Introduction to Unconventional Superconductivity

Manfred Sigrist

Theoretische Physik, ETH-Hönggerberg, 8093 Zürich, Switzerland

Abstract. This lecture gives a basic introduction into some aspects of the unconventional superconductivity. First we analyze the conditions to realize unconventional superconductivity in strongly correlated electron systems. Then an introduction of the generalized BCS theory is given and several key properties of unconventional pairing states are discussed. The phenomenological treatment based on the Ginzburg-Landau formulations provides a view on unconventional superconductivity based on the concept of spontaneous symmetry breaking. Finally some aspects of two examples of unconventional superconductors will be discussed: high-temperature superconductivity and spin-triplet superconductivity in Sr_2RuO_4.

Keywords: Unconventional superconductivity, high-temperature superconductivity, Sr_2RuO_4

INTRODUCTION

Superconductivity remains to be one of the most fascinating and intriguing phases of matter even nearly hundred years after its first observation. Owing to the breakthrough in 1957 by Bardeen, Cooper and Schrieffer we understand superconductivity as a condensate of electron pairs, so-called Cooper pairs, which form due to an attractive interaction among electrons. In the superconducting materials known until the mid-seventies this interaction is mediated by electron-phonon coupling which gises rise to Cooper pairs in the most symmetric form, i.e. vanishing relative orbital angular momentum and spin singlet configuration (nowadays called *s*-wave pairing). After the introduction of the BCS concept, also studies of alternative pairing forms started. Early on Anderson and Morel [1] as well as Balian and Werthamer [2] investigated superconducting phases which later would be identified as the A- and the B-phase of superfluid ^{3}He [3]. In contrast to the *s*-wave superconductors the A- and B-phase are characterized by Cooper pairs with angular momentum 1 and spin-triplet configuration. This was the beginning of the era of *unconventional* superconductivity, condensates of Cooper pairs of lower symmetry, in contrast to the *conventional* superconductors with the most symmetric Cooper pairs.

The discovery of superfluidity in the ^{3}He in 1971 by Osheroff, Richardson and Lee gave the first example of unconventional Cooper pairing [4]. In ^{3}He other pairing mechanisms are obviously of non-phononic origin, based on van der Waals and spin fluctuation mediated interactions [3, 5]. Moreover, ^{3}He is the prime example for a strongly correlated Fermi liquid where the short range repulsive interaction leads to strong renormalisations of the quasiparticle mass and other quantities. Alternative pairing mechanism and strong correlation effects are key elements to prevent electrons from undergoing conventional *s*-wave pairing.

The natural aim to find among solids a system with unconventional Cooper pairing

was not satisfied until much latter when at the end of seventies and beginning of the eighties two novel classes of strongly correlated materials were found among which some were superconducting - the heavy Fermion compounds [6, 7, 8] and organic conductors [9, 10]. The first type of materials are intermetallics containing rare earth ions and the second are highly anisotropic conductors based organic units. Although it is not clear until today which form of Cooper pairing is realized in many of these materials, some of them possess complex phase diagrams with several different superconducting phases, firmly establishing the unconventional nature. In both types of material superconductivity emerges out of phase that are nearly magnetic or evolve under pressure from a magnetically ordered state. In 1986 the discovery of high-temperature superconductivity in cuprate compounds with layered perovskite structure announced the era of unconventional superconductivity to a wider community [11]. This system dominates to the present days the study of superconductivity. A few years were necessary to establish the unconventional character to pairing for the cuprates. Cooper pairs possess in the quasi-two-dimensional systems a so-called spin singlet $d_{x^2-y^2}$-wave structure [12, 13]. In cuprate materials the important role of magnetism in the context of the unusual metallic properties and superconductivity is underlined by the fact that this superconductor emerges from an antiferromagnetic Mott-insulator upon carrier doping [14].

The essential role which magnetism could play for unconventional superconductivity became one of the guiding strategies in the nineties in the search for new materials. Striking examples of superconductivity associated with magnetic phases are several Ce-based compounds where superconductivity is associated with a quantum critical point of an antiferromagnetically ordered phase. $CeIn_3$ [15], $CePd_2Si_2$ [15, 16] and $CeMIn_5$ (M=Co,Rh,Ir) [17, 18] are a few examples of this type. Surprisingly superconductivity was also found inside a ferromagnetic phases in UGe_2 [19], $URhGe$ [20] and $ZrZn_2$ [21], possibly connected with the corresponding magnetic quantum phase transition.

Sr_2RuO_4 whose superconductivity was discovered in 1994 deserves a special place as an exemplary case of an unconventional superconductor resulting from a strongly correlated Fermi liquid phase [22]. In various respects it may be considered as an analog to ^3He, including the pairing symmetry which is closely related to the A-phase of the superfluid. Many aspects of this superconductor have been explored in much detail during the last ten years [23, 24]

More recently the superconducting skutterudites such as $PrOs_4Sb_{12}$ have been aroused much interest as new examples of heavy Fermion materials with multiple superconducting phases [25]. The exploration of superconductivity in materials with geometrically frustrated crystall lattices has been a further recent focus. This includes Na_xCoO_4 intercalated with water which has been considered as a realization of superconductivity on a triangular lattice [26]. Also superconductivity in metalls with the pyrochlor structure belong to this class such as $Cd_2Re_2O_7$ [27] and AOs_2O_6 (A=Cs,Rb,K) [28], although it is not clear whether they are unconventional. Crystal structure can have an even crucial impact on superconductivity than in the case of frustrated lattices, if inversion symmetry is missing. As we will see later inversion together with time reversal invariance are among the key symmetries for Cooper pair formation. The discovery of superconductivity in the heavy Fermion systems $CePt_3Si$ and UIr have reopened the discussion of superconductivity in this kind of systems [29].

During the past two decades we experience important developments in the field of

unconventional superconductivity, from the side of new materials as well as theoretical understanding. New strategies for the discovery of unconventional superconductors bear fruits besides the tremendous progress in sample production which is a mandatory accessory for the observation of unconventional superconducting phases which are very sensitive to material disorder effects. These lecture notes cover a few aspects and developments in the field of unconventional superconductivity. Naturally this overview is selective and the viewpoint is biased by the preferences of the lecturer.

CONVENTIONAL VERSUS UNCONVENTIONAL SUPERCONDUCTIVITY

The most fundamental experimental aspect of superconductivity is the screening of a magnetic field, the Meissner-Ochsenfeld effect, which implies also the existence of persistent electric currents. The microscopic theory which provides such a feature is based on the coherent state introduced by Bardeen, Cooper and Schrieffer. In this chapter we will give a brief introduction to this BCS state (screening effects, however, will be only addressed later in the context of the phenomenological Ginzburg-Landau formulation) and motivate the generalization beyond the standard BCS theory of conventional superconductivity. We will compare also the electron-phonon mechanism for superconductivity with possible alternative mechanisms, in particular, based on effective interaction originating from spin fluctuations.

Standard BCS theory

It is convenient for the further discussion to first introduce the basics of the meanfield formulation of the BCS theory using a very simple model. The formation of Cooper pairs which is at the heart of the microscopic theory of Bardeen, Cooper and Schrieffer, requires the presence of an attractive interaction between electrons. For our purpose it is sufficient to use a structureless contact interaction which yields the following Hamiltonian in a second-quantization language,

$$\mathcal{H} = \sum_{\vec{k},s} \xi_{\vec{k}} c^{\dagger}_{\vec{k}s} c_{\vec{k}s} + g \sum_{\vec{k},\vec{k}',\vec{q}} c^{\dagger}_{\vec{k}+\vec{q},\uparrow} c^{\dagger}_{\vec{k}'-\vec{q},\downarrow} c_{\vec{k}'\downarrow} c_{\vec{k}\uparrow}. \tag{1}$$

where $c^{\dagger}_{\vec{k}s}$ ($c_{\vec{k}s}$) creates (annihilates) an electron with momentum $\vec{k}$ and spin s. The first term is the kinetic energy accounting for the band structure of the metal, where $\xi_{\vec{k}}$ is measured relative to the chemical potential μ, i.e. $\xi_{\vec{k}} = \varepsilon_{\vec{k}} - \mu = \frac{\hbar^2}{2m}(\vec{k}^2 - k_F^2)$ for a parabolic band. The second term describes the two-particle interaction which is represented by a structureless scattering matrix element g. This corresponds to a attractive contact interaction $U(\vec{r} - \vec{r}') = g\delta(\vec{r} - \vec{r}')$ (with $g < 0$) such that $V_{\vec{k},\vec{k}'} = V(\vec{q} = \vec{k} - \vec{k}') = \int d^3 r U(\vec{r}) e^{i\vec{q}\cdot\vec{r}} = g$. Note that in this case only particle of opposite spin interact.

For the BCS theory the relevant scattering processes are those of particle pairs with vanishing total momentum, belonging to the set of states $\{|\vec{k}\uparrow\rangle \otimes |-\vec{k}\downarrow\rangle\}$. Therefore we concentrate on the reduced Hamiltonian

$$\mathscr{H} = \sum_{\vec{k},s} \xi_{\vec{k}} c_{\vec{k}s}^\dagger c_{\vec{k}s} + g \sum_{\vec{k},\vec{k}'} c_{\vec{k}\uparrow}^\dagger c_{-\vec{k}\downarrow}^\dagger c_{-\vec{k}'\downarrow} c_{\vec{k}'\uparrow}. \tag{2}$$

ignoring all other pair scattering events. Bardeen, Cooper and Schrieffer introduced the following variational ground state

$$|\Phi_{\text{BCS}}\rangle = \prod_{\vec{k}} \left\{ u_{\vec{k}} + v_{\vec{k}} c_{\vec{k}\uparrow}^\dagger c_{-\vec{k}\downarrow}^\dagger \right\} |\text{vac}\rangle \tag{3}$$

where $|\text{vac}\rangle$ denotes the electron vacuum ($|u_{\vec{k}}|^2 + |v_{\vec{k}}|^2 = 1$). This is a coherent states of electron pairs (Cooper pairs) giving a lower energy than the bare Fermi gas.

An alternative approach which provides also straightforwardly the quasiparticle spectrum of the coherent state is given by the mean field theory which allows us to reduce the interaction part. Among the possible meanfields we use the off-diagonal

$$b_{\vec{k}} = \left\langle c_{-\vec{k}\downarrow} c_{\vec{k}\uparrow} \right\rangle \tag{4}$$

which connects states of particle numbers different by 2, as suggested by the variational state (3). Note that the expectation value $\langle A \rangle = \text{tr}[\exp(-\beta\mathscr{H})A]/\text{tr}[\exp(-\beta\mathscr{H})]$. We may interpret $b_{\vec{k}}$ as the wavefunction of the Cooper pairs in momentum space. Inserting $c_{-\vec{k}\downarrow} c_{\vec{k}\uparrow} = b_{\vec{k}} + \{c_{-\vec{k}\downarrow} c_{\vec{k}\uparrow} - b_{\vec{k}}\}$ into the Hamiltonian and neglecting terms quadratic in $\{\ldots\}$ (we assume $\langle|\{\ldots\}|^2\rangle \ll |b_{\vec{k}}|^2$) we obtain the meanfield Hamiltonian

$$\begin{aligned} \mathscr{H} &= \sum_{\vec{k},s} \xi_{\vec{k}} c_{\vec{k}s}^\dagger c_{\vec{k}s} + g \sum_{\vec{k},\vec{k}'} b_{\vec{k}'}^* c_{-\vec{k}\downarrow} c_{\vec{k}\uparrow} + b_{\vec{k}'} c_{\vec{k}\uparrow}^\dagger c_{-\vec{k}\downarrow}^\dagger - b_{\vec{k}}^* b_{\vec{k}'} \tag{5} \\ &= \sum_{\vec{k},s} \xi_{\vec{k}} c_{\vec{k}s}^\dagger c_{\vec{k}s} - \sum_{\vec{k}} \left(\Delta^* c_{-\vec{k}\downarrow} c_{\vec{k}\uparrow} + \Delta c_{\vec{k}\uparrow}^\dagger c_{-\vec{k}\downarrow}^\dagger \right) - \Delta^* b_{\vec{k}} \tag{6} \end{aligned}$$

with $\Delta = -g\sum_{\vec{k}'} b_{\vec{k}'}$. It is now straightforward to find the quasiparticle spectrum of this one-particle Hamiltonian by introducing new Fermion operators $\gamma_{\vec{k}s}$ with the property $\dot{\gamma}_{\vec{k}s}^\dagger = i[\mathscr{H}_{mf}, \gamma_{\vec{k}s}^\dagger] = E_{\vec{k}} \gamma_{\vec{k}s}^\dagger$. To reach such a diagonalization of the Hamiltonian we use the Bogolyubov transformation

$$c_{\vec{k}\uparrow} = u_{\vec{k}}^* \gamma_{\vec{k}1} + v_{\vec{k}} \gamma_{\vec{k}2}^\dagger \quad \text{and} \quad c_{-\vec{k}\downarrow} = -v_{\vec{k}}^* \gamma_{\vec{k}1} + u_{\vec{k}} \gamma_{\vec{k}2}^\dagger \tag{7}$$

with $|u_{\vec{k}}|^2 + |v_{\vec{k}}|^2 = 1$ and indices 1 and 2 stands for the electron like and hole like quasiparticle. Note that the functions $u_{\vec{k}}$ and $v_{\vec{k}}$ are identical with those of the variational state (3). The Hamiltonian acquires the diagonal form

$$\mathscr{H}_{mf} = \sum_{\vec{k}} [\xi_{\vec{k}} - E_{\vec{k}} + \Delta b_{\vec{k}}] + \sum_{\vec{k}} E_{\vec{k}} (\gamma_{\vec{k}1}^\dagger \gamma_{\vec{k}1} + \gamma_{\vec{k}2}^\dagger \gamma_{\vec{k}2}) \tag{8}$$
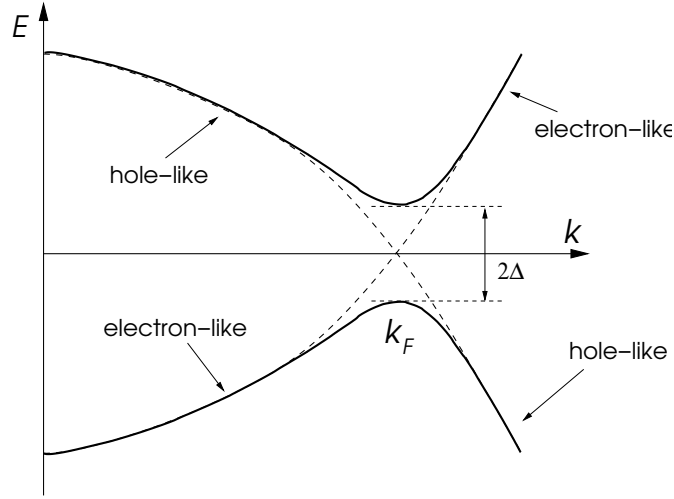
FIGURE 1. Schematic quasiparticle spectrum: The solid line shows the spectrum with a finite energy gap and the dashed line corresponds to the spectrum for $\Delta = 0$ with the same quasiparticle occupation. States with $E < 0$ are occupied by quasiparticles and empty for $E > 0$. Obviously the opening of the gap lowers the groundstate energy.

where the quasiparticle energy is given by $E_{\vec{k}} = \sqrt{\xi_{\vec{k}}^2 + \Delta^2}$, The spectrum of the Hamiltonian has two branches which originate from electron and hole branches. The attractive interaction g leads to an instability of the Fermi surface and the opening of a gap 2Δ (see Fig.1). The gap is the result of 'hybridizing' electron-like and hole-like quasiparticles leading to new quasiparticles as a superposition of electron- and hole-like character.

The energy gap has to be determined self-consistently from the "gap equation":

$$\Delta = -g \sum_{\vec{k}} b_{\vec{k}} = -g \sum_{\vec{k}} u_{\vec{k}}^* v_{\vec{k}} [1 - f(E_{\vec{k}})] = -g \sum_{\vec{k}} \frac{\Delta}{2E_{\vec{k}}} \tanh\left(\frac{E_{\vec{k}}}{k_B T}\right) \qquad (9)$$

with the Fermi factor $f(E) = 1/(1 + e^{E/k_B T})$. Note that this energy gap $\Delta(T)$ only depends on temperature. We define the critical temperature T_c as the temperature where the gap vanishes. In the limit $\Delta \to 0$ of Eq.(9) we obtain the linearized gap equation determining T_c:

$$\Delta = -g\Delta \sum_{\vec{k}} \frac{1}{2\xi_{\vec{k}}} \tanh\left(\frac{\xi_{\vec{k}}}{k_B T}\right) \quad \Rightarrow \quad 1 = -g \int d\xi \frac{N(\xi)}{2\xi} \tanh\left(\frac{\xi}{k_B T_c}\right). \qquad (10)$$

where $N(\xi)$ is the density of states of the electrons. This integral has a logarithmic divergence for $\xi \to \pm\infty$. Thus we need to introduce a cutoff energy ε_c to obtain sensible result. This corresponds to a characteristic energy scale of the attactive interaction and is assumed to be much smaller than the Fermi energy or the band width, the electronic energy scale. In other words we may say that the attractive interaction is only present in a narrow energy range around the Fermi surface. Then it seems legitimate to assume

that the density of states is constant, $N(\xi) \to N_0$, yielding:

$$1 = -gN_0 \int_{-\varepsilon_c}^{\varepsilon_c} \frac{d\xi}{\xi} \tanh\left(\frac{\xi}{2k_B T_c}\right) = -gN_0 \ln\left(\frac{1.14\varepsilon_c}{k_B T_c}\right) \tag{11}$$

from which we derive

$$k_B T_c = 1.14\varepsilon_c e^{-1/|g|N_0} . \tag{12}$$

The critical temperature T_c depends on the cutoff energy ε_c.

The energy gap at zero temperature is also straightforwardly calculated using the same energy cutoff:

$$1 = -gN_0 \int_0^{\varepsilon_c} \frac{d\xi}{\sqrt{\xi^2 + \Delta^2}} = -gN_0 \sinh^{-1} \frac{\varepsilon_c}{\Delta} \tag{13}$$

such that

$$\Delta(T = 0) \approx 2\varepsilon_c e^{-1/|g|N_0} = 1.764 k_B T_c . \tag{14}$$

Obviously we can express the gap by T_c with a universal proportionality factor and without the appearance of ε_c. This is the signature of the scheme which we call "weak-coupling" approximation. It is possible to express physical quantities cutoff-free, if T_c is known.

Finally we estimate the condensation energy at $T = 0$ which corresponds to the energy gain due to the opening of the gap. Since this gap is very small the condensation energy originates from the modification of the quasi particle states very close to the Fermi energy. Therefore we obtain

$$E_{\text{cond}} = \sum_{\vec{k}} \left[\xi_{\vec{k}} - E_{\vec{k}} + \Delta b_{\vec{k}}\right] \approx -\frac{1}{2} N_0 |\Delta|^2 . \tag{15}$$

The condensation energy depends on the density of states at the Fermi surface and the zero-temperature gap magnitude. Thus within the weak coupling meanfield treatment E_{cond} is determined by the modified quasiparticle spectrum only (Fig.1).

Electron-Phonon interaction and Coulomb Repulsion

So far the nature of the model interaction was not specified in our discussion. We now turn to the electron-phonon mediated interaction and which closely connected with the Coulomb interaction. Thus, it is necessary examine also the effect of Coulomb repulsion on the pairing of electrons. Electron possesses charge and spin degrees of freedom. In a metal Coulomb interaction coupling to charge is renormalized through many body effects.

$$V_{\vec{k},\vec{k}'} = \frac{4\pi e^2}{q^2 \varepsilon(\vec{q}, \omega)} \tag{16}$$

where $\vec{q} = \vec{k} - \vec{k}'$. The dielectric constant $\varepsilon(\vec{q}, \omega)$ describes the effect of dynamical screening of charge fluctuations. This occurs due to the rearrangement of the electrons

as well as the polarization of the elastic (positively charged) ionic lattice of the metal i.e. due to phonons. We can decompose the renormalized interaction into two corresponding parts

$$V_{\vec{k},\vec{k}'}^{\text{eff}} = \underbrace{\frac{4\pi e^2}{q^2 + k_{TF}^2}}_{\text{renorm. Coulomb}} + \underbrace{\frac{4\pi e^2}{q^2 + k_{TF}^2} \frac{\omega_q^2}{\omega^2 - \omega_q^2}}_{\text{electron-phonon}}, \tag{17}$$

with $\hbar\omega = \varepsilon_{\vec{k}} - \varepsilon_{\vec{k}'}$. where the first is due Thomas-Fermi screening which is considered as instantaneous so that we ignore the frequency dependence. The screening length is

$$\lambda_{TF} = k_{TF}^{-1} \quad \text{with} \quad k_{TF}^2 = \frac{6\pi e^2 n_e}{\varepsilon_F}, \tag{18}$$

which is of the order of a few lattice constants, making the interaction very short ranged. The second part due to the phonons, in the same way short ranged, involves the dynamics of the ions which slow compared electronic time scales. Here ω_q describes the spectrum of the acoustic phonons $\omega_q = sq$ at long wave-lengths, implying the Debye energy $\hbar\omega_D$ as a characteristic energy scale. This interaction is attractive for frequencies $|\omega| < \omega_q \leq \omega_D$ and repulsive otherwise. In this way the Debey frequency appears as a natural energy cutoff ε_c. We will now use a simple model given by Anderson and Morel to discuss the superconducting instability including the repulsive part of the Coulomb interaction which we had ignored in the introduction above [30].

Anderson-Morel-Model

Including now also the effect of the repulsive Coulomb interaction we set up a simplified weak-coupling model which keeps the most essential features of the electron band and the structure of the interaction (17). The electron band is characterized by its width $W = 2E_F$ with the chemical potential in the center and a constant density of states $N(\xi) = N_0$. The interaction is divided into a repulsive and an attractive part V_{ee} and V_{ep}, respectively, originating from the two parts in (17). The energy range of the attractive part is centered around the Fermi energy bounded by the cutoff energy $\varepsilon_D = \hbar\omega_D$ while the repulsive part extends over the whole band width. Thus we define

$$\tilde{V}_{\vec{k},\vec{k}'} = V_{\vec{k},\vec{k}'}^{ee} + V_{\vec{k},\vec{k}'}^{ep},$$

$$\Rightarrow \begin{cases} N_0 V_{\vec{k},\vec{k}'}^{ee} = N_0 V^{ee}(\xi_{\vec{k}}, \xi_{\vec{k}'}) = \begin{cases} \mu > 0 & \text{for } -W \leq \xi_{\vec{k}}, \xi_{\vec{k}'} \leq W \\ 0 & \text{else} \end{cases} \\ \\ N_0 V_{\vec{k},\vec{k}'}^{ep} = N_0 V^{ep}(\xi_{\vec{k}}, \xi_{\vec{k}'}) = \begin{cases} -\lambda < 0 & \text{for } -\varepsilon_D \leq \xi_{\vec{k}}, \xi_{\vec{k}'} \leq \varepsilon_D \\ 0 & \text{else} \end{cases} \end{cases}$$

$$\tag{19}$$

with $\xi_{\vec{k}} = \varepsilon_{\vec{k}} - \varepsilon_F$. We set up the corresponding BCS-type Hamiltonian with the mo-
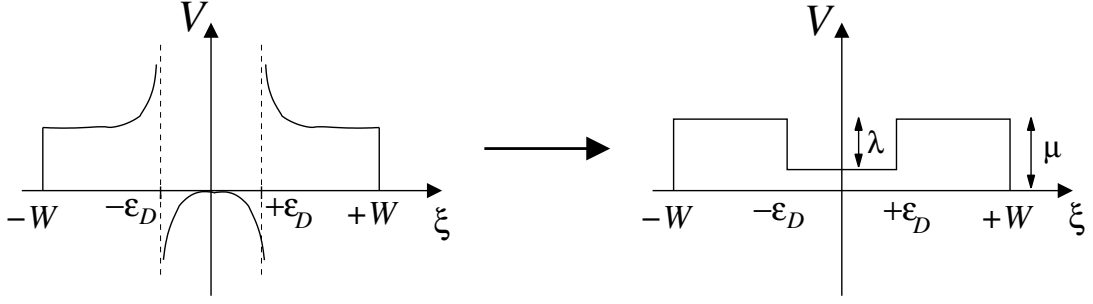
FIGURE 2. Model interaction: The left panel shows the basic energy dependence of the interaction (17). The right panel is a very simplified model interaction with the essential features of an overall repulsive interaction with an attractive part around the Fermi energy.

mentum dependent interaction

$$\mathscr{H} = \sum_{\vec{k},s} \xi_{\vec{k}} c^{\dagger}_{\vec{k},s} c_{\vec{k},s} + \frac{1}{2\Omega} \sum_{\vec{k},\vec{k}'} \tilde{V}_{\vec{k},\vec{k}'} c^{\dagger}_{\vec{k}\uparrow} c^{\dagger}_{-\vec{k}\downarrow} c_{-\vec{k}'\downarrow} c_{\vec{k}'\uparrow} \tag{20}$$

which we decouple in the analogous way as in the previous section leading to the gap equation

$$\Delta_{\vec{k}} = -\sum_{\vec{k}'} \tilde{V}_{\vec{k},\vec{k}'} \langle c_{-\vec{k}'\downarrow} c_{\vec{k}'\uparrow} \rangle , \qquad \Delta^{*}_{\vec{k}} = -\sum_{\vec{k}'} \tilde{V}_{\vec{k},\vec{k}'} \langle c^{\dagger}_{\vec{k}'\uparrow} c^{\dagger}_{-\vec{k}'\downarrow} \rangle . \tag{21}$$

We introduce the simplifying form

$$\Delta_{\vec{k}} = \Delta(\xi_{\vec{k}}) g_{\vec{k}} , \tag{22}$$

where $g_{\vec{k}}$ describes the angular structure of the gap which is also a function of the energy. We reduce the linearized gap equation to the form

$$\Delta(\xi) = -N_0 \int d\xi' \tilde{V}(\xi,\xi') \frac{\tanh(\beta \xi'/2)}{\xi'} \Delta(\xi') , \tag{23}$$

where $\tilde{V}(\xi,\xi')$ is defined as

$$\tilde{V}(\xi,\xi') = \frac{1}{\Omega} \sum_{\vec{k},\vec{k}'} g^{*}_{\vec{k}} V_{\vec{k},\vec{k}'} g_{\vec{k}'} \delta(\xi - \xi_{\vec{k}}) \delta(\xi' - \xi_{\vec{k}'}) . \tag{24}$$

where $V_{\vec{k},\vec{k}'}$ is taken from (19). This interaction requests that $g_{\vec{k}} = 1$. Sinc the approximation for the band structure and the pairing interaction in (19) give to distinct energy regions we also put the analogous parametrization ansatz for the gap

$$\Delta(\xi) = \begin{cases} \Delta_1 & \text{for} \quad |\xi| < \varepsilon_D \\ \Delta_2 & \text{for} \quad \varepsilon_D < |\xi| < W \end{cases} . \tag{25}$$
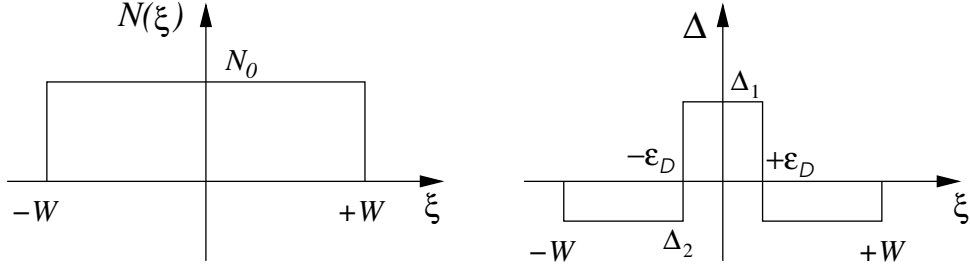
FIGURE 3. The left panel shows the density of states of the simple model and the right panel gives the schematic energy dependence of the gap as a function of ξ.

With this simplifications we arrive at the following two linearized coupled gap equations

$$
\begin{aligned}
\Delta_1 &= (\lambda - \mu)\Delta_1 \int_0^{\varepsilon_D} d\xi' \frac{\tanh(\beta\xi'/2)}{\xi'} - \mu\Delta_2 \int_{\varepsilon_D}^W d\xi' \frac{\tanh(\beta\xi'/2)}{\xi'} \\
&= (\lambda - \mu)\Delta_1 \ln(1.14\varepsilon_D/k_BT) - \mu\Delta_2 \ln(W/\varepsilon_D)
\end{aligned}
$$

$$
\begin{aligned}
\Delta_2 &= -\mu\Delta_1 \int_0^{\varepsilon_D} d\xi' \frac{\tanh(\beta\xi'/2)}{\xi'} - \mu\Delta_2 \int_{\varepsilon_D}^W d\xi' \frac{\tanh(\beta\xi'/2)}{\xi'} \\
&= -\mu\Delta_1 \ln(1.14\varepsilon_D/k_BT) - \mu\Delta_2 \ln(W/\varepsilon_D) \,.
\end{aligned}
\tag{26}
$$

The condition that $\Delta_{1,2} \neq 0$ (non-zero determinant) defines T_c:

$$
k_BT_c = 1.14\varepsilon_D \exp\left(-\frac{1}{\lambda - \mu^*}\right)
\tag{27}
$$

with

$$
\mu^* = \frac{\mu}{1 + \mu\ln(W/\varepsilon_D)} \,.
\tag{28}
$$

This has a structure similar to that of the previous section apart from the fact that the effect of the attractive potential is slightly diminished. A finite transition temperature exist as long as $\lambda > \mu^*$. The important result is that the effect of the repulsive Coulomb interaction does not enter in its full strength but is renormalized. The reduction depends on the ration W/ε_D, i.e. the ratio of the energy scales involved. This renormalization of the Coulomb repulsion displays the retardation effect of the electron-phonon interaction. The polarization of the ionic lattice due to electron persists on time scales much longer the characteristic time scale of the electron ($\sim \hbar/E_F \ll \omega_D^{-1}$. Thus an electron interact with another electron via lattice deformation without having to be at the same time at the same position in the lattice.

The gap as a function of ξ changes sign at ε_D which allows to optimize the pairing energy taking the different sign of the interaction into account.

A similar form for T_c comes out of the full retarded solution of the equations of the superconducting instability by means of the Eliashberg-formulation in the so-called

strong coupling limit:

$$k_B T_c = 0.7\varepsilon_D \exp\left(-\frac{1.04(1+\lambda)}{\lambda - \mu^*(1+0.62\lambda)}\right) . \tag{29}$$

This form is due to Mac Millan and takes also the effect of the quasiparticle renormalization due to the electron-phonon interaction into account [31], contained in the factor $(1+\lambda)$ of the numerator in the exponent. While the most simple weak-coupling form for T_c gives that $T_c \propto \omega_D$ we expect to observe the so-called isotope effect, i.e. $T_c \propto M_{ion}^{-1/2}$, since $\omega_D \propto M_{ion}^{-1/2}$. Including retardation effects, however, gives a new dependence of T_c on the cutoff energy so that we find deviation from the simple form of the isotope effect.

Strongly correlated electron systems

In simple metals it is rather easy for the electron-phonon interaction to overcome the Coulomb repulsion through the retardation effect. The conduction electrons are much faster than the ions and move basically as free particles. In so-called strongly correlated electron systems, however, electrons are often more close associated with atomic orbitals and retain more of their localized character, like in transition metal oxides or rare-earth intermetallics forming so-called heavy Fermion systems. The nearly localized electrons are considerably slower in their motion such that Coulomb interactions are comparable to the kinetic energy or even larger. In the heavy Fermion materials the characteristic energy scale associated with the carriers at the Fermi energy is even smaller that the Debye energy. Under such conditions the retardation effect does not provide sufficient help and Coulomb interaction dominates over the attractive electron-phonon coupling.

Symmetry of the pair wave function

Both the Coulomb and the electron-phonon interaction are very short ranged and may be viewed practically as contact interactions so that they are felt by two electrons only if they can be found with a finite probability at the same spot. Considering the pair wavefunction

$$\psi(\vec{r}, s; \vec{r}', s') = f(|\vec{r} - \vec{r}'|)\chi(s, s') \tag{30}$$

the obital part $f(\vec{r})$ has to be in the $l = 0$-channel for a rotationally symmetric systems and the spin configuration has spin-singlet character (only particles of the opposite spin can meet at the same point). For $\lambda < \mu^*$ the Cooper pairing instability is suppressed by Coulomb interaction. The short-ranged repulsive interaction can be avoided by electron pairs with a non-vanishing orbital angular momentum $l > 0$. Then the pair wavefunction vanishes for the two electrons at the same place ($f(r) \propto r^l$ for $r \to 0$). Cooper pairs in a rotationally symmetric environment satisfy the following basic symmetry requirements. The fact that two identical Fermions pair requires that their wave functions is

antisymmetric under exchange of the two electrons yields following conditions:

$$\psi(\vec{r}',s';\vec{r},s) = -\psi(\vec{r},s;\vec{r}',s') = f(-\{\vec{r}-\vec{r}'\})\chi_{s',s}$$

$$\Rightarrow \quad \begin{cases} f(-\vec{r}) = f(\vec{r}), & \chi_{s,s'} = -\chi_{s',s}, & l = 0,2,4,..., & S = 0 \\ f(-\vec{r}) = -f(\vec{r}), & \chi_{s,s'} = \chi_{s',s}, & l = 1,3,5,..., & S = 1 \end{cases} \qquad (31)$$

As parity is given by $(-1)^l$, even partity means spin singlet and odd parity means spin triplet pairing. From this viewpoint we define a conventional superconductor as a condensate of $l = 0$ Cooper pairs, i.e. the most symmetric pairing state. Unconventional are all other states with $l > 0$. This distinction is not restricted to rotation symmetric systems, but can be applied in the modified form also to real metals which possess (lower) point group symmetry of the crystalline lattices. There the angular momentum is replaced by the irreducible representations of the point group, as we will see later.

Alternative mechanisms

If the short-ranged Coulomb repulsion jams the electron-phonon interaction for pairing, alternative pairing interactions have to be found. Both interactions are of less importance, if pairing is realized in a channel different from the most symmetric one.

$$g_{\vec{k};s,s'} = \langle c_{-\vec{k},s} c_{\vec{k}s'} \rangle \quad \text{with} \quad \sum_{\vec{k}} g_{\vec{k};s,s'} = 0 \qquad (32)$$

which means that there is no pairing amplitude for electrons on the same position. Mechanisms giving rise to this kind of pairing should provide a not too short-ranged interaction.

Kohn and Luttinger asked in 1965 the question whether pairing would be possible based poorly on Coulomb interaction [32]. Their pairing mechanism is based on a part of the renormalized Coulomb interaction which we had ignored. Due to the sharp Fermi edge in metals the renormalized Coulomb interaction possesses also a long-range oscillatory tail. These are the Friedel oscillations giving rise to a potential of the large-r form

$$V(r) = \frac{\cos 2k_F r}{r^3}. \qquad (33)$$

which has obviously both attractive as well as repulsive parts. Pairing states of higher angular momentum would be able to take advantage of the attractive portion of $V(r)$. The resulting critical temperature obtained from this interaction is

$$\frac{T_c}{T_F} \simeq e^{-(2l)^4} \qquad (34)$$

with $l > 0$. Although the relevant energy scale is the Fermi energy or band width, this mechanism is irrelevant for real superconductivity, since even for $l = 1$ the achievable T_c

would be of order of $10^{-7} \times T_F$. Nevertheless it is possible to undergo a superconducting transition at very low temperature if no other instability has happened. An approach resulting in more feasible critical temperatures was given by Berk and Schrieffer [33], who studied the exchange of spin fluctuations. In contrast to the electron-phonon interaction and the Kohn-Luttinger mechanism which are based on the electron charge only, the spin plays the key role in this case.

Mechanism based on spin-fluctuation exchange

The electron-phonon mechanism is based on the polarizability of the elastic ionic lattice in a metal. In a similar way also spins can form a polarizable medium and yield an effective interaction among electrons. These polarizable spins can be localized degrees of freedom or the spins of the conduction electrons themselves. Nearly magnetic materials are most suitable for this type of interaction. We will illustrate this here on the example of a nearly ferromagnetic metal, described by the Stoner model.

We consider an electron with spin $\vec{S}$ at the position $\vec{r}$ and time t. By means of the exchange interaction (exchange hole) the electron spin polarizes the spin of the surrounding electrons. In this way it acts like a local magnetic field of the form

$$\vec{H}(\vec{r},t) = -\frac{I}{\mu_B \hbar} \vec{S}(\vec{r},t) \tag{35}$$

where μ_B is the Bohr magneton and $I = U/\Omega$ is derived from the exchange interaction

$$\mathscr{H}_{ex} = \int d^3 r d^3 r' U \delta(\vec{r} - \vec{r}') \rho_\uparrow(\vec{r}) \rho_\downarrow(\vec{r}') \tag{36}$$

which appears here as a repulsive contact interaction of strength U between electrons of opposite spin ($\rho_s(\vec{r})$ denotes the density of electrons of spin s at $\vec{r}$, Ω is the volume). According to linear response theory, the electron spins will respond to the local field as described by the dynamical spin susceptibility

$$\vec{S}(\vec{r}',t') = \mu_B \int d^3 r \, dt \, \chi(\vec{r}' - \vec{r}, t' - t) \vec{H}(\vec{r},t) \tag{37}$$

assuming $\chi(\vec{r},t)$ to be isotropic in spin space. Again invoking the exchange interaction it is possible to derive an effective Zeeman energy for the spin density at $(\vec{r}',t')$.

$$\Delta E = -\frac{\mu_B}{\hbar} \vec{S}(\vec{r}',t') \cdot \vec{H}(\vec{r}',t') = \frac{I}{\hbar} \vec{S}(\vec{r}',t') \cdot \mu_B \int d^3 r \, dt \, \chi(\vec{r}' - \vec{r}, t' - t) \vec{H}(\vec{r},t) \tag{38}$$

which can be reformulated in terms of electron spin densities,

$$\mathscr{H}_{sf} = -\frac{I^2}{\hbar^2} \int d^3 r \, d^3 r' \int dt \, dt' \, \chi(\vec{r} - \vec{r}'; t - t') \, \vec{S}(\vec{r},t) \cdot \vec{S}(\vec{r}',t') \,. \tag{39}$$
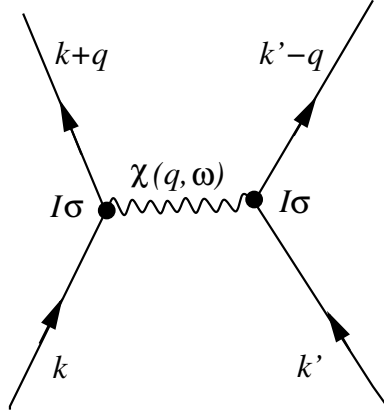
FIGURE 4. Process of pair scattering of electrons due to spin flucutions, i.e. paramagnon exchange.

and can be rewritten in momentum space as

$$\mathcal{H}_{sf} = -\frac{1}{\Omega}\frac{I^2}{4}\int d\omega \sum_{\vec{q},\vec{k},\vec{k}'} Re(\chi(\vec{q},\omega))$$

$$\times \sum_{s_1,s_2,s_3,s_4} \{c^{\dagger}_{\vec{k}+\vec{q},s_1}\vec{\sigma}_{s_1s_2}c_{\vec{k},s_2}\} \cdot \{c^{\dagger}_{\vec{k}'-\vec{q},s_3}\vec{\sigma}_{s_3s_4}c_{\vec{k}',s_4}\} \tag{40}$$

This scattering process is shown diagrammatically in Fig.4. In order to be specific in the form of the interaction we approximate the spin susceptibility by its RPA form:

$$\chi(\vec{q},\omega) = \frac{\chi_0(\vec{q},\omega)}{1-I\chi_0(\vec{q},\omega)} \tag{41}$$

with

$$\chi_0(\vec{q},\omega) \approx N_0\left(1 - \frac{\vec{q}^2}{12k_F^2} + i\frac{\pi}{2}\frac{\omega}{v_F|\vec{q}|}\right) \quad q \ll 2k_F \;,\; \omega \ll \varepsilon_F \tag{42}$$

where $\chi_0(\vec{q},\omega)$ is the bare dynamical susceptibility of the isotropic electron gas. For a parabolic band (i.e. no nesting features) the static susceptibility is maximal for $\vec{q} = 0$ where $\chi(\vec{q}=0,\omega=0) = N_0/(1-IN_0)$. The divergence of the susceptibility for $1 = IN_0$ is the well-known Stoner's instability corresponding to the onset of ferromagnetic order. Turning to the imaginary part of χ we find for a given $\vec{q}$ a maximum as a function of ω, which is interpreted as a rather broad resonance, called *paramagnon*, with the approximate dispersion $\omega_{0q} = \frac{2}{\pi IN_0}(1-IN_0)v_Fq$ for small $\vec{q}$ (Fig.5).

By analogy to the electron-phonon interaction, we use the electron-paramagnon coupling as a pairing potential (spin fluctuation exchange mechanism). Limiting ourselves to the Cooper pairing channel the interaction term is written as

$$\mathcal{H}'_{sf} = \sum_{\vec{k},\vec{k}'}\sum_{s_1,s_2,s_3,s_4} V_{\vec{k},\vec{k}';s_1s_2s_3s_4} c^{\dagger}_{\vec{k},s_1} c^{\dagger}_{-\vec{k},s_2} c_{-\vec{k}',s_3} c_{\vec{k}',s_4} \tag{43}$$
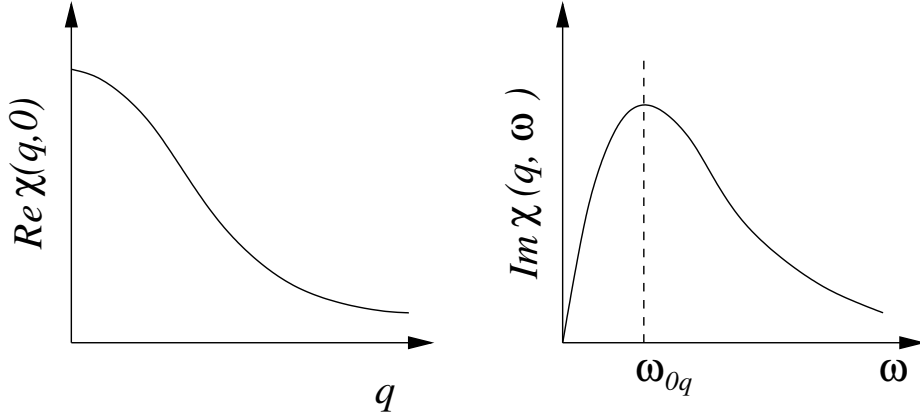
FIGURE 5. Real and imaginary part of the dynamical susceptibility. The static real part of χ has a maximum at $\vec{q} = 0$. The imaginary part shows a broak peak whose center is used to give an ω-$\vec{q}$ relation describing the paramagnon as a strongly damped collective excitation.

with

$$V_{\vec{k},\vec{k}';s_1 s_2 s_3 s_4} = -\frac{I^2}{4} Re\chi(\vec{k} - \vec{k}', \omega = \varepsilon_{\vec{k}} - \varepsilon_{\vec{k}'}) \, \vec{\sigma}_{s_1 s_4} \cdot \vec{\sigma}_{s_2 s_3} \,. \tag{44}$$

Since the Cooper scattering matrix element is spin dependent, we obtain different values for the spin-singlet and spin-triplet configuration:

$$V_{\vec{k},\vec{k}'}^{s} = \frac{3I^2}{4} Re\chi(\vec{k} - \vec{k}', \omega = \varepsilon_{\vec{k}} - \varepsilon_{\vec{k}'}) \quad \text{for} \quad S = 0 \,,$$

$$V_{\vec{k},\vec{k}'}^{t} = -\frac{I^2}{4} Re\chi(\vec{k} - \vec{k}', \omega = \varepsilon_{\vec{k}} - \varepsilon_{\vec{k}'}) \quad \text{for} \quad S = 1 \,, \tag{45}$$

Obviously this is repulsive for the singlet, but attractive in the triplet channel. Thus odd-parity pairing states are favored with $l = 1, 3, 5, \dots$. Similar to electron-phonon interaction retardation effects play a role. The attraction is obtained roughly within an energy range $\omega < \omega_{0q}$ providing the natural energy cutoff from the maximal paramagnon resonance energy for $q \sim 2k_F$:

$$\varepsilon_c = \frac{8}{\pi I N_0}(1 - I N_0)E_F \tag{46}$$

It is important to notice that $\varepsilon_c \ll E_F$ near the Stoner instability, an effect of the so-called critical slowing down (spin fluctuations become slower). Examining all possibilities we find that the $l = 1$-state is the most favored odd-parity state of this interaction. We choose for the gap function $\Delta_{\vec{k}} = \Delta g_{\vec{k}}$ with

$$g_{\vec{k}}^{\alpha} = Y_{l\alpha}(\hat{k}) = \begin{cases} \dfrac{1}{\sqrt{2}k}(k_x + i k_y) & \alpha = +1 \\[2mm] \dfrac{k_z}{k} & \alpha = 0 \\[2mm] \dfrac{1}{\sqrt{2}k}(k_x - i k_y) & \alpha = -1 \end{cases}, \tag{47}$$

the three $l = 1$ spherical harmonics ($\hat{k} = \vec{k}/k$). Projecting with this $g_{\vec{k}}$ we define

$$\tilde{V}(\xi, \xi') = -\frac{I^2}{4\Omega} \sum_{\vec{k}, \vec{k}'} g_{\vec{k}}^{\alpha} \chi(\vec{k} - \vec{k}', \omega = 0) g_{\vec{k}'}^{\alpha} \delta(\xi - \xi_{\vec{k}}) \delta(\xi' - \xi_{\vec{k}'})$$

$$\approx \begin{cases} V_1 & |\xi|, |\xi'| < \varepsilon_c \\ 0 & \text{otherwise} \end{cases} \tag{48}$$

where

$$V_1 = -\frac{I}{12} \frac{IN_0}{(1 - IN_0)^2} . \tag{49}$$

Since we are now left with a BCS-like formulation, it is straightforward to derive the critical temperature is

$$k_B T_c = \varepsilon_c e^{-1/\lambda_s} , \tag{50}$$

with

$$\lambda_s = N_0 V_1 = \frac{1}{12} \left(\frac{IN_0}{1 - IN_0} \right)^2 . \tag{51}$$

Assuming the Coulomb repulsion as a contact interaction we do not have a correction in the exponent in the case of $l > 0$. It is important note here that while the Coulomb and electron-phonon interaction has usually the range of the Thomas-Fermi screening length, the paramagnon mediated interaction is longer ranged with the magnetic correlation length ξ as the length scale. The correlation length is defined as

$$\xi_s^2 \sim \int d^3 r r^2 \langle \vec{S}(\vec{r}) \cdot \vec{S}(0) \rangle \tag{52}$$

Since we have an Ornstein-Zernike form for the static susceptibility, we can write for the static susceptibility

$$\chi(\vec{q}) \propto \frac{1}{1 + \xi_s^2 \vec{q}^2} \tag{53}$$

which compared with (42, 41) leads to

$$\xi_s^2 = \frac{1}{12 k_F^2} \frac{IN_0}{1 - IN_0} . \tag{54}$$

The correlation length diverges at the Stoner instability point favoring higher angular momentum pairing. Eventually the $\vec{q}$-dependence of the pairing interaction apart from the spin dependence, is decisive for the choice of the pairing state.

Superconducivitity in the vicinity of magnetic quantum critical point

Based on these considerations we construct now a phase diagram for the spin triplet state near a quantum phase transition to ferromagnetic order. Although we have done
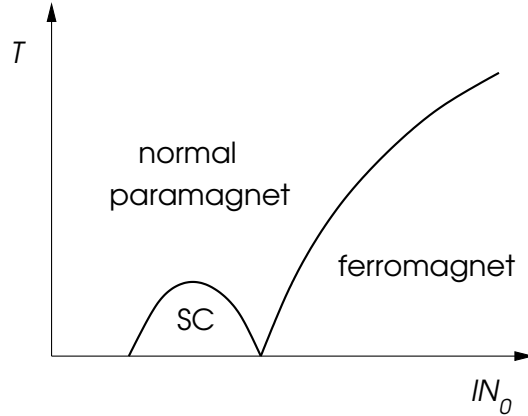
FIGURE 6. Schematic phase diagram of the superconducting phase (SC) near the ferromagnetic quantum critical point.

some rough approximations, a qualitative view is still illustrative. The Stoner-criterion $1 - IN_0 = 0$ defines the zero-temperature transition point so that we may take IN_0 as the controlling parameter which might be changed in real material, for example, by applying pressure. For $IN_0 > 1$ the metal has a finite Curie-temperature $T_C \propto (IN_0 - 1)^{1/2}$ (in the standard mean field approach).

In the paramagnetic region there are two basic trends determining the superconducting transition temperature T_c. The coupling constant V_1 diverges while the cutoff energy ε_c vanishes at the quantum critical point. This gives rise to the non-monotonous behavior of T_c which passes a maximum with increasing IN_0 and vanishing at the quantum critical point. While the exact behavior is modified by the renormalization of the quasiparticle weight close to the quantum critical point which has been ignored here, the fact that T_c goes through a maximum and disappears right at the quantum critical point. [34, 35].

We do not touch here the question whether superconductivity would also appear inside the ferromagnetic phase within our theory. It has been shown by Fay and Appel that spin polarized pairing states (so-called non-unitary states) are possible [34]. This kind of finding is very interesting in the context of the earlier mentioned superconductivity in UGe$_2$, URhGe and ZrZn$_2$ which are superconducting inside the ferromagnetic region. In these materials there is no superconductivity in the paramagnetic region which is difficult to understand within our discussion. So far there is no system known where the phase diagram of Fig.6 would apply. The situation in the very recently discovered superconducting phase at the ferromagnetic quantum critical point in UIr is not clear yet [36] In particular, this material has the complication that it has no inversion center. On the other hand, there are many examples for superconductivity in connection with quantum phase transitions to antiferromagnetic order as also discussed in the introduction.

GENERALIZED BCS-THEORY

After having discussed the motivation to consider superconductivity due to Cooper pairs of general structure, we would like to introduce here the generalize formulation of the

BCS theory and discuss some of the basic properties of unconventional superconductors [37]. For this purpose we do not invoke any particular pairing mechanism nor assume a special symmetry of the metal. Nevertheless, in some cases complete rotation symmetry will be imposed to do concrete calculations.

The Gap Function

The generalized BCS theory relies on an extended form of the microscopic interaction where we consider again only the scattering of electron pairs with vanishing total momentum which is attractive. The correspondig Hamiltonian can be written as

$$\mathscr{H} = \sum_{\vec{k},s} \xi_{\vec{k}} c_{\vec{k}s}^{\dagger} c_{\vec{k}s} + \frac{1}{2} \sum_{\vec{k},\vec{k}'} \sum_{s_1,s_2,s_3,s_4} V_{\vec{k},\vec{k}';s_1 s_2 s_3 s_4} c_{\vec{k}s_1}^{\dagger} c_{-\vec{k}s_2}^{\dagger} c_{-\vec{k}'s_3} c_{\vec{k}'s_4} \tag{55}$$

with pair scattering matrix elements

$$V_{\vec{k},\vec{k}';s_1 s_2 s_3 s_4} = \langle -\vec{k}, s_1; \vec{k}, s_2 | \widehat{V} | -\vec{k}', s_3; \vec{k}', s_4 \rangle . \tag{56}$$

Due to Fermionic anticommutation rules the following relations must hold

$$V_{\vec{k},\vec{k}';s_1 s_2 s_3 s_4} = -V_{-\vec{k},\vec{k}';s_2 s_1 s_3 s_4} = -V_{\vec{k},-\vec{k}';s_1 s_2 s_4 s_3} = V_{-\vec{k},-\vec{k}';s_2 s_1 s_4 s_3} . \tag{57}$$

We consider a weak-coupling approach with an interaction attractive in an energy range defined by a cutoff ε_c, i.e. the scattering matrix elements are non-zero for $-\varepsilon_c < \xi_{\vec{k}}, \xi_{\vec{k}'} < \varepsilon_c$ ε_c and $\varepsilon_c \ll E_F$.

Analogous to the simple case we introduce an off-diagonal mean-field

$$b_{\vec{k},ss'} = \langle c_{-\vec{k}s} c_{\vec{k}s'} \rangle \tag{58}$$

which leads to the mean field Hamiltonian

$$\mathscr{H}' = \sum_{\vec{k},s} \xi_{\vec{k}} c_{\vec{k}s}^{\dagger} c_{\vec{k}s} - \frac{1}{2} \sum_{\vec{k},s_1,s_2} \left[\Delta_{\vec{k},s_1 s_2} c_{\vec{k}s_1}^{\dagger} c_{-\vec{k}s_2}^{\dagger} + \Delta_{\vec{k},s_1 s_2}^{*} c_{\vec{k}s_1} c_{-\vec{k}s_2} \right] + K + \text{small terms} ,$$

$$\tag{59}$$

where

$$K = -\frac{1}{2} \sum_{\vec{k},\vec{k}'} \sum_{s_1,s_2,s_3,s_4} V_{\vec{k},\vec{k}';s_1 s_2 s_3 s_4} \langle c_{\vec{k}s_1}^{\dagger} c_{-\vec{k}s_2}^{\dagger} \rangle \langle c_{-\vec{k}'s_3} c_{\vec{k}'s_4} \rangle . \tag{60}$$

The generalized gap $\Delta_{\vec{k};ss'}$ are defined as a function of $\vec{k}$ and the spins (s,s') by the self-consistent equations

$$\Delta_{\vec{k},ss'} = -\sum_{\vec{k}',s_3 s_4} V_{\vec{k},\vec{k}';ss's_3 s_4} b_{\vec{k},s_3 s_4} ,$$

$$\Delta_{\vec{k},ss'}^{*} = -\sum_{\vec{k}'s_1 s_2} V_{\vec{k}',\vec{k};s_1 s_2 s' s} b_{\vec{k},s_2 s_3}^{*} . \tag{61}$$

The gap function is now a complex 2×2 complex matrix in spin space

$$\widehat{\Delta}_{\vec{k}} = \begin{pmatrix} \Delta_{\vec{k},\uparrow\uparrow} & \Delta_{\vec{k},\uparrow\downarrow} \\ \Delta_{\vec{k},\downarrow\uparrow} & \Delta_{\vec{k},\downarrow\downarrow} \end{pmatrix}. \tag{62}$$

The structure of the gap function is related to the wave function of the Cooper pairs, $b_{\vec{k},s_1 s_2}$. In order to get a deeper insight into the symmetry properties of the gap function, we separate $b_{\vec{k},s_1,s_2}$ into an orbital part and a spin part

$$b_{\vec{k},s_1 s_2} = \phi(\vec{k})\chi_{s_1 s_2} , \tag{63}$$

The parity of the orbital part and the spin configuration are linked due to the antisymmetry condition of the many-Fermion wave functions as mentioned above:

Even Parity: $\quad \phi(\vec{k}) = \phi(-\vec{k}) \quad \Leftrightarrow \quad \chi_{s_1 s_2} = \frac{1}{\sqrt{2}}(|\uparrow\downarrow\rangle - |\downarrow\uparrow\rangle) \qquad$ spin singlet

Odd Parity: $\quad \phi(\vec{k}) = -\phi(-\vec{k}) \quad \Leftrightarrow \quad \chi_{s_1 s_2} = \begin{cases} |\uparrow\uparrow\rangle \\ \frac{1}{\sqrt{2}}(|\uparrow\downarrow\rangle + |\downarrow\uparrow\rangle) \quad \text{spin triplet} \\ |\downarrow\downarrow\rangle \end{cases}$

$$\tag{64}$$

Consequently, the gap function obeys the following rules:

$$\Delta_{\vec{k},s_1 s_2} = -\Delta_{-\vec{k},s_2 s_1} = \begin{cases} \Delta_{-\vec{k},s_1 s_2} = -\Delta_{\vec{k},s_2 s_1} & \text{even} \\[2mm] -\Delta_{-\vec{k},s_1 s_2} = \Delta_{\vec{k},s_2 s_1} & \text{odd} \end{cases} \tag{65}$$

or in short notation

$$\widehat{\Delta}_{\vec{k}} = -\widehat{\Delta}^T_{-\vec{k}} \tag{66}$$

Based on these points, we parametrize the form of the 2×2 matrix representing the gap function. For even parity (spin singlet), we only need a scalar function $\psi(\vec{k})$,

$$\widehat{\Delta}_{\vec{k}} = \begin{pmatrix} \Delta_{\vec{k},\uparrow\uparrow} & \Delta_{\vec{k},\uparrow\downarrow} \\ \Delta_{\vec{k},\downarrow\uparrow} & \Delta_{\vec{k},\downarrow\downarrow} \end{pmatrix} = \begin{pmatrix} 0 & \psi(\vec{k}) \\ -\psi(\vec{k}) & 0 \end{pmatrix} = i\hat{\sigma}_y \psi(\vec{k}) . \tag{67}$$

which satisfies $\psi(\vec{k}) = \psi(-\vec{k})$. For the odd parity case, the spin triplet configuration has to be represented by three components which we introduce as the vector function $\vec{d}(\vec{k})$ in the following form

$$\begin{aligned} \widehat{\Delta}_{\vec{k}} &= \begin{pmatrix} \Delta_{\vec{k},\uparrow\uparrow} & \Delta_{\vec{k},\uparrow\downarrow} \\ \Delta_{\vec{k},\downarrow\uparrow} & \Delta_{\vec{k},\downarrow\downarrow} \end{pmatrix} \\[2mm] &= \begin{pmatrix} -d_x(\vec{k}) + id_y(\vec{k}) & d_z(\vec{k}) \\ d_z(\vec{k}) & d_x(\vec{k}) + id_y(\vec{k}) \end{pmatrix} = i\left(\vec{d}(\vec{k}) \cdot \hat{\vec{\sigma}}\right)\hat{\sigma}_y , \end{aligned} \tag{68}$$

with $\vec{d}(\vec{k}) = -\vec{d}(-\vec{k})$. This notation will turn out to be very useful considering rotations in spin space as will see shortly. We find that

$$
\begin{aligned}
\widehat{\Delta}_{\vec{k}}\widehat{\Delta}_{\vec{k}}^{\dagger} &= |\psi(\vec{k})|^2 \hat{\sigma}_0 & \text{spin singlet} \\
\widehat{\Delta}_{\vec{k}}\widehat{\Delta}_{\vec{k}}^{\dagger} &= |\vec{d}|^2 \hat{\sigma}_0 + i(\vec{d} \times \vec{d}^{*}) \cdot \hat{\vec{\sigma}} & \text{spin triplet} .
\end{aligned}
\tag{69}
$$

While for the spin singlet case leads always to $\widehat{\Delta}_{\vec{k}}\widehat{\Delta}_{\vec{k}}^{\dagger} \propto \hat{\sigma}_0$, the unit matrix, in the spin triplet channel also components different from $\hat{\sigma}_0$ is possible. Pairing states with non-zero $\vec{q}(\vec{k}) = i\vec{d}(\vec{k}) \times \vec{d}(\vec{k})^{*}$ are called *non-unitary* and are related to pairing with some intrinsic spin polarization, since $\vec{q}(\vec{k})$ is connected with the spin expectation value $\text{tr}[\widehat{\Delta}_{\vec{k}}\widehat{\Delta}_{\vec{k}}^{\dagger}\hat{\vec{\sigma}}]$ for momentum $\vec{k}$. As will become clear below a necessary condition for $\vec{q} \neq 0$ is broken time reversal symmetry.

Symmetry aspects

Cooper pairs consist of two electrons of opposite momentum ($\Rightarrow$ zero-momentum pairs) which are degenerate in energy. There are certain key symmetries which guarantee the possibility to find such states at the Fermi energy.

For spin singlet pairing the key symmetry is time reversal invariance [38]. Starting with an electronic state with momentum $\vec{k}$ and spin up $\uparrow$, we obtain a proper degenerate partner state by time reversal $\widehat{K}$:

$$
\widehat{K}|\vec{k} \uparrow\rangle = |-\vec{k}, \downarrow\rangle
\tag{70}
$$

such that we have the necessary partner states to form spin singlet Cooper pairs: $|\vec{k} \uparrow\rangle, |-\vec{k} \downarrow\rangle$.

Spin triplet pairing requires in addtion to time reversal the inversion symmetry $\widehat{I}$ to generate the proper partner states [39]. We start from the same state and obtain

$$
\widehat{K}|\vec{k} \uparrow\rangle = |-\vec{k}, \downarrow\rangle , \quad \widehat{I}|\vec{k} \uparrow\rangle = |-\vec{k}, \uparrow\rangle , \quad \widehat{IK}|\vec{k} \uparrow\rangle = |\vec{k}, \downarrow\rangle
\tag{71}
$$

which allows us to form all possible spin triplet configurations.

We want to review the important symmetries and examine their effect on the gap functions. This will be important in the future discussion of the superconducting phases, in particular, in the context of phenomenological description. The symmetries relevant to us are rotations in real and spin space, time reversal, inversion and $U(1)$-gauge symmetry.

Orbital rotation:

$$
g c_{\vec{k},s} = c_{R(g)\vec{k},s} \qquad\qquad g c_{\vec{k},s}^{\dagger} = c_{R(g)\vec{k},s}^{\dagger}
\tag{72}
$$

$$
g\widehat{\Delta}_{\vec{k}} = \widehat{\Delta}_{R(g)\vec{k}}
\tag{73}
$$

where $R(g)$ is the rotation matrix in three dimensiona corresponding the operation of g.
Spin rotation:

$$gc_{\vec{k}s} = \sum_{s'} D_{\mathscr{S}}(g)_{ss'} c_{\vec{k}s'} \qquad \text{and} \qquad gc^{\dagger}_{\vec{k}s} = \sum_{s'} D_{\mathscr{S}}(g)^*_{s's} c^{\dagger}_{\vec{k}s'} \tag{74}$$

$$g\widehat{\Delta}_{\vec{k}} = \hat{D}^{\tau}_{\mathscr{S}}(g)\widehat{\Delta}_{\vec{k}}\hat{D}_{\mathscr{S}}(g). \tag{75}$$

where

$$\hat{D}_{\mathscr{S}}(g) = e^{i\vec{S}\cdot\vec{\phi}} \tag{76}$$

with $\vec{\phi}$ the rotation vector of the operation g. Spin rotation has naturally no influence on a singlet configuration because the total spin is zero. On the other hand, the triplet case corresponds to the usual rotation applied on the $\vec{d}$-vector

$$g\vec{d}(\vec{k}) = \tilde{R}_{\mathscr{S}}(g)\vec{d}(\vec{k}) \tag{77}$$

with $\tilde{R}_{\mathscr{S}}(g)$ the three-dimensional representation of the corresponding rotation. One would note that the gap function is then represented in spin space as a spin pointing along the $\vec{d}$-vector

$$d_x\{-|\uparrow\uparrow\rangle + |\downarrow\downarrow\rangle\} - id_y\{|\uparrow\uparrow\rangle + |\downarrow\downarrow\rangle\} + d_z\{|\uparrow\downarrow\rangle + |\downarrow\uparrow\rangle\} \tag{78}$$

This rather simple behavior under spin rotation is the benefit of the above parametrization of the gap function.

Time-reversal symmetry $\widehat{K}$

$$\widehat{K}c_{\vec{k}s} = \sum_{s'} (-i\hat{\sigma}^y)_{ss'} c^{\dagger}_{-\vec{k},s'} \tag{79}$$

$$\widehat{K}\widehat{\Delta}_{\vec{k}} = \hat{\sigma}^y \widehat{\Delta}^*_{\vec{k}} \hat{\sigma}^y \tag{80}$$

We used $\widehat{K} = -i\hat{\sigma}^y\widehat{C}$ with $\widehat{C}$ the operator of complex-conjugation. Note that $\widehat{K}$ is antilinear.

Inversion symmetry $\hat{I}$

$$\hat{I}c_{\vec{k},s} = c_{-\vec{k},s} \qquad \Rightarrow \qquad \hat{I}\widehat{\Delta}_{\vec{k}} = \widehat{\Delta}_{-\vec{k}} = \begin{cases} +\widehat{\Delta}_{\vec{k}} & \text{spin-singlet} \\ \\ -\widehat{\Delta}_{\vec{k}} & \text{spin-triplet} \end{cases} \tag{81}$$

U(1)-gauge symmetry:

$$\widehat{\Phi}c_{\vec{k}s} = e^{i\phi/2} \qquad \Rightarrow \qquad \widehat{\Phi}\widehat{\Delta}_{\vec{k}} = \widehat{\Delta}_{\vec{k}}e^{i\phi} \tag{82}$$

Results for the scalar function ψ and the vector function $\vec{d}$ are summarized below.

Operation	Singlet	Triplet
Fermion exchange	$\psi(\vec{k}) = \psi(-\vec{k})$	$\vec{d}(\vec{k}) = -\vec{d}(-\vec{k})$
Orbital rotation	$g\psi(\vec{k}) = \psi(R(g)\vec{k})$	$g\vec{d}(\vec{k}) = \vec{d}(R(g)\vec{k})$
Spin rotation	$g\psi(\vec{k}) = \psi(\vec{k})$	$g\vec{d}(\vec{k}) = \tilde{R}_{\mathscr{S}}(g)\vec{d}(\vec{k})$
Time-reversal	$\widehat{K}\psi(\vec{k}) = \psi^*(-\vec{k})$	$\widehat{K}\vec{d}(\vec{k}) = -\vec{d}^*(-\vec{k})$
$U(1)$-gauge	$\widehat{\Phi}\psi(\vec{k}) = e^{i\phi}\psi(\vec{k})$	$\widehat{\Phi}\vec{d}(\vec{k}) = e^{i\phi}\vec{d}(\vec{k})$

Examples of Gap functions

We introduce here several typical forms of gap functions on a spherical Fermi surface, which will later used as examples to discuss some properties of the unconventional superconducting phases. In particular, we are interested in the quasiparticle gap which is given in the general formulation of the gap function by

$$|\Delta_{\vec{k}}|^2 = \frac{1}{2}tr\left(\widehat{\Delta}_{\vec{k}}^{\dagger}\widehat{\Delta}_{\vec{k}}\right) = \begin{cases} |\psi(\vec{k})|^2 & \text{spin singlet} \\ \\ |\vec{d}(\vec{k})|^2 & \text{spin triplet} \end{cases} \tag{83}$$

and is essential for the discussion of the elementary low-energy excitations in the superconducting phase. Note that for non-unitary states

$$|\Delta_{\vec{k}\pm}|^2 = |\vec{d}(\vec{k})|^2 \pm |\vec{d}^*(\vec{k}) \times \vec{d}(\vec{k})| \tag{84}$$

with two different gaps.

Isotropic pairing: There are conventional and unconventional pairing states which have isotropic properties. The conventional spin singlet pairing in the $l = 0$ (*s*-wave) channel is given by

$$\psi(\vec{k}) = \Delta_0 , \tag{85}$$

which gives obviously rise to an isotropic quasiparticle gap $|\Delta_{\vec{k}}| = |\Delta_0|$.

Among the unconnventional states there is one spin triplet state, the Balian-Werthamer-state which also has an isotropic gap [2]. Its $\vec{d}$-vector is given by

$$\vec{d}(\vec{k}) = \frac{\Delta_0}{k_F}(\hat{x}k_x + \hat{y}k_y + \hat{z}k_z) = \frac{\Delta_0}{k_F}\begin{pmatrix} k_x \\ k_y \\ k_z \end{pmatrix} , \tag{86}$$
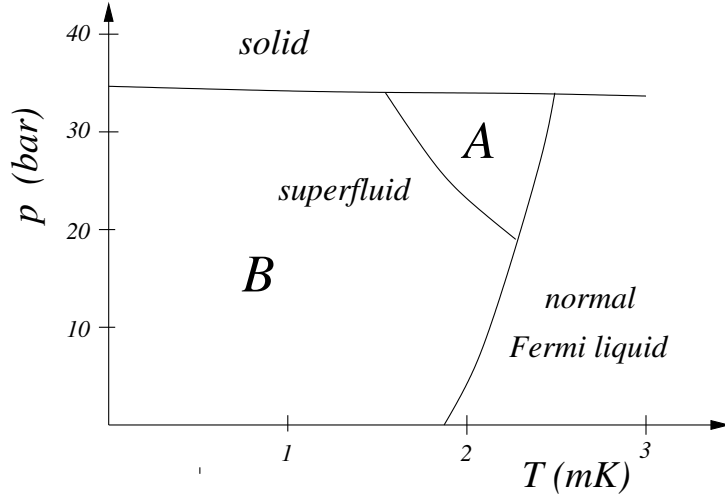
FIGURE 7. Phase diagram of ^{3}He.

so that the $\vec{d}$ is pointing isotropically outwards on the Fermi surface. The gap is then

$$|\Delta_{\vec{k}}|^2 = \frac{1}{2}\text{tr}(\widehat{\Delta}^\dagger_{\vec{k}}\widehat{\Delta}_{\vec{k}}) = |\vec{d}(\vec{k})|^2 = |\Delta_0|^2\frac{|\vec{k}|^2}{k_F^2} = |\Delta_0|^2 , \tag{87}$$

While the quasiparticle gap is the same for both states, we will see below that they are different in their spin susceptibility. Note that the Balian-Werthamer state corresponds to the *B*-phase of superfluid ^{3}He [3, 5].

Anisotropic spin-singlet state: We consider here one example for $l = 2$, a so-called *d*-wave pairing state:

$$\psi(\vec{k}) = \frac{\Delta_0}{k_F}(k_x^2 - k_y^2) \tag{88}$$

It has line nodes for $(k_x, k_y) \parallel (\pm 1, \pm 1)$ and represents the pairing realized in high-temperature superconductors. Other good candidates for related forms of "*d*-wave" pairing are found among the heavy fermions superconductors, such as UPd$_2$Al$_3$, CeIn$_3$, CePd$_2$Si$_2$, etc. which are associated with quantum phase transitions to antiferromagnetic order.

Anisotropic spin-triplet state: One of the most interesting anisotropic spin triplet pairing ($l = 1$ or *p*-wave) states is

$$\vec{d}(\vec{k}) = \frac{\Delta_0}{k_F}\hat{z}(k_x \pm ik_y) , \tag{89}$$

with

$$|\Delta_{\vec{k}}|^2 = |\Delta_0|^2\frac{k_x^2 + k_y^2}{k_F^2} . \tag{90}$$

This gap has point nodes for $\vec{k} \parallel (0, 0, \pm 1)$. Interestingly this this state has a finite orbital angular momentum along the z axis, $L_z = \pm 1$, so that it is sometimes called chiral *p*-wave

state or ABM-phase (Anderson Brinkmann Morel) [1, 40]. This type of Cooper pairing is realized in ^{3}He under pressure as the so-called *A-Phase* [3, 5] and in the quasi-two dimensional metal Sr_2RuO_4 [23].

Nonunitary state: All previous examples have been so-called unitary states, $(\widehat{\Delta}_{\vec{k}}^\dagger \widehat{\Delta}_{\vec{k}} \propto \sigma^0)$. A well-known example of a non-unitary state is

$$\vec{d}(\vec{k}) = \frac{\Delta_0}{k_F}(\hat{x} - i\hat{y})k_z \qquad \Rightarrow \qquad \widehat{\Delta}_{\vec{k}} = \begin{pmatrix} -k_z & 0 \\ 0 & 0 \end{pmatrix}, \qquad (91)$$

which corresponds to the A_1-*Phase* of ^{3}He. This state shows pairing only in one of the two spin state $(|\uparrow\uparrow\rangle$, and not in the state $|\downarrow\downarrow\rangle)$. We see that

$$i\vec{d}(\vec{k})^* \times \vec{d}(\vec{k}) = \hat{z}\frac{|\Delta_0|^2 k_z^2}{k_F^2} \qquad (92)$$

gives the spin expectation value for the Cooper pair. This state leaves half of all electrons unpaired and is hard to stabilize due to reduced condensation energy. In ^{3}He it appears only in magnetic field which provides a bias for different spin directions. A similar bias appears of course also in ferromagnetic metals. Thus the superconducting phases in UGe_2, URhGe and $ZnZr_2$ are most likely non-unitary.

Bogolyubov Quasiparticles and Self-Consistent Equations

We can diagonalize the mean-field Hamiltonian (59) by means of Bogolyubov transformation. It is convenient to rewrite (59) in the following form

$$\mathcal{H} = \sum_{\vec{k}} \mathbf{C}_{\vec{k}}^\dagger \widehat{\mathscr{E}}_{\vec{k}} \mathbf{C}_{\vec{k}} + K, \qquad (93)$$

with

$$\mathbf{C}_{\vec{k}} = \begin{pmatrix} c_{\vec{k}\uparrow} \\ c_{\vec{k}\downarrow} \\ c_{-\vec{k}\uparrow}^\dagger \\ c_{-\vec{k}\downarrow}^\dagger \end{pmatrix} \qquad \text{and} \qquad \widehat{\mathscr{E}}_{\vec{k}} = \frac{1}{2}\begin{pmatrix} \xi_{\vec{k}}\widehat{\sigma}_0 & \widehat{\Delta}_{\vec{k}} \\ \widehat{\Delta}_{\vec{k}}^\dagger & -\xi_{\vec{k}}\widehat{\sigma}_0 \end{pmatrix}. \qquad (94)$$

We are now searching the diagonalized form

$$\mathcal{H} = \sum_{\vec{k}} \mathbf{A}_{\vec{k}}^\dagger \widehat{E}_{\vec{k}} \mathbf{A}_{\vec{k}} + K \qquad (95)$$

where

$$\mathbf{A}_{\vec{k}} = \begin{pmatrix} a_{\vec{k}\uparrow} \\ a_{\vec{k}\downarrow} \\ a_{-\vec{k}\uparrow}^\dagger \\ a_{-\vec{k}\downarrow}^\dagger \end{pmatrix} \qquad \text{and} \qquad \widehat{E}_{\vec{k}} = \begin{pmatrix} E_{\vec{k}+} & 0 & 0 & 0 \\ 0 & E_{\vec{k}-} & 0 & 0 \\ 0 & 0 & -E_{-\vec{k}+} & 0 \\ 0 & 0 & 0 & -E_{\vec{k}-} \end{pmatrix}. \qquad (96)$$

The Bogolyubov transformation is given by the unitary matrix $\widehat{U}_{\vec{k}}$ with

$$\widehat{U}_{\vec{k}} = \begin{pmatrix} \widehat{u}_{\vec{k}} & \widehat{v}_{\vec{k}} \\ \widehat{v}^*_{-\vec{k}} & \widehat{u}^*_{-\vec{k}} \end{pmatrix} \qquad \Rightarrow \qquad \mathbf{C}_{\vec{k}} = \widehat{U}_{\vec{k}} \mathbf{A}_{\vec{k}} \quad \text{and} \quad \widehat{E}_{\vec{k}} = \widehat{U}^\dagger_{\vec{k}} \widehat{\mathscr{E}}_{\vec{k}} \widehat{U}_{\vec{k}} \qquad (97)$$

and $\widehat{U}_{\vec{k}} \widehat{U}^\dagger_{\vec{k}} = \widehat{U}^\dagger_{\vec{k}} \widehat{U}_{\vec{k}} = \widehat{1}$.

We restrict ourselves to the case of unitary pairing. This ensures that $E_{\vec{k}} = E_{\vec{k}+} = E_{\vec{k}-}$. The solution of the eigenvalue problem leads to $\widehat{u}_{\vec{k}}$ and $\widehat{v}_{\vec{k}}$

$$\widehat{u}_{\vec{k}} = \frac{(E_{\vec{k}} + \xi_{\vec{k}})\widehat{\sigma}_0}{\sqrt{2E_{\vec{k}}(E_{\vec{k}} + \xi_{\vec{k}})}} \qquad \text{and} \qquad \widehat{v}_{\vec{k}} = \frac{-\widehat{\Delta}_{\vec{k}}}{\sqrt{2E_{\vec{k}}(E_{\vec{k}} + \xi_{\vec{k}})}} \qquad (98)$$

and the energy

$$E_{\vec{k}} = \sqrt{\xi_{\vec{k}}^2 + |\Delta_{\vec{k}}|^2} \qquad \text{with} \qquad |\Delta_{\vec{k}}|^2 = \frac{1}{2}\text{tr}\left(\widehat{\Delta}^\dagger_{\vec{k}} \widehat{\Delta}_{\vec{k}}\right). \qquad (99)$$

With the new quasiparticle operators (61) we can express the self-consistence or gap equation using $\langle a^\dagger_{\vec{k}s} a_{\vec{k}'s'} \rangle = \delta_{\vec{k}\vec{k}'} \delta_{ss'} f(E_{\vec{k}})$ where $f(E) = 1/(\exp(E/k_BT)+1)$ is the Fermi distribution function:

$$\Delta_{\vec{k},s_1s_2} = -\sum_{\vec{k}',s_3s_4} V_{\vec{k},\vec{k}';s_1s_2s_3s_4} \left\{ \sum_{s'} v_{\vec{k}s_4s'} u_{\vec{k}s's_3} \langle a_{-\vec{k}s'} a^\dagger_{\vec{k}s'} \rangle - u_{\vec{k}s_4s'} v_{\vec{k}s's_3} \langle a^\dagger_{\vec{k}s'} a_{\vec{k}s'} \rangle \right\}$$

$$= -\sum_{\vec{k}',s_3s_4} V_{\vec{k},\vec{k}';s_1s_2s_3s_4} \frac{\Delta_{\vec{k}',s_4s_3}}{2E_{\vec{k}}} \tanh\left(\frac{E_{\vec{k}}}{2k_BT}\right)$$

$$(100)$$

We introduce now a newly parametrized pairing interaction term in order to obtain a simpler form of the self-consistence equation,

$$V_{\vec{k},\vec{k}';s_1s_2s_3s_4} = J^0_{\vec{k},\vec{k}'} \widehat{\sigma}^0_{s_1s_4} \widehat{\sigma}^0_{s_2s_3} + J_{\vec{k},\vec{k}'} \widehat{\vec{\sigma}}_{s_1s_4} \cdot \widehat{\vec{\sigma}}_{s_2s_3}, \qquad (101)$$

consisting of a spin independent or density-density term and spin-spin exchange coupling. In the following we assume that these interactions are only non-zero in a certain range around the Fermi energy with a cutoff energy ε_c. For spin singlet pairing the gap equation can be expressed for $\psi(\vec{k})$,

$$\psi(\vec{k}) = -\sum_{\vec{k}'} \underbrace{(J^0_{\vec{k},\vec{k}'} - 3J_{\vec{k},\vec{k}'})}_{= v^s_{\vec{k},\vec{k}'}} \frac{\psi(\vec{k}')}{2E_{\vec{k}'}} \tanh\left(\frac{E_{\vec{k}'}}{2k_BT}\right) \qquad (102)$$

and $|\Delta_{\vec{k}}|^2 = |\psi(\vec{k})|^2$. For spin triplet channel, the gap equation takes the form

$$\vec{d}(\vec{k}) = -\sum_{\vec{k}'} \underbrace{(J^0_{\vec{k},\vec{k}'} + J_{\vec{k},\vec{k}'})}_{= v^t_{\vec{k},\vec{k}'}} \frac{\vec{d}(\vec{k}')}{2E_{\vec{k}'}} \tanh\left(\frac{E_{\vec{k}'}}{2k_B T}\right) \tag{103}$$

with $|\Delta_{\vec{k}}|^2 = |\vec{d}(\vec{k})|^2$.

Critical tempeature and gap magnitude at $T = 0$

The linearized gap equation can now be used to determine the critical temperature. We consider first the spin singlet case

$$\begin{aligned}\psi(\vec{k}) &= -\sum_{\vec{k}'} v^s_{\vec{k},\vec{k}'} \frac{\psi(\vec{k}')}{2\xi_{\vec{k}'}} \tanh\left(\frac{\xi_{\vec{k}'}}{2k_B T}\right) \\ &= -N_0 \langle v^s_{\vec{k},\vec{k}'} \psi(\vec{k}')\rangle_{\vec{k}',FS} \underbrace{\int_0^{\varepsilon_c} d\xi \frac{1}{\xi} \tanh\left(\frac{\xi}{2k_B T}\right)}_{= \ln(1.13\varepsilon_c/k_B T)}\end{aligned} \tag{104}$$

where $\langle \ldots \rangle_{\vec{k},FS}$ denotes the angular average over the Fermi surface. This equation can be expressed as a eigenvalue problem

$$-\lambda\,\psi(\vec{k}) = -N_0 \langle v^s_{\vec{k},\vec{k}'} \psi(\vec{k}')\rangle_{\vec{k}',FS}\,, \tag{105}$$

leading to

$$k_B T_c = 1.14\varepsilon_c e^{-1/\lambda}\,. \tag{106}$$

Here λ is a dimensionless and positive parameter. The superconducting instability corresponds to the highest eigenvalue (highest T_c) of (105) which determines also the structure of the Cooper pairs.

The spin-triplet case has an analogous gap equation which for the evaluation of T_c takes the form

$$-\lambda\,\vec{d}(\vec{k}) = -N_0 \langle v^t_{\vec{k},\vec{k}'} \vec{d}(\vec{k}')\rangle_{\vec{k}',FS} \tag{107}$$

and the same type of solutions. Naturally the solution of the instability problem is specific to the pairing interaction.

We now turn to the zero-temperature limit and determine the gap for the case of spin singlet pairing. We introduce Δ_m as the maximal gap and write $\psi(\vec{k}) = \Delta_m \tilde{g}_{\vec{k}}$ with $|\tilde{g}_{\vec{k}}| \leq 1$. The gap at $T = 0$ is obtained from the equation

$$\Delta_m \tilde{g}_{\vec{k}} = -N_0 \left\langle v^s_{\vec{k},\vec{k}'} \Delta_m \tilde{g}_{\vec{k}'} \int_0^{\varepsilon_c} d\xi \frac{1}{\sqrt{\xi^2 + |\Delta_m \tilde{g}_{\vec{k}'}|^2}} \right\rangle_{\vec{k}',FS}\,. \tag{108}$$

Multiplying both sides with $\tilde{g}^*_{\vec{k}}$ and averaging $\vec{k}$ over the Fermi surface, using (105) and integrating over ξ, we obtain eventually

$$1 = -\lambda \left\langle |\tilde{g}_{\vec{k}}|^2 \ln\left(\frac{2\varepsilon_c}{|\Delta_m \tilde{g}_{\vec{k}}|}\right) \right\rangle_{\vec{k}',FS} = -\lambda \, \ln\left(\frac{2\varepsilon_c}{\Delta_m}\right) \left\{ 1 - \langle |\tilde{g}_{\vec{k}'}|^2 \ln(|\tilde{g}_{\vec{k}'}|) \rangle_{\vec{k}',FS} \right\} . \tag{109}$$

From this we get the ratio of the maximal gap and T_c to be

$$\frac{\Delta_m}{k_B T_c} = 1.76 \exp\left(-\langle |\tilde{g}_{\vec{k}'}|^2 \ln(|\tilde{g}_{\vec{k}'}|) \rangle_{\vec{k}',FS} \right) \geq 1.76 , \tag{110}$$

While this ratio is universal for the isotropic Fermi surface in the case $\tilde{g}_{\vec{k}} = 1$, we see that it in general depends on the gap anisotropy. Like in conventional superconductors, in this ratio the cutoff energy has been eliminated, such that we can express the gap magnitude by T_c, i.e. we are dealing with the weak-coupling limit.

Condensation energy at $T = 0$

We now compute the condensation energy at $T = 0$ within the weak coupling approach. Starting from Hamiltonian (59), we obtain in the Bogolyubov transformed formulation

$$\mathcal{H}' = \frac{1}{2} \sum_{\vec{k},s} E_{\vec{k}} \left(a^\dagger_{\vec{k},s} a_{\vec{k},s} - a_{-\vec{k},s} a^\dagger_{-\vec{k},s} \right) + K . \tag{111}$$

with

$$K = \frac{1}{2} \sum_{\vec{k},s_1,s_2} \frac{\Delta^*_{\vec{k},s_1 s_2} \Delta_{\vec{k},s_2 s_1}}{2 E_{\vec{k}}} \tanh\left(\frac{E_{\vec{k}}}{2 k_B T}\right) . \tag{112}$$

Then, the condensation energy at $T = 0$ is given by

$$\begin{aligned} E_{cond} &= \langle \mathcal{H}' \rangle_\Delta - \langle \mathcal{H}' \rangle_{\Delta=0} = \frac{1}{2} \sum_{\vec{k},s} (\xi_{\vec{k}} - E_{\vec{k}}) + \frac{1}{2} \sum_{\vec{k},s_1,s_2} \frac{\Delta^*_{\vec{k},s_1 s_2} \Delta_{\vec{k},s_2 s_1}}{2 E_{\vec{k}}} \\ &= 2 N_0 \int_0^{\varepsilon_c} d\xi \, (\xi - \langle \sqrt{\xi^2 + |\Delta_{\vec{k}}|^2} \rangle_{\vec{k},FS}) + \left\langle |\Delta_{\vec{k}}|^2 \int_0^{\varepsilon_c} d\xi \, \frac{1}{\sqrt{\xi^2 + |\Delta_{\vec{k}}|^2}} \right\rangle_{\vec{k},FS} \\ &\approx -\frac{N_0}{2} \langle |\Delta_{\vec{k}}|^2 \rangle_{\vec{k},FS} = -\frac{N_0}{2} |\Delta_m|^2 \langle |\tilde{g}_{\vec{k}}|^2 \rangle_{\vec{k},FS} , \end{aligned} \tag{113}$$

under the assumptions that $|\Delta_{\vec{k}}| \ll \varepsilon_c$ and for simplicity, that N_0 is isotropic. (For an anisotropic Fermi density $N_0(\hat{k})$, we can extend this expression $E_{cond} = -(1/2) \langle N_0(\hat{k}) |\Delta_{\vec{k}}|^2 \rangle_{\vec{k},FS}$.) Using now (110) we can compare different condensation

energies

$$E_{cond} = -\frac{N_0}{2} \langle |\Delta_m \tilde{g}_{\vec{k}}|^2 \rangle_{\vec{k},FS}$$

$$= -\frac{1}{2} N_0 \, (1.76 \, k_B T_c)^2 \, \langle |\tilde{g}_{\vec{k}}|^2 \rangle_{\vec{k},FS} \exp(-\langle |\tilde{g}_{\vec{k}}|^2 \ln |\tilde{g}_{\vec{k}}| \rangle_{\vec{k},FS})$$

(114)

It is now obvious that an isotropic gap under these conditions gives the largest gain in condensation energy and explains why among the spin triplet state the BW-state is most stable, if no bias in the pairing interaction (spin-orbit coupling and strong coupling effects) favors a different state.

Specific heat discontinuity at T_c

A characteristic feature of the second order normal-superconductor phase transition is the jump in specific heat at T_c which is related to the release of entropy through the opening of the gap at the Fermi surface. First, we write the specific heat starting from the general form for the entropy:

$$S = -\frac{2k_B}{\Omega} \sum_{\vec{k}} \left\{ f(E_{\vec{k}}) \ln(f(E_{\vec{k}})) + (1 - f(E_{\vec{k}})) \ln(1 - f(E_{\vec{k}})) \right\}$$

(115)

leading to

$$C = T\frac{dS}{dT} = -\frac{2}{\Omega} \sum_{\vec{k}} E_{\vec{k}} \frac{df(E_{\vec{k}})}{dT}$$

$$= -\frac{2N_0}{T} \int_{-\infty}^{+\infty} d\xi \, \left\langle \frac{\partial f(E_{\vec{k}})}{\partial E_{\vec{k}}} \left\{ E_{\vec{k}}^2 - \frac{T}{2} \frac{\partial |\Delta_m(T)|^2}{\partial T} |\tilde{g}_{\vec{k}}|^2 \right\} \right\rangle_{\vec{k},FS}$$

(116)

The specific heat of the normal state is easily obtained by setting $\Delta_m = 0$,

$$C_n = -\frac{2N_0}{T} \int_{-\infty}^{+\infty} d\xi \, \frac{\partial f(\xi)}{\partial \xi} \, \xi^2 \approx \frac{2\pi^2 k_B^2}{3} N_0 T \, ,$$

(117)

with the standard Sommerfeld T-linear dependence. The jump in specific heat depends on the variation of the gap with temperature. It can be expressed as

$$\frac{\Delta C}{C_n}\bigg|_{T=T_c} = \frac{C - C_n}{C_n}\bigg|_{T=T_c}$$

$$= \frac{3}{2\pi^2 k_B^2 T} \langle |\tilde{g}_{\vec{k}}|^2 \rangle_{\vec{k},FS} \frac{\partial |\Delta_m(T)|^2}{\partial T}\bigg|_{T \to T_{c-}} = 1.43 \frac{\langle |\tilde{g}_{\vec{k}}|^2 \rangle_{\vec{k},FS}^2}{\langle |\tilde{g}_{\vec{k}}|^4 \rangle_{\vec{k},FS}}$$

(118)

This result infers that the specific heat discontinuity is less pronounced in anisotropic gap functions than in the isotropic case. The entropy change is smaller for a given gap size Δ_m in the anisotropic case, since quasiparticle excitations with lower energy are still allowed.

To show the last equality in (118), the temperature dependence of Δ_m has to be determined. For this purpose we return to the gap equation which we want to consider near T_c. Using the definition of λ we have the relation

$$\frac{1}{\lambda} = -\ln\left(\frac{T}{T_c}\right) - \int_0^{\varepsilon_c} d\xi \frac{1}{\xi} \tanh\left(\frac{\xi}{2k_B T}\right) . \tag{119}$$

With this expression of λ for an arbitrary T, we find

$$\langle |\tilde{g}_{\vec{k}}|^2 \rangle_{\vec{k},FS} \ln\left(\frac{T}{T_c}\right) = \int_0^{\varepsilon_c} d\xi \left\langle |\tilde{g}_{\vec{k}}|^2 \frac{1}{E_{\vec{k}}} \tanh\left(\frac{E_{\vec{k}}}{2k_B T}\right) \right\rangle_{\vec{k},FS}$$

$$- \langle |\tilde{g}_{\vec{k}}|^2 \rangle_{\vec{k},FS} \int_0^{\varepsilon_c} d\xi \frac{1}{\xi} \tanh\left(\frac{\xi}{2k_B T}\right) \tag{120}$$

$$= |\Delta_m|^2 b \langle |\tilde{g}_{\vec{k}}|^4 \rangle_{\vec{k},FS}$$

with

$$b = -\int_{-\infty}^{+\infty} d\xi \frac{d}{d\xi^2} \left\{ \frac{\tanh(\xi/2k_B T_c)}{2\xi} \right\} = \frac{7\zeta(3)}{8\pi^2 k_B^2 T_c^2} . \tag{121}$$

Note that $\zeta(3) = \sum_{n=1}^{\infty} n^{-3} \approx 1.2$ is the ζ Riemann function. Thus, in the vicinity of T_c, we have

$$|\Delta_m(T)|^2 \approx \frac{\langle |\tilde{g}_{\vec{k}}|^2 \rangle_{\vec{k},FS}}{b \langle |\tilde{g}_{\vec{k}}|^4 \rangle_{\vec{k},FS}} \left(1 - \frac{T}{T_c}\right) = 9.4 \, (k_B T_c)^2 \frac{\langle |\tilde{g}_{\vec{k}}|^2 \rangle_{\vec{k},FS}}{\langle |\tilde{g}_{\vec{k}}|^4 \rangle_{\vec{k},FS}} \left(1 - \frac{T}{T_c}\right)$$

$$\tag{122}$$

$$= 5.3 \, |\Delta_m(0)|^2 \left(1 - \frac{T}{T_c}\right) \frac{\langle |\tilde{g}_{\vec{k}}|^2 \rangle_{\vec{k},FS}}{\langle |\tilde{g}_{\vec{k}}|^4 \rangle_{\vec{k},FS}} \exp(\langle |\tilde{g}_{\vec{k}}|^2 \ln |\tilde{g}_{\vec{k}}| \rangle_{\vec{k},FS})$$

which inserted into (118) gives the result presented for the specific heat discontinuity. This behavior of $\Delta_m(T)$ is general for the mean-field description of a second-order phase transition.

Low Temperature Properties

The low temperature properties of superconductors are governed by the low-energy quasiparticle excitations. Thus, in the frame of generalized BCS theory, the key quantity which controls the thermodynamics is the quasiparticles density of states. As will become clear immediately, the topology of the nodes in the gap function is very decisive in this respect.

The density of states is defined as

$$N(E) = \frac{2}{\Omega} \sum_{\vec{k}} \delta(E_{\vec{k}} - E) .$$

(123)

where we use the Bogolyubov quasiparticles spectrum

$$E_{\vec{k}} = \sqrt{\xi_{\vec{k}}^2 + |\Delta_{\vec{k}}|^2} .$$

(124)

We decompose the $\vec{k}$-integral into the (radial) energy ξ part and the angular part (average over the Fermi surface):

$$
\begin{aligned}
N(E) &= N_0 \int \frac{d\Omega_{\vec{k}}}{4\pi} \int d\xi\, \delta(\sqrt{\xi^2 + |\Delta_m \tilde{g}_{\vec{k}}|^2} - E) \\
&= N_0 \int \frac{d\Omega_{\vec{k}}}{4\pi} \frac{E}{\sqrt{E^2 - |\Delta_m \tilde{g}_{\vec{k}}|^2}} = N_0 \langle \frac{E}{\sqrt{E^2 - |\Delta_m \tilde{g}_{\vec{k}}|^2}} \rangle_{\vec{k},FS} .
\end{aligned}
$$

(125)

The density of states for an isotropic gap function $\tilde{g}_{\vec{k}} = 1$ is straightforward :

$$
N(E) = N_0 \begin{cases} 0 & |E| < \Delta_m \\[2mm] \dfrac{E}{\sqrt{E^2 - |\Delta_m|^2}} & \Delta_m \le |E| \end{cases}
$$

(126)

No state can be found with energies below Δ_m and a characteristic square-root singularity signals the onset of continuous spectrum above Δ_m. At higher energies the density of states approaches the normal state value, so that the influence of superconductivity is restricted to an energy range of several times the gap.

Turning to anisotropic gap functions we find an important change in the density of states, since "subgap" states appear. First we consider a gap with line nodes. As a simple example we take $\Delta_{\vec{k}} = \Delta_m \cos\theta$ which has a line node in the x-y-plane. We obtain

$$
N(E) = N_0 \frac{E}{\Delta_m} \int_{-1}^{+1} dx\, Re\left(\frac{1}{\sqrt{(E/\Delta_m)^2 - x^2}} \right) = N_0 \frac{E}{\Delta_m} \begin{cases} \dfrac{\pi}{2} & |E| < \Delta_m \\[3mm] \arcsin\left(\dfrac{\Delta_m}{E}\right) & \Delta_m \le |E| \end{cases}
$$

(127)

Indeed a finite density of states is found below the maximal gap, down to zero energy. However, the density of states vanishes in a characteristic way at $E = 0$, In the case of line nodes it is a linear behavior. The singularity at $E = \Delta_m$ is replaced by a cusp. The anisotropy smoothens the singularity found for the isotropic gap.

The second class of node topology are the point nodes. As an example we consider $|\Delta_{\vec{k}}| = \Delta_m \sin\theta$ which has z-axial symmetry with point nodes along z-direction. The
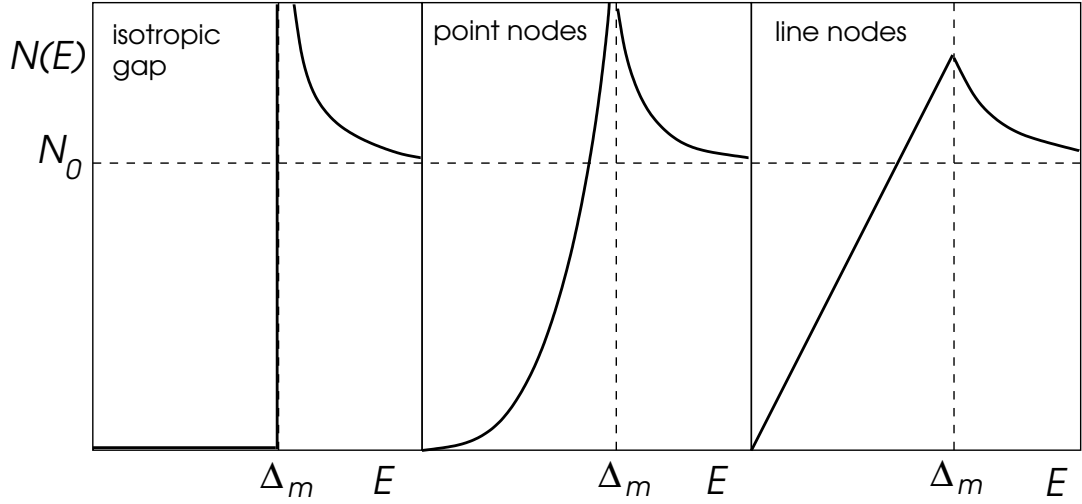
FIGURE 8. Quasiparticle density of states $N(E)$ for the isotropic gap, the gap with point nodes and line nodes.

density of states has then the form

$$N(E) = N_0 \frac{E}{\Delta_m} \int dx Re \left(\frac{1}{\sqrt{x^2 + ((E/\Delta_m)^2 - 1)}} \right) = N_0 \frac{E}{\Delta_m} \ln \left| \frac{1 + \frac{E}{\Delta_m}}{1 - \frac{E}{\Delta_m}} \right| \qquad (128)$$

which also vanishes continuously when $E \to 0$. but here with a quadratic behavior $N(E) \propto E^2$, due the fact that fewer excitations with nearly zero-energy are accessible than in the case of line nodes. At $E = \Delta_m$ $N(E)$ is logarithmically divergent.

We examine now the influence of the node topology on the low-temperture thermodynamics using the example of the specific heat. The isotropic gap leads us to the result of a conventional superconductor. We can safely assume that at very low temperature the gap magnitude has saturated and does not change much anymore. Therefore the behavior of the specific heat is dominated by the quasiparticle density of states.

$$C(T) \quad = \frac{2}{\Omega} \sum_{\vec{k}} E_{\vec{k}} \frac{df(E_{\vec{k}})}{dT} = \int dE \, N(E) \, E \, \frac{df(E)}{dT}$$

$$= \int dE \, N(E) \, \frac{E^2}{k_B T^2} \frac{1}{4 \cosh^2(E/2k_B T)}$$

$$\approx \frac{N_0}{4 k_B T^2} \int_{\Delta_m}^{\infty} dE \, \frac{E^3}{\sqrt{E^2 - \Delta_m^2}} e^{E/k_B T} \approx N_0 k_B \left(\frac{\Delta_m}{k_B T} \right)^2 \sqrt{2\pi k_B T \Delta_m} e^{-\Delta_m/k_B T} \, .$$

$$(129)$$

This exponential behavior is typical of a gaped system (thermally activated), like in a semiconductor. The gap sets a natural energy scale which can be derived from the exponential behavior.

For line or point nodes this thermally activated behavior is covered by the low-lying quasiparticle states. Simple scaling in the integrals show that the powerlaw in the density of states at $E \to 0$, $N(E) \propto E^n$, translates directly to a powerlaw in the temperature dependence:

$$
\begin{aligned}
C(T) &= \int dE \, N(E) \, \frac{E^2}{k_B T^2} \frac{1}{4\cosh^2(E/2k_B T)} \\
&\propto \int dE \, E^n \, \frac{E^2}{k_B T^2} \frac{1}{4\cosh^2(E/2k_B T)} \propto T^{n+1} \ .
\end{aligned}
\tag{130}
$$

The prefactor is determined by the detailed form of the angle dependence and is not necessarily connected with Δ_m in a simple way. It is important to note that this behavior is only really valid for $T \ll T_c$, and is not easily observed in experiments, since various other influences can complicate the behavior. In particular, impurity scattering changes the low-energy density of states strongly.

More generally, thermodynamic quantities are governed by the density of states so that they usually have a powerlaw behavior for nodal superconductors. Here are a few examples of such thermodynamic quantities. A particularly important quantity is the London penetration depth, because here only contributions of the superconducting part are involved, while for most other quantities also the crystal lattice or other contributions are involved. For an arbitrary field direction we find

$$
\lambda(0)^{-2} - \lambda(T)^{-2} = 2 \int dE N(E) \left(-\frac{\partial f(E)}{\partial E} \right) \overset{T \to 0}{\to} const.T^n
\tag{131}
$$

for $N(E) \propto E^n$. Thus the London penetration depth approaches its zero-temperature value also in a powerlaw, if the nodes can be found in the gap. For specific direction where the screening currents are moving parallel to node directions these powerlaws are corrected to higher exponents.

Quantity	Line nodes	Point nodes
spec. heat $C(T)$	T^2	T^3
London penetration length $\lambda(T) - \lambda(0)$	$T \quad (T^3)$	$T^2 \quad (T^4)$
NMR $1/T_1$	T^3	T^5
heat conductivity $\kappa(T)$	T^2	T^3
ultrasound absorption $\alpha(T)$	$T \quad (T^3)$	$T^2 \quad (T^4)$

Items with T^a (T^b) are direction dependent and possess different powerlaws depending on the orientation of fields or polarizations of the ultrasound.

Spin Susceptibility

The spin susceptibility provides an excellent means to distinguish between spin singlet and spin triplet pairing. In spin singlet superconductors the spin susceptibility is suppressed because Cooper pairs have to be broken up in order to polarize the electron spins. Spin triplet superconductors are more easily spin polarized since the Cooper pairs keep an $S = 1$ degree of freedom, at least for certain orientations.

We consider here superconductor were the external magnetic field only couples through Zeeman coupling, i.e. we ignore the orbital coupling which is responsible for Meissner screening. The external magnetic field is chosen to lie along the z-axis:

$$\mathscr{H}_Z = -\mu_B H_z \sum_{\vec{k}} \left\{ c^\dagger_{\vec{k}\uparrow} c_{\vec{k}\uparrow} - c^\dagger_{\vec{k}\downarrow} c_{\vec{k}\downarrow} \right\} \tag{132}$$

We tackle the problem by distinguishing two distinct cases of the gap matrix. First, consider a superconducting state with only off-diagonal gap matrix elements, i. e. $\Delta_{\vec{k}\uparrow\uparrow} = \Delta_{\vec{k}\downarrow\downarrow} = 0$. This includes both spin-singlet pairing ($\Delta_{\vec{k}\uparrow\downarrow} = -\Delta_{\vec{k}\downarrow\uparrow}$) as well as triplet-pairing ($\Delta_{\vec{k}\uparrow\downarrow} = \Delta_{\vec{k}\downarrow\uparrow} \Rightarrow \vec{d} \parallel \hat{z}$ with equal spin-pairing in the x-y-plane). In this case the quasiparticles Hamiltonian becomes diagonal

$$H_{QP} = \sum_{\vec{k}} \left\{ E_{\vec{k}\uparrow} a^\dagger_{\vec{k}\uparrow} a_{\vec{k}\uparrow} + E_{\vec{k}\downarrow} a^\dagger_{\vec{k}\downarrow} a_{\vec{k}\downarrow} \right\} \tag{133}$$

with $E_{\vec{k}s} = \sqrt{\xi_{\vec{k}}^2 + |\Delta_{\vec{k}}|^2} - s\mu_B H_z$ and $s = \uparrow, \downarrow$ or $+, -$. The induced magnetization is

$$M_z = \mu_B \sum_{\vec{k}} \langle c^\dagger_{\vec{k}\uparrow} c_{\vec{k}\uparrow} - c^\dagger_{\vec{k}\downarrow} c_{\vec{k}\downarrow} \rangle \tag{134}$$

with

$$\langle c^\dagger_{\vec{k}s} c_{\vec{k}s} \rangle = \sum_{s'=\pm} \left\{ |u_{\vec{k}ss'}|^2 f(E_{\vec{k}s'}) + |v_{\vec{k}ss'}|^2 \left(1 - f(E_{\vec{k}s'}) \right) \right\} . \tag{135}$$

Note that $|u_{\vec{k}ss'}|^2 \propto \delta_{ss'}$, $|v_{\vec{k}ss'}|^2 \propto |\Delta_{\vec{k}ss'}|^2$ and $|u_{\vec{k}\uparrow\uparrow}|^2 + |v_{\vec{k}\uparrow\downarrow}|^2 = 1$. It follows that

$$M_z = \mu_B \sum_{\vec{k}} \left(f(E_{\vec{k}\uparrow}) - f(E_{\vec{k}\downarrow}) \right) \xrightarrow{H_z \to 0} -2\mu_B^2 H_z \sum_{\vec{k}} \frac{\partial f(E_{\vec{k}})}{\partial E_{\vec{k}}} . \tag{136}$$

Finally the spin susceptibility reads

$$\begin{aligned} \chi_\perp &= \frac{M_z}{H_z} = 2\mu_B^2 N_0 \int \frac{d\Omega_{\vec{k}}}{4\pi} \int d\xi \frac{1}{4k_B T \cosh^2(E_{\vec{k}}/2k_B T)} \\[2mm] &= \chi_P \int \frac{d\Omega_{\vec{k}}}{4\pi} Y(\hat{k}; T) = \chi_P Y(T) \end{aligned} \tag{137}$$
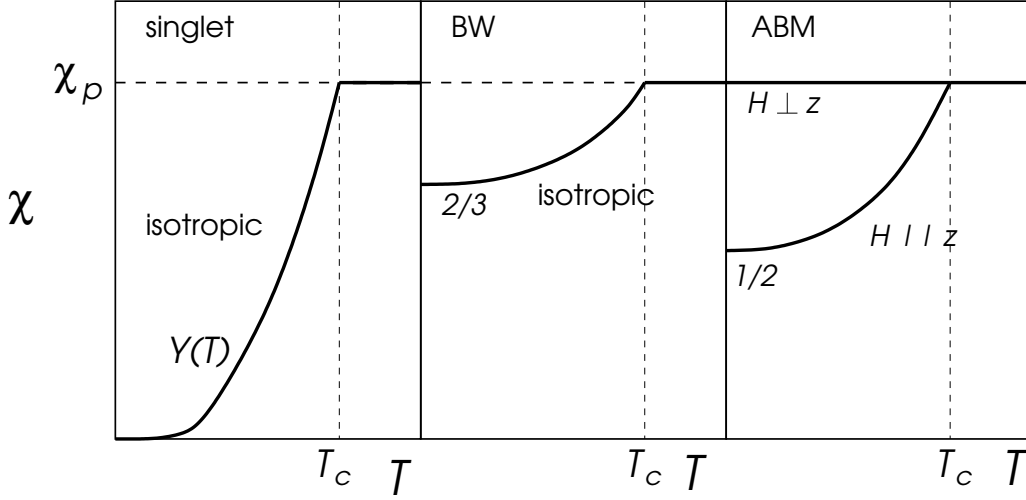
FIGURE 9. Spin susceptibility in the superconducting phase: For spin singlet pairing the susceptibility vanishes at $T = 0$. The precise T-dependence is determined by the gap structure. For the BW-phase the spin susceptibility drops to $2\chi_p/3$ in all field directions. The ABM-phase has an anisotropic susceptibility which remains constant for $\vec{d} \cdot \vec{H} = 0$.

with $\chi_P = 2\mu_B^2 N_0$ the Pauli spin susceptibility of the normal state. The function $Y(\hat{k}; T)$ is the $\vec{k}$-dependent Yosida function, and $Y(T)$ is the angle-average Yosida function. Note that both functions depends on the precise $\vec{k}$-dependence of the quasiparticle spectrum. Above $T = T_c$, it is equal to 1, and below T_c the T-dependence depends on the concrete shape of the gap function. In any case for a finite gap Y goes to zero at $T = 0$.

The resulting spin susceptibility parallel to the field in the superconducting phase is suppressed both for spin-singlet pairing and spin-triplet pairing (Fig.9). This is due to the fact that in the spin-triplet superconducting state the spin orientation is confined in the x-y-plane. We do not consider here that the Zeeman coupling might induce a change of the superconducting phase.

We now move on to the case of the diagonal gap matrix $\Delta_{\vec{k}\uparrow\downarrow} = \Delta_{\vec{k}\downarrow\uparrow} = 0$ and $\Delta_{\vec{k}\uparrow\uparrow} = \Delta_{\vec{k}\downarrow\downarrow}$ ($\vec{d} \perp \hat{z}$). This corresponds to spin-triplet pairing with a spin orientation parallel to the z-axis. The energies in the quasiparticle-spectrum (133) are now $E_{\vec{k}s} = \sqrt{\xi_{\vec{k}s}^2 + |\Delta_{\vec{k}ss}|^2}$ with $\xi_{\vec{k}s} = \xi_{\vec{k}} - s\mu_B H_z$.

The expectation value (135) of the magnetization (134) now reads

$$M_z = \mu_B \sum_{\vec{k}} \left\{ \frac{\xi_{\vec{k}\uparrow}}{E_{\vec{k}\uparrow}} \tanh\left(\frac{E_{\vec{k}\uparrow}}{2k_B T}\right) - \frac{\xi_{\vec{k}\downarrow}}{E_{\vec{k}\downarrow}} \tanh\left(\frac{E_{\vec{k}\downarrow}}{2k_B T}\right) \right\}$$

(138)

$$\xrightarrow{H_z \to 0} -2\mu_B^2 H_z N_0 \int \frac{d\Omega_{\vec{k}}}{4\pi} \int d\xi \frac{d}{d\xi} \left\{ \frac{\xi}{E_{\vec{k}}} \tanh\left(\frac{E_{\vec{k}}}{2k_B T}\right) \right\} = \chi_P H_z$$

In this case the spin susceptibility remains unchanged. Indeed, if the magnetic field

lies parallel to the spin orientation of the triplet Cooper pair there is no need for pair breaking in order to polarize the spin. Also the essential conditions to form Cooper pairs of degenerate electron states with both spins parallel (or antiparallel) to the magnetic field is satisfied.

Based on the two special results there are two cases for the spin susceptibility in spin triplet superconductors:

$$\chi(T) = \chi_P \begin{cases} 1 & \vec{d}(\vec{k}) \perp \vec{H} \\ \int \frac{d\Omega_{\vec{k}}}{4\pi} Y(\hat{k};T) & \vec{d}(\vec{k}) \parallel \vec{H} \end{cases}, \qquad (139)$$

It becomes obvious that the susceptibility remains unchanged if the $\vec{d}$-vector lies for all $\vec{k}$ in the plane perpendicular to the magnetic field. On the other hand, the susceptibility vanishes at $T = 0$, if $\vec{d}$ is parallel to the field for all $\vec{k}$. The generalization for arbitrary fields and spin triplet gap functions yields

$$\chi(T)_{\mu\nu} = \chi_P \int \frac{d\Omega_{\vec{k}}}{4\pi} \left\{ \delta_{\mu\nu} - Re\frac{d_\mu(\vec{k})^* d_\nu(\vec{k})}{|\vec{d}(\vec{k})|^2}(1 - Y(\hat{k};T)) \right\} \qquad (140)$$

in which $M_\mu = \sum_\nu \chi_{\mu\nu} H_\nu$.

We consider here as a first example the BW-phase for which $\vec{d}(\vec{k}) = \Delta_0(\hat{x}k_x + \hat{y}k_y + \hat{z}k_z)$. The calculation by (140) leads to

$$\chi^{BW}(T)_{\mu\nu} = \chi_P \delta_{\mu\nu} \left(1 - \frac{1}{3}(1 - Y(T)) \right). \qquad (141)$$

The spin susceptibilty is isotrop and reaches $2\chi_P/3$ for $T = 0$. A further example is the ABM-state for which we have $\vec{d}(\vec{k}) = \Delta_0\hat{z}(k_x + ik_y)$. In this case the susceptibility reads

$$\chi(T) = \chi_P \begin{cases} \bar{Y}^{ABM}(T) & \vec{H} \parallel z \\ 1 & \vec{H} \perp z \end{cases}, \qquad (142)$$

with $\bar{Y}^{ABM}(T)$ the Yosida-Function for the ABM-state after integration over the Fermi surface. This phase might be realized in Sr_2RuO_4 from spin susceptibility measurements for fields in the x-y-plane [82].

Obviously it is not only possible to distinguish between spin singlet and spin triplet pairing, but also between different spin triplet state as long as the $\vec{d}$-vector is sufficiently "pinned" due to spin-orbit coupling. The spin susceptibility cannot be measured directly by the sample magnetization because of Meissner-screening. However, a local probe like nuclear magnetic resonance (NMR) measurements allow us to observe the temperature dependence of the local susceptibility in the mixed phase (vortex phase) of the superconductor, by looking at the Knight shift, the shift of resonance lines in the NMR spectrum [41]. Similar measurements are also possible with muon spin relaxation.

The Paramagnetic Limit

The response to Zeeman coupling can play an important role in superconductors with very short coherence lengths $\xi_0 = \hbar v_f / \pi |\Delta|$. The coherence length can be viewed as the extension of the Cooper pairs. The upper critical field H_{c2} due to the orbital depairing depends on ξ_0 in the following way

$$H_{c2} = \frac{\Phi_0}{2\pi\xi_0^2} \tag{143}$$

so that H_{c2} can acquire large values for small ξ_0. If this is the case depairing due to Zeeman spin splitting can become decisive for the destruction of the superconductivity. This phenomenon is called paramagnetic limiting (or Pauli- , Chandrasker- or Clogston-limiting). The paramagnetic limiting field is connected with the spin susceptibility in the following way. We have to compare the superconducting condensation energy with the magnetization energy which could be reached by the application of a magnetic field:

$$E_Z = -\frac{1}{2}\sum_{\mu,\nu}(\chi_P\delta_{\mu\nu} - \chi(T)_{\mu\nu})H_\mu H_\nu \qquad \Leftrightarrow \qquad E_{cond} = -\frac{N_0}{2}|\Delta_m|^2\langle|g_{\vec{k}}|^2\rangle_{\vec{k},FS} \tag{144}$$

where we have restricted the comparison to $T = 0$ and $\chi_p = 2\mu_B^2 N_0$. For spin-singlet superconductors, we immediately find that a critical field where the two energies are identical.

$$H_P = \frac{1}{\mu_B\sqrt{2}}|\Delta_m|\sqrt{\langle|g_{\vec{k}}|^2\rangle_{\vec{k},FS}} \,. \tag{145}$$

Thus for $H_{c2} > H_p$ superconductivity would break down at $H = H_p$, actually as a discontinuous first order transition unlike the second order transition for orbital depairing at H_{c2}. This condition on H_{c2} is generally quite restrictive, so that it is generally not so easy to find superconductors displaying paramagnetic limiting.

If paramagnetic limiting is absent, it can be taken as a sign for spin triplet pairing. However, the effect is field direction dependent in general, since the magnetic energy

$$E_Z = -\frac{\chi_P}{2}Re\left\langle\frac{d_\mu(\vec{k})^*d_\nu(\vec{k})}{|\vec{d}(\vec{k})|^2}\right\rangle_{\vec{k},FS}H_\mu H_\nu \,, \tag{146}$$

has to be compared with the condensation energy. For instance the the ABM-phase discussed earlier would not be paramagnetically limited for fields in the *x-y* plane.

PHENOMENOLOGICAL THEORY AND SYMMETRIES

The description of superconductivity based on the theory of phase transition by Ginzburg-Landau is one of the corner stones of our phenomenological understanding of superconductivity in general. The particular strength of this phenomenological theory lies in its generality allowing a formulation even without any detailed microscopic understanding of a superconductor. The key quantity is the *order parameter* describing the superconducting phase. This order parameter vanishes in the normal state, $T > T_c$, and grows continuously from zero below T_c. The crucial aspect of the Ginzburg-Landau theory lies in the concept of spontaneous symmetry breaking at a (continuous) second order phase transition. This suggests to base the theory on symmetrical grounds which is a powerful strategy as we will show below. The fundamental symmetry to be broken in the superconducting phase is $U(1)$-gauge symmetry. This suggests an order parameter which would change under the operation of $\widehat{\Phi} \in U(1)$. While this is the only important symmetry for conventional superconductors, we will see below that time reversal and point group symmetry of a crystal can also appear in general as broken symmetries in unconventional superconductors [42, 43]

Conventional Superconductors

In order to introduce some basic concepts, it is useful to study first the Ginzburg-Landau phenomenology of conventional superconductors. One choice for the order parameter is the gap function $\Delta = -g b_{\vec{k}}$ which indeed changes under $U(1)$-gauge operation by a phase and becomes continuously finite below T_c. Alternatively we could choose $b_{\vec{k}}$ itsself as the pair wavefunction. In any case we define an order parameter η as $\Delta = \eta(\vec{r}, T)$ as a space and temperature dependent complex wavefunction describing the superconducting condensate (related also with the density of coherent Cooper pairs). This order parameter changes under basic symmetries as

$$\text{time reversal}: \quad \widehat{K}\eta = \eta^*$$

$$\text{(147)}$$

$$U(1) \text{ gauge}: \quad \widehat{\Phi}\eta = \eta e^{i\phi}$$

where the vector potential and the electron field operators change under gauge transformation as

$$\widehat{\Psi}(\vec{r}), \qquad \vec{A}(\vec{r}) \qquad \Leftrightarrow \qquad \widehat{\Psi}(\vec{r})e^{ie\chi(\vec{r})/\hbar c}, \qquad \vec{A}(\vec{r}) + \vec{\nabla}\chi(\vec{r}) \qquad (148)$$

with $\phi = 2ie\chi/\hbar c$, since $\eta \propto \langle \widehat{\Psi}\widehat{\Psi} \rangle$. Consequently a finite order parameter picks a certain phase which can be changed by $U(1)$-gauge transformation, breaking this symmetry.

Following Landau we expand the free energy around T_c in the order parameter η. The free energy is a scalar under symmetry operations belonging to the group $\mathscr{G} = \mathscr{K} \times U(1)$. The most general form including the possibility of spatial variations of the

order parameter is given by

$$F[\eta, \vec{A}; T] = \int_{\Omega} d^3r \left[a(T)|\eta|^2 + b(T)|\eta|^4 + K(T)|\vec{\Pi}\eta|^2 + \frac{1}{8\pi}(\vec{\nabla} \times \vec{A})^2 \right], \quad (149)$$

with

$$\vec{\Pi} = \frac{\hbar}{i}\vec{\nabla} + \frac{2e}{c}\vec{A}. \quad (150)$$

the canonical "momentum" (gradient) of the Cooper pairs of charge $2e$. Only powers of $\eta^*\eta$ appear which are invariant under time reversal as well as $U(1)$-gauge operations. We stop the expansion at fourth order. The third term describes the stiffness of the order parameter against spatial modulations and contains the minimal coupling between the order parameter and the vector potential and giving this term a gauge invariant form. This term reflects one of the important consequences of a state with broken $U(1)$-gauge symmetry as we will see below. Finally the last term is the magnetic field energy. The

$$a(T) \approx a'(T - T_c), \ a' > 0,$$

$$b(T) \approx b(T_c) = b > 0, \quad (151)$$

$$K(T) \approx K(T_c) = K > 0,$$

so that $a(T)$ changes sign at $T = T_c$ and F is bound towards negative values. For given temperature we find the equilibrium state by minimizing the free energy variationally with respect to η and $\vec{A}$.

We discuss first the uniform superconducting phase ignoring spatial variations and the magnetic field:

$$0 = \frac{\partial F}{\partial \eta^*} = a(T)\eta + 2b\eta|\eta|^2 \quad \Rightarrow \quad |\eta|^2 = \begin{cases} 0 & T > T_c \\ -\dfrac{a(T)}{2b} & T \le T_c \end{cases} \quad (152)$$

The order parameter satisfies the requirement to be only non-zero below T_c and to grow continuously from zero. We can now use this solution to calculate some thermodynamic quantities such as entropy and specific heat:

$$-S = \frac{dF}{dT} = -S_n + |\eta|^2\frac{da}{dT} + \underbrace{\frac{\partial F}{\partial \eta}\frac{d\eta}{dT} + \frac{\partial F}{\partial \eta^*}\frac{d\eta^*}{dT}}_{=0},$$

$$C = T\frac{dS}{dT} \approx C_n + a'T\frac{d|\eta|^2}{dT} \quad (153)$$

$$\Rightarrow \quad \Delta C|_{T=T_c} = C - C_n|_{T=T_c} = \frac{a'^2}{2b} = \frac{8\pi^2 k_B^2 T_c N_0}{7\zeta(3)}\Omega.$$

Using the specific heat result we can related the ratio a/b to the microscopic parameter. The latest enables us to relate a'^2/b to the microscopic parameters of the BCS theory. Assuming that the order parameter corresponds to the gap we can derive the coefficients as

$$a' = \Omega \frac{N_0}{T_c} \qquad \text{and} \qquad b = \Omega \frac{7\zeta(3)N_0}{16\pi^2 k_B^2 T_c^2} \; . \tag{154}$$

Now we turn to the general inhomogenous form of the order parameter and the vector potential. The given expansion of the free energy is valid for variations of the order parameter on length scales much longer the zero-temperature coherence length ξ_0. The variational minimization of the free energy with respect to both η and $\vec{A}$ leads to the Ginzburg-Landau equations

$$a\eta + 2b\eta|\eta|^2 - K \vec{\Pi}^* \cdot \vec{\Pi}\eta = 0$$

$$\frac{2e}{c} K \left\{ \eta^* \vec{\Pi}\eta + \eta \vec{\Pi}^* \eta^* \right\} - \frac{1}{4\pi} \vec{\nabla} \times (\vec{\nabla} \times \vec{A}) = 0 \tag{155}$$

The second equation can be rewritten as the stationary Maxwell equations which links current and magnetic field

$$\vec{\nabla} \times \vec{B} = \frac{4\pi}{c} 2eK \left\{ \eta^* \vec{\Pi}\eta + \eta \vec{\Pi}^* \eta^* \right\} = \frac{4\pi}{c} \vec{j} \; , \tag{156}$$

with $\vec{j}$ as the supercurrent. For a uniform order parameter $|\eta|$, this equation can be simplified into an equation for the magnetic field only

$$\vec{\nabla} \times (\vec{\nabla} \times \vec{B}) = -\frac{4\pi}{c} \frac{8e^2}{c} K|\eta|^2 \vec{B} \qquad \Rightarrow \qquad \vec{\nabla}^2 \vec{B} = \frac{1}{\lambda_L^2} \vec{B} \; , \tag{157}$$

which is the London equation describing the screening of the magnetic field. This is an essential consequence of the broken $U(1)$-gauge symmetry and corresponds to the Higgs-mechanism in gauge field theories making gauge fields massive by violating gauge symmetries. A result of the London equation is that an external magnetic field can only penetrate a sample on length λ_L, the London penetration length:

$$\lambda_L^{-2} = \frac{32\pi e^2}{c^2} K|\eta|^2 = \frac{4\pi e^2 n_s}{mc^2} \tag{158}$$

where the second equality gives the standard form of λ_L with n_s as the superfluid density. Note that n_s is the electronic density n_e at $T = 0$. Near the phase transition one finds

$$n_s(T) = 2n_e \left(1 - \frac{T}{T_c} \right) = \frac{7\zeta(3)n_e}{8(\pi k_B T_c)^2} |\eta|^2 \; , \tag{159}$$

which relates K to microscopic parameters

$$K = \frac{7\zeta(3)n_e}{64\pi m(\pi k_B T_c)^2} \; . \tag{160}$$

There is a second important length scale in the Ginzburg-Landau equation, the coherence length ξ. We look at the terms of the first equation in (155), which are linear in the order parameter. Here we can define ξ naturally as a characteristic length.

$$\left(a(T) - K\hbar^2 \vec{\nabla}^2 \right) \eta = a(T) \left\{ 1 - \xi^2 \vec{\nabla}^2 \right\} \eta$$

$$\Rightarrow \qquad \xi(T)^2 = -\frac{\hbar^2 K}{a(T)} = \frac{\hbar^2 K}{2b|\eta|^2} = \frac{\hbar^2 v_F^2}{8\pi|\eta|^2} \propto \frac{T_c}{T_c - T} ,$$

(161)

which we may compare with coherence length $\xi_0 = \hbar v_F / \pi |\Delta|$ at $T = 0$.

Generalization to unconventional order parameters

The extension of the phenomenological theory to general superconducting order parameters requires to include further symmetries of the system. This leads us to the classification of the possible order parameters in terms of the irreducible representations of the corresponding symmetry group analogous to the stationary states in quantum mechanics. In the standard case the second order phase transition can be restricted to a single representation.

To explain this point we consider again the linearized gap equations we had derived ealier for spin singlet and spin triplet pairing with the gap functions $\psi(\vec{k})$ and $\vec{d}(\vec{k})$, respectively.

$$-\lambda \, \psi(\vec{k}) = -N_0 \langle v^s_{\vec{k},\vec{k}'}, \psi(\vec{k}') \rangle_{\vec{k}',FS} \qquad \text{for spin singlet pairing}$$

$$-\lambda \, \vec{d}(\vec{k}) = -N_0 \langle v^t_{\vec{k},\vec{k}'}, \vec{d}(\vec{k}') \rangle_{\vec{k}',FS} \qquad \text{for spin triplet pairing}$$

(162)

where all symmetries are incorporated in the pairing interaction. This is an eigenvalue problem which gives possible transition tempertures T_c. The largest one defines the real physical instability temperature of the normal state. This corresponds here to the largest eigenvalue λ. The eigenfunctions belong to irreducible representations whose dimensionality gives the degeneracy of a given eigenvalue. We have shown in the previous chapter how the gap functions is transformed under symmetry operations. These operations include besides the time reversal and the $U(1)$-gauge symmetry also the orbital and the spin rotation. In solids the orbital rotation is limited to the point group operation of the crystal lattice. Thus we will not be allowed to use the relative angular momentum l to label the irreducible representations of $SO(3)$. We will also assume that spin-orbit coupling is sufficiently strong, so that one can consider the spin to be "frozen" to the lattice and rotate together with the orbital rotations.

We now would like to construct a free energy that describes a phase transition to an unconventional superconducting phase. Following Landau's recipe we pick the gap function with the highest T_c and decompose in the independent basis functions of this

representation, $\{\psi_m(\vec{k})\}$ or $\{\vec{d}_m(\vec{k})\}$:

$$\psi(\vec{k}) = \sum_l \eta_m \psi_m(\vec{k}) \qquad \text{and} \qquad \vec{d}(\vec{k}) = \sum_l \eta_m \vec{d}_m(\vec{k}) \,. \qquad (163)$$

where the sum runs over all basis functions of the relevant irreducible representation. It is thus assumed that all other representations have sufficiently lower critical temperatures to be ignored safely. We will use the coefficients η_m as order parameters in the free energy. The free energy F must be real and a scalar functional of the general order parameter η_m and also of the vector potential so it is denoted $F[\eta_m, \vec{A}; T]$, with T the temperature parameter. All η_m transform under symmetry operations like coordinates in the basis of functions $\{\psi_m(\vec{k})\}$ or $\{\vec{d}_m(\vec{k})\}$, and transform as $\eta \to \eta^*$ ($\eta \to e^{i\phi}\eta$) under time-reversal ($U(1)$-gauge) operation. The generic form of the scaler F is given by

$$\begin{aligned} F[\eta_m, \vec{A}; T] &= F_n(T) + \int d^3r \Bigg\{ a \sum_m |\eta_m|^2 + \sum_{m_1,\cdots,m_4} b_{m_1,\cdots,m_4} \eta_{m_1}^* \eta_{m_2}^* \eta_{m_3} \eta_{m_4} \\ &\quad + \sum_{m_1,m_2} \sum_{n_1,n_2} K_{m_1 m_2, n_1 n_2} (\Pi_{n_1} \eta_{m_1})^* (\Pi_{n_2} \eta_{m_2}) + \frac{1}{8\pi} (\vec{\nabla} \times \vec{A})^2 \Bigg\} \end{aligned} \qquad (164)$$

where

$$a = a'(T - T_c) \,, \quad a', b_m, K_{mm',nn'} > 0 \quad \text{and} \quad \vec{\Pi} = \vec{\nabla} + i\frac{2e}{\hbar c}\vec{A} \,, \qquad (165)$$

and $F_n(T)$ the normal state free energy, which will omitted from now on. The parameters are chosen to satisfy the symmetry condition. The important merit of this formulation is that the we can formulate this theory based on a few material dependent parameters which should be determined either experimentally or derived from a microscopic theory. This theory goes beyond the weak-coupling approach we had used in the previous chapter and is therefore more general.

Superconductor with tetragonal crystal structure

We consider here a superconductor in a system with tetragonal crystal structure and strong spin-orbit coupling. This provides one of the most illustrative examples among the possible unconventional superconductors. In addition there are important unconventional superconductors of this symmetry, e.g. the high-temperature superconductors and Sr_2RuO_4. Thus the releventa point group is D_{4h} and complete the symmetry group $\mathscr{G} = D_{4h} \times \mathscr{K} \times U(1)$ (spin rotation due to spin-orbit coupling is tied to orbital rotation). For this symmetry group we give the irreducible representations labeled as for D_{4h} with their character table and basis functions for both the even- and odd-parity case (label g for "gerade") and odd parity (label u for "ungerade").

Γ	E	$2C_4$	C_2	$2C_2'$	$2C_2''$	I	$2S_4$	σ_h	$2\sigma_v$	$2\sigma_d$	Basis function
A_{1g}	1	1	1	1	1	1	1	1	1	1	$\psi = 1$
A_{2g}	1	1	1	-1	-1	1	1	1	-1	-1	$\psi = k_x k_y (k_x^2 - k_y^2)$
B_{1g}	1	-1	1	1	-1	1	-1	1	1	-1	$\psi = k_x^2 - k_y^2$
B_{2g}	1	-1	1	-1	1	1	-1	1	-1	1	$\psi = k_x k_y$
E_g	2	0	-2	0	0	2	0	-2	0	0	$\psi = \{k_x k_z, k_y k_z\}$
A_{1u}	1	1	1	1	1	-1	-1	-1	-1	-1	$\vec{d} = \hat{x} k_x + \hat{y} k_y$
A_{2u}	1	1	1	-1	-1	-1	-1	-1	1	1	$\vec{d} = \hat{x} k_y - \hat{y} k_x$
B_{1u}	1	-1	1	1	-1	-1	1	-1	-1	1	$\vec{d} = \hat{x} k_x - \hat{y} k_y$
B_{2u}	1	-1	1	-1	1	-1	1	-1	1	-1	$\vec{d} = \hat{x} k_y + \hat{y} k_x$
E_u	2	0	-2	0	0	-2	0	2	0	0	$\vec{d} = \{\hat{z} k_x, \hat{z} k_y\}$

Reading from the characters of the identity element E, we have four one dimensional irreducible representations and one two-dimensional representation for even and odd parity. Note that the representation A_{1g} includes the conventional superconducting phase while all others are necessarily unconventional.

It is easy to see that all one-dimensional representations will lead to a Ginzburg-Landau theory identical to that of the conventional superconductor, since there is only one order parameter component, $\psi(\vec{k}) = \eta \psi_0(\vec{k})$ or $\vec{d}(\vec{k}) = \eta \vec{d}_0(\vec{k})$. The two-dimensional representation is much more interesting because of its two basis function and thus a functional that depends on two complex order parameter components $\vec{\eta} = (\eta_x, \eta_y)$

$$\psi(\vec{k}) = \eta_x k_x k_z + \eta_y k_y k_z \qquad \text{or} \qquad \vec{d}(\vec{k}) = \eta_x \hat{z} k_x + \eta_y \hat{z} k_y \qquad (166)$$

This additional degrees of freedom yield a more complicated general form of the free energy:

$$F[\vec{\eta}, \vec{A}; T] = \int d^3 r \left[a(T)|\vec{\eta}|^2 + b_1 |\vec{\eta}|^4 + \frac{b_2}{2} \{\eta_x^{*2} \eta_y^2 + \eta_x^2 \eta_y^{*2}\} + b_3 |\eta_x|^2 |\eta_y|^2 \right.$$

$$+ K_1 \{|\Pi_x \eta_x|^2 + |\Pi_y \eta_y|^2\} + K_2 \{|\Pi_x \eta_y|^2 + |\Pi_y \eta_x|^2\}$$

$$+ K_3 \{(\Pi_x \eta_x)^* (\Pi_y \eta_y) + c.c.\} + K_4 \{(\Pi_x \eta_y)^* (\Pi_y \eta_x) + c.c.\}$$

$$\left. + K_5 \{|\Pi_z \eta_x|^2 + |\Pi_z \eta_y|^2\} + \frac{1}{8\pi} (\vec{\nabla} \times \vec{A})^2 \right]$$

$$(167)$$

with $a(T), b_i$ and K_i real material dependent coefficients. It is important to realize that the two components are closely connected with each other as can be seen in the forth-order and the gradient terms.

Uniform phases

First we address the homogeneous superconducting phase without external magnetic fields. Thus we ignore the gradient terms and minimize the remaining free energy. A convenient parametrization simplifies the discussion:

$$\vec{\eta} = \eta_0(\cos\alpha, e^{i\gamma}\sin\alpha) \quad \Rightarrow \quad F = a\eta_0^2 + [4b_1 + \frac{1}{4}\sin^2 2\alpha(b_3 + b_2\cos 2\gamma)]\eta_0^4 \quad (168)$$

Since the free energy should always be bound below the following constraints for the coefficients have to be satisfied,

$$4b_1 - b_2 + b_3 > 0 \qquad \text{and} \qquad 4b_1 + b_2 + b_3 > 0 . \qquad (169)$$

We find that for $b_3 + b_2\cos 2\gamma > 0$ the angle $\alpha = 0, \pi/2$ minimizes the free energy. The condition $b_3 + b_2\cos 2\gamma < 0$ yields $\alpha = \pm\pi/4$ as a stable angle. Depending on the sign of b_2 either $\gamma = 0, \pi$ or $\gamma = \pm\pi/2$ gives a minimal free energy. This leads to three distinct superconducting phases whose range in parameter space (b_2, b_3) is shown in the phase diagram. We call these phase A, B and C.

Phase	$\psi(\vec{k})$	$\vec{d}(\vec{k})$	broken symmetry
A	$k_z(k_x \pm ik_y)$	$\hat{z}(k_x \pm ik_y)$	$U(1), \mathscr{K}$
B	$k_z(k_x \pm k_y)$	$\hat{z}(k_x \pm k_y)$	$U(1), D_{4h} \rightarrow D_{2h}$
C	$k_z k_x, k_z k_y$	$\hat{z}k_x, \hat{z}k_y$	$U(1), D_{4h} \rightarrow D_{2h}$

Each phase is two-fold degenerate besides the continuous $U(1)$-gauge degeneracy. Besides the $U(1)$ gauge symmetry also other symmetries are broken: the *A*-phase violates time reversal symmetry and the *B*- and *C*-phases break rotation symmetry reducing D_{4h} (tetragonal) to D_{2h} (orthorhombic). Time reversal violation is connected with special magnetic properties as we will show below. The reduced crystal symmetry yields lattice deformation, although these are rather small. The structure of the quasiparticle gap allows us to make a statement on the relative stability of the three phases within the weak-coupling scheme. The *B*- and *C*-phase have an equivalent gap structure and are degenerate for a spherical Fermi surface. The *A*-phase has less nodes than the *B*- and *C*-phase, e.g. in the triplet case *A* has only two point nodes while the other two have two line nodes. Consequently, the *A*-phase is more stable. Naturally, Fermi surface anisotropies and other corrections may shift the situation towards the *B*- and *C*-phase. It is a general trend that time reversal symmetry breaking phases gain more condensation energy within weak-coupling theory of multi-component BCS condensates.
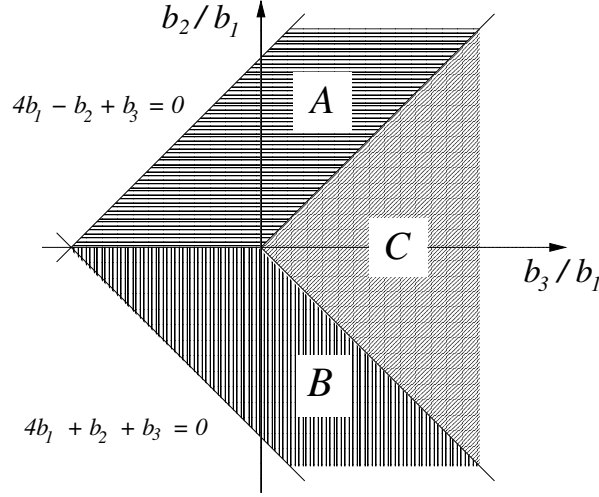
FIGURE 10. Phase diagram of the three stable phases of the $E_{g,u}$-representation.

London equation

The complex structure of the gradient terms is reflected in the supercurrent density which enters the London equation. The currents result from the variation of the free energy function with respect to $\vec{A}$, $\vec{j} = -c\partial F/\partial \vec{A}$:

$$j_x = 8\pi e \left[K_1 \eta_x^* \Pi_x \eta_x + K_2 \eta_y^* \Pi_x \eta_y + K_3 \eta_x^* \Pi_y \eta_y + K_4 \eta_y^* \Pi_y \eta_x + c.c. \right]$$

$$j_y = 8\pi e \left[K_1 \eta_y^* \Pi_y \eta_y + K_2 \eta_x^* \Pi_y \eta_x + K_3 \eta_y^* \Pi_x \eta_x + K_4 \eta_x^* \Pi_x \eta_y + c.c. \right] \tag{170}$$

$$j_z = 8\pi e K_5 \{ \eta_x^* \Pi_z \eta_x + \eta_y^* \Pi_z \eta_y + c.c. \} \ .$$

This structure yields a tensorial form for the London equations

$$\begin{aligned}
\vec{\nabla}^2 B_x &= \lambda_1^{-2} B_x + \lambda_3^{-2} B_y \\
\vec{\nabla}^2 B_y &= \lambda_3^{-2} B_x + \lambda_2^{-2} B_y \\
\vec{\nabla}^2 B_z &= \lambda_4^{-2} B_z
\end{aligned} \tag{171}$$

where the coefficients for homogeneous order parameters are given by

$$\lambda_1^{-2} = \frac{32\pi^2 e^2}{c^2} \{ K_1 |\eta_x|^2 + K_2 |\eta_y|^2 \} , \qquad \lambda_2^{-2} = \frac{32\pi^2 e^2}{c^2} \{ K_1 |\eta_y|^2 + K_2 |\eta_x|^2 \} ,$$

$$\lambda_3^{-2} = \frac{32\pi^2 e^2}{c^2} (K_3 + K_4)(\eta_x^* \eta_y + \eta_x \eta_y^*) , \qquad \lambda_4^{-2} = \frac{32\pi^2 e^2}{c^2} K_5 |\vec{\eta}|^2 \ .$$

$$\tag{172}$$

We find a diagonal form for the A-phase with $\lambda_3^{-2} = 0$ and $\lambda_1 = \lambda_2$ which is isotropic in the x-y-plane. On the other hand, the B- and C-phase lead to main axis forms which are anisotropic in the x-y-plane. This means also that the screening currents and, thus,

the London penetration depths are different for different orientations in the plane. This may observed, for example, in the structure of the vortex lattice, whose structure is depending on the vortex-vortex interaction. If the vortex lattice for fields along the z-axis has orthorhombic symmetry, the B- or C-phase would be realized.

Broken time-reversal symmetry and magnetism

The A-phase characterized by the gap functions

$$\psi(\vec{k}) = \eta k_z (k_x \pm ik_y) \quad \text{and} \quad \vec{d}(\vec{k}) = \eta \hat{z}(k_x \pm ik_y) \,. \tag{173}$$

has Cooper pair states with a finite angular momentum along the z-axis.

$$\vec{M} = \langle \psi^*(\vec{k}) i\vec{k} \times \vec{\nabla}_{\vec{k}} \psi(\vec{k}) \rangle_{FS} = \pm\hat{z}\langle k_z^2(k_x^2 + k_y^2)\rangle_{FS} \neq 0 \tag{174}$$

Such states with a finite angular momentum average over the Fermi surface have been called "ferromagnetic" by Volovik and Gorkov [44, 42]There are also time reversal symmetry breaking phases where the Cooper pairs do not possess a net angular momentum, which are called "antiferromagnetic". An example for an antiferromagnetic time reversal symmetry breaking phase is the so-called $d + is$-wave state which is a complex superposition of a conventional s-wave pairing state and the B_{1g} d-wave state of the tetragonal system.

$$\psi(\vec{k}) = s + id(k_x^2 - k_y^2) \quad \Rightarrow \quad \vec{M} = \left\langle \begin{pmatrix} 2dk_zk_y\{s - id(k_x^2 - k_y^2)\} \\ -2dk_zk_x\{s - id(k_x^2 - k_y^2)\}, \\ -4dk_xk_y\{s - id(k_x^2 - k_y^2)\} \end{pmatrix} \right\rangle_{FS} = 0 \,. \tag{175}$$

Because Cooper pairs are charged the angular momentum $L_z = \pm 1$ of the A-phase generates a magnetic moment which introduces intrinsic magnetism into the superconducting state. However, this magnetism cannot be so easily observed. The Cooper pairs overlapp and the "orbital currents" which induce the magnetic moment cancel each other in the depth of the superconductor. Moreover Meissner-Ochsenfeld screening would expell any magnetization from the bulk. Hence the only realm for the observation of magnetism is in regions where both effects are diminished. Such region can be provided by inhomogeneties and interfaces in the superconductor, e.g. impurities or surfaces.

Magnetism near the surface

We consider now the time-reversal violating A-phase in the vicinity of a surface. The boundary conditions are not trivial as they require a closer view on the interference behavior of Cooper pairs scattered at the surface. Let us assume that the normal vector of the planar surface is directed along the x-axis. For specular reflection the parallel components k_y and k_z of the momentum are conserved, while the perpendicular component k_x is inverted, i.e. $k_x \to -k_x$. This behavior leads to a different behavior of the two order parameter components at the surface. Under reflection k_zk_x ($\hat{z}k_x$) changes and k_zk_y

($\hat{z}k_y$) conserves the sign. Due to this property the former suffers a destructive, the latter a constructive interference, leading to a suppression of the order parameter component η_x and leaving η_y constant or even slightly enhanced. We use a variational approach to the behavior of the order parameter with the boundary conditon

$$\eta_x|_{x=0} = 0 \,, \quad \left.\frac{\partial \eta_y}{\partial x}\right|_{x=0} = 0 \tag{176}$$

and

$$\eta_x(x) = \eta_0 \tanh\left(\frac{x}{\xi}\right) \quad \text{and} \quad \eta_y = \pm i\eta_0 \tag{177}$$

for $x \geq 0$ and the surface at $x = 0$. Here ξ is the coherence length and the bulk value of the order parameter is given by

$$\eta_0^2 = \frac{a'(T_c - T)}{4b_1 - b_2 + b_3} \,. \tag{178}$$

This simple form captures the essential features of the superconducting phase at the surface. In particular, it is now interesting to study the supercurrents near the surface. We use the expressions in Eq.(170) and find that there is naturally no current running perpendicular to the surface: $j_x = 0$. Moreover there is no current along the z-axis. Neglecting the vector potential, we obtain for the current density parallel to the y-direction a finite value:

$$j_y(x) = 16\pi e\hbar K_3 \eta_y \frac{\partial \eta_x}{\partial x} = -\frac{16\pi e\hbar}{\xi} \frac{i\eta_y \eta_0}{\cosh^2(x/\xi)} \,. \tag{179}$$

This corresponds to a current spontaneously flowing parallel to the surface without applying a magnetic field. The extension of the current density towards the bulk is characterized by ξ. The direction of the current depends on the sign of η_y and is thus directly related to the orientation of in Cooper pair angular moment.

If the magnetic field outside of the superconductor vanishes, the obtained current layer would result in a constant magnetic field inside. This unphysical result is corrected, if we include the vector potential and solve corresponding "London equation" with the source current $j_y(x)$ of (179).

$$\frac{\partial^2 A_y}{\partial x^2} - \frac{1}{\lambda^2}A_y = \frac{4\pi}{c}j_y(x) \tag{180}$$

The magnetic field inside the superconductor dacays to zero with the length scale λ, which is realized by a screening current density flowing in opposite direction to the spontaneous current such that the net integrated current vanishes at the surface (Fig.11). The net magnetization remains finite in the complete solution and shows that the intrinsic magnetism of the angular momentum of the Cooper pairs is only visible at the edge of the superconductor.

It can be shown in an analogous manner that spontaneous currents occur around impurities and other defects in the superconductor. Such defects are also domain walls in the
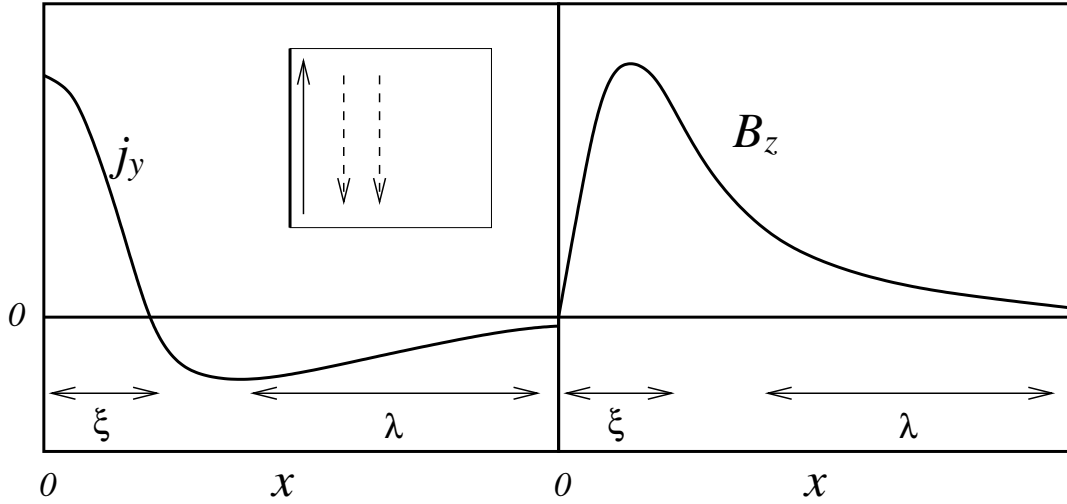
FIGURE 11. Distribution of spontaneous currents parallel to the surface and magnetic field. Screening currents in opposite direction ensure that the magnetic field vanishes in the bulk of the superconductor. The spontaneous current possesses the length scale ξ, the screening currents λ.

superconducting phase between the two stable states with $L_z = +1$ and $L_z = -1$. Consequently, a time reversal symmetry breaking superconductor would possess a rather broadly scattered internal magnetization due to inhomogeneities of the superconducting condensate. Such a random field distribution can be observed by local probes of the magnetic field. Most suitable are muons which by means of zero-field muon relaxation techniques provides a very suitable means to detect a randomly distributed field by means of the muon spin depolarization rate. In this way intrinsic spontaneous magnetism has been observed in the superconducting phase, giving a rough estimate of the generated fields of $0.1 - 1$ Gauss. These materials are the spin-triplet superconductor Sr_2RuO_4 [45], the heavy Fermion superconductor $U_{1-x}Th_xBe_{13}$ with $0.018 \leq x \leq 0.045$ [46], UPt_3 [49] and in skutterudite $PrOs_4Sb_{12}$ [52]. These results have been interpreted as evidence for time reversal symmetry breaking superconducting phases.

Multiple Superconducting Phase Transitions

Unconventional superconductors are characterized by the symmetries which are broken at the onset of superconductivity. Since a conventional superconductor only breaks $U(1)$-gauge symmetry, only one kind of phase transition is possible. In contrast the possibility of violating several symmetries allows for several superconducting phase transitions and complex phase diagrams of superconducting phases. Thus the observation of multiple superconducting phase transitions and different phases is a clear proof for unconventional superconductivity as long as the materials are of highquality to exclude different material phases in the same sample.

We would like here to illustrate the problem of multiple transitions on a simple model. For this purpose we use again the case of the two-component order parameter leading

to the *A*-, *B*- or *C*-phase. The situation will now be modified slightly be reducing the crystal symmetry, say by a uniaxial distortion in a specific direction (e.g. *x*-direction) to reduce the tetragonal symmetry (D_{4h}) to a orthorhombic one (D_{2h}). This lifts the degeneracy to the two components leading to different transition temperatures in the instability analysis, or the second order term of the Ginzburg-Landau free energy:

$$a'(T - T_c)|\vec{\eta}|^2 \quad \rightarrow \quad a'(T - T_{cx})|\eta_x|^2 + a'(T - T_{cy})|\eta_y|^2 \tag{181}$$

The splitting of the transition temperatures is assumed to be small compared to T_c ($|T_{cx} - T_{cy}| \ll T_{cx,y}$) so that we do not need to alter any of the other parameters in the free energy expansion. We replace now the second order term in the free energy $F[\vec{\eta}, T]$ and analyze the phase transitions. We take $T_{cx} > T_{cy}$. Thus the first instability goes to a phase with only the η_x-component finite:

$$\vec{\eta}(T) = \begin{pmatrix} \eta_x(T) \\ 0 \end{pmatrix} = \begin{pmatrix} \dfrac{a'(T_{cx} - T)}{2b_1} \\ 0 \end{pmatrix} \tag{182}$$

for temperatures just below T_{cx}. Now consider the question at which temperature the other component would appear. We tackle this problem by studying the instability conditions for η_y in the Ginzburg-Landau free energy. Thus we extract the effective second order term in η_y:

$$\left\{ a'(T - T_{cy}) + (2b_1 + b_3)|\eta_x(T)|^2 \right\} |\eta_y|^2 + \frac{b_2}{2}\eta_x^2(T)(\eta_y^{*2} + \eta_y^2) \tag{183}$$

where η_x is real given by (182). This is a bilinear form in (η_y, η_y^*) and can written with a component form for (η_y, η_y^*).

$$(\eta_y^*, \eta_y)\hat{A}\begin{pmatrix} \eta_y \\ \eta_y^* \end{pmatrix} \tag{184}$$

with

$$\hat{A} = \begin{pmatrix} a'(T - T_{cy}) + (2b_1 + b_3)|\eta_x(T)|^2 & b_2\eta_x^2(T) \\ b_2\eta_x^2(T) & a'(T - T_{cy}) + (2b_1 + b_3)|\eta_x(T)|^2 \end{pmatrix} \tag{185}$$

The new critical temperature is defined by the first zero of the determinant when the temperature is lowered, i.e. :

$$a'(T - T_{cy}) + (2b_1 - b_2 + b_3)|\eta_x(T)|^2 = 0 \quad \Rightarrow \quad \eta_y^* + \eta_y = 0, \tag{186}$$

$$a'(T - T_{cy}) + (2b_1 + b_2 + b_3)|\eta_x(T)|^2 = 0 \quad \Rightarrow \quad \eta_y^* - \eta_y = 0. \tag{187}$$

This yields to the following possible transition temperatures :

$$T'_{cy\pm} = T_{cy}\frac{1 - R_\pm T_{cx}/T_{cy}}{1 - R_\pm} \quad \text{with} \quad R_\pm = \frac{2b_1 \pm b_2 + b_3}{2b_1}. \tag{188}$$
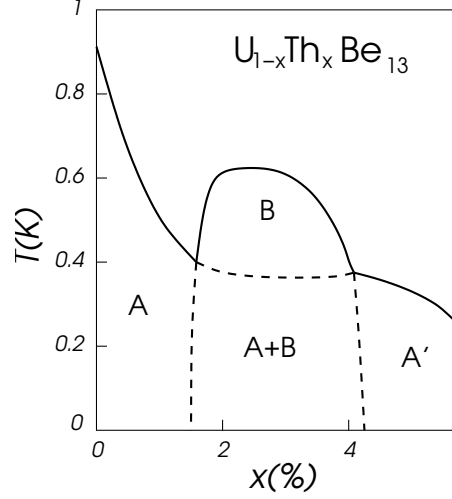
FIGURE 12. Phase diagram of $U_{1-x}Th_xBe_{13}$: Th-substitution for U gives four superconducting phases [47]. The phase A and A' are most likely identical. The phase $A + B$ is reached through multiple superconducting phase transitions. This phase has been found to be time reversal symmetry breaking by muon-spin relaxation experiments [46]. The symmetry of the different pairing states have not been identified so far [48].

where $+$ and $-$ signs yield the imaginary (186) or real solution (187), respectively, for η_y. The larger T'_{cy} determines a physical second phase transition and is determined by the coefficients b_2 and b_3. The phase diagram in Fig.10 yields the region. In the range of the A-phase η_y is imaginary, in B real and no second phase transition occurs in region C of the phase diagram.

The two phase transitions are both of second order in our example and lead to a sequential symmetry breaking:

$$\mathscr{G} = D_{2h} \times \mathscr{K} \times U(1) \xrightarrow{T_{cx}} D_{2h} \times \mathscr{K} \xrightarrow{T'_{cy}} \begin{cases} D_{2h} & \text{range } A \\ \mathscr{K} & \text{range } B \end{cases} \quad (189)$$

The first transition removes the $U(1)$-gauge symmetry yielding superconductivity. In the range A the time reversal symmetry is broken and in the range B the orthorhombic symmetry is removed. Note that the phase previously associated with range C in the phase diagram has the same crystal symmetry reduction as induce by the assumed uniaxial distortion. For this reason there is no further symmetry breaking possible in this range.

How can we observe consecutive superconducting transtions? The resistivity vanishes already at the frist transtions and shows no features at the second. The most common quantity is the specific heat which shows a discontinuity at each second order phase transition. However, also collective modes are very suitable for detection of phase transitions. The sound velocity of ultrasound shows rather pronounced change at phase transitions for longitudinal polarization. There are, however, interesting selection rules for transverse polarized sound waves which can be used to obtain more information about the nature of the superconducting phase transition. Anomalies in the lower critical magnetic field H_{c1} give a further possibility to locate a second superconducting transition.
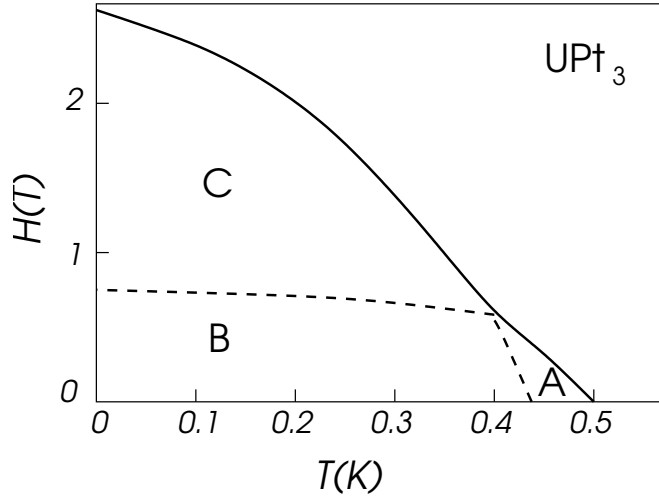
FIGURE 13. Phase diagram of UPt$_3$: There are two consecutive superconducting transitions in zero magnetic field, distinguishing the phase *A* and *B* [50]. The phase *B* is likely time reversal symmetry breaking [49]. In a magnetic field a third phase *C* is observed [51, 48].

Anomalies of the upper critical field H_{c2} can give an indication for additional transitions, however, this requires a careful extrapolation to zero field in order to find the corresponding T_c'. If the second transition involves the violation of time reversal symmetry the onset of a signal in the zero-field muon spin relaxation determines the transition [46, 49]. In fact in all systems where one has observed multiple superconducting phase transitions the signature of broken time reversal symmetry was detected. Such systems are $U_{1-x}Th_xBe_{13}$ $(0.018 < x < 0.045)$ (Fig.12), UPt$_3$ (Fig.13) and PrOs$_4$Sb$_{12}$.

HIGH-TEMPERATURE SUPERCONDUCTORS

High-temperature cuprate superconductors have been in the focus of condensed matter research ever since their discovery by Bednorz and Müller in 1986 [11]. Although the roughly twenty years have brought much insight in this complex system, it is fair to say that our knowledge of many essential points is still limited. One aspect which can be considered as established is the unconventionality of the superconducting phase. The evidence for a so-called $d_{x^2-y^2}$-wave state is overwhelming and it seems not so difficult to argue for this pairing symmetry from theoretical point of view. Even more intriguing is the fact that this superconducting phase emerges from a strongly correlated electron system with a pronounced trend towards antiferromagnetism. In the chapter we will give a brief overview on two of the most popular points of view on the issue of high-temperature superconductivity, keeping in mind that this field is still widely open. Then we will review also the most important experiments which have been used for the high-temeprature superconductors to test the pairing symmetry.

Electronic model

High-temperature superconductors belong to a class of transition metal oxides with a layered perovskite structure. Copper is the only transition metal yielding high-temperature superconductivity. One of the most simple compounds is $La_{2-x}Sr_xCuO_4$ where x corresponds to the carrier-doping concentration as we will point out later. We start with the "parent"-compound La_2CuO_4 ($x = 0$) which consists of copper-oxide-layers separated by La-ions. This is an ionic crystal where the elements enter as La^{3+}, Cu^{2+} and O^{2-}. While La- and O-ions are electronically in a nobel gas configuration the Cu-ion has a partially filled $3d$-shell. Starting from the $3d^{10}4s^1$-configuration we end up with $3d^9$, i.e. one d-electron missing. The d-orbital degeneracy is lifted by the crystal field in particular the octahedral oxigene cage around each Cu-ion which gives rise to an essential cubic symmetry, such that the d-level splitts into two subsets:

$$e_g : \begin{cases} 3d_{x^2-y^2} \\ 3d_{3z^2-r^2} \end{cases} \qquad t_{2g} : \begin{cases} 3d_{yz} \\ 3d_{zx} \\ 3d_{xy} \end{cases} \tag{190}$$

A slight tetragonal deformation of the O-octahedra splits these levels additionally such that the electron vacancy would reside in the e_g-$d_{x^2-y^2}$-orbital. Strong Coulomb repulsion essentially prevents the Cu-3d-orbitals from being doubly occupied by a second hole and gives rise to the formation of a filled lower and an empty upper Hubbard-band spitted by the Coulomb energy $U_d \approx 10$eV. Inbetween the oxigene 2p-hole band is located with a finite gap Δ to the upper $3d_{x^2-y^2}$-Hubbard band ($U_d > \Delta$). Any dispersion of the $3d_{x^2-y^2}$-hole would occur through the completely occupied O-2p-states lying between to Cu sites. This is prevented by the charge transfer gap to the 2p-levels, corresponding to the situation of a charge transfer insulator (Fig.14). Thus every Cu-site carries a spin $S = 1/2$ spin which interact through superexchange yielding a quasi-two-dimensional Heisenberg antiferromagnet:

$$\mathscr{H}_H = J \sum_{\langle i,j \rangle} \hat{\vec{S}}_i \cdot \hat{\vec{S}}_j , \tag{191}$$

where $J \sim 0.12$eV is the coupling strength. The stochiometric compound is an insulator with antiferromagnetic order. Only carrier doping leads to a metallic state which eventually provides the condition for superconductivity.

We know both types of high-temperature superconductors, electron- and hole-doped systems. La_2CuO_4 is the parent compound for a hole-doped compound. We will concentrate to this case of hole-doping which is much better explored than the electron-doped compounds. From Fig.14 it is obvious that doped holes (in contrast to doped electrons) do not enter the Cu $3d$-orbitals, but the 2p-orbitals of the oxigenes. Hole-doping is realized chemically by replacing La^{3+}-ions by Sr^{2+}-ions removing an additional electron from the copper-oxide plane.

Zhang and Rice have shown that the additional holes spread over the four O 2p-orbitals around a Cu-site hybridizing with the $3d_{x^2-y^2}$-orbital to form a strong spin singlet, the so-called Zhang-Rice singlet [53]. The singlet formation leads to the removal
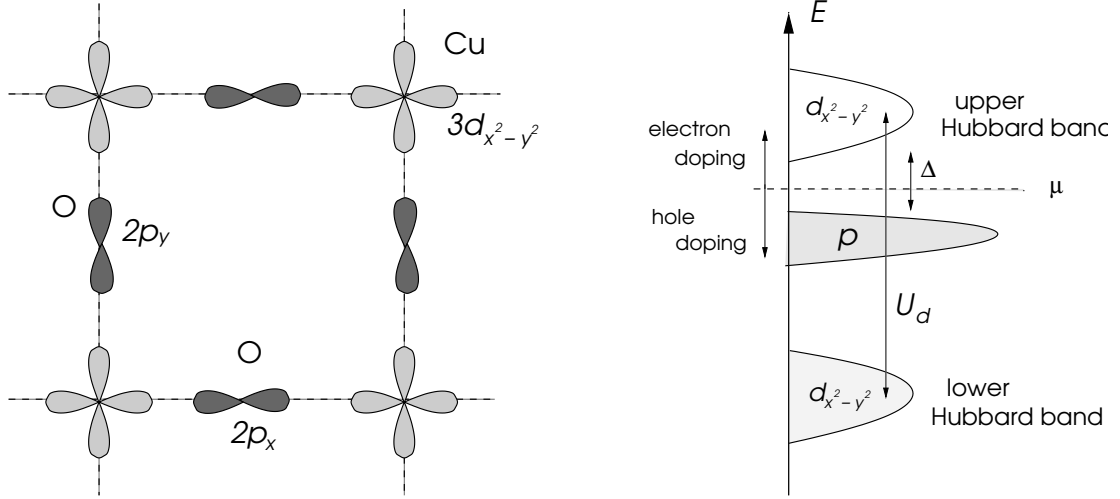
FIGURE 14. Relevant electron configurations in the copper-oxide plane: For the $3d_{x^2-y^2}$-orbital on the Cu-ion the σ-hybridization with the O-$2p$-orbitals is most important for dispersion (left panel). However, the right panel with the schematic density of states of the different orbitals shows that this system is in the charge transfer insulator regime. There is a gap Δ between the filled p- and the empty upper Hubbard band of the $d_{x^2-y^2}$-orbitals.
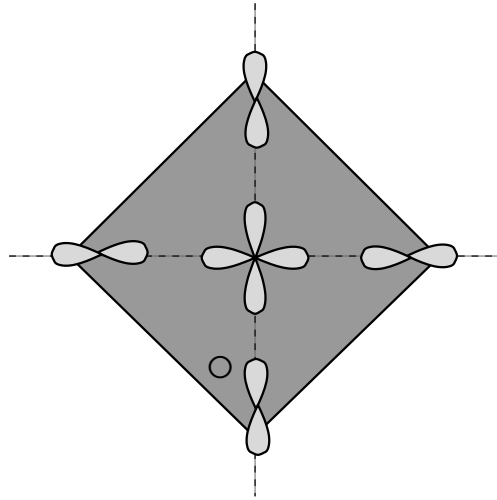

FIGURE 15. Zhang-Rice singlet: Superposition of four O-$2p$-orbitals hybridizing with the Cu-$3d_{x^2-y^2}$-orbital.

of the $S = 1/2$ spin degree of freedom which was associated with the Cu site. The Zhang-Rice singlet can also hop between the Cu-sites yielding mobile vacancies in the spin lattice (Fig.15). The dynamics of the doped system is described by the so-called t-J-model, the natural extension of the Heisenberg-Hamiltonian in this context:

$$\mathcal{H}_{tJ} = -t \sum_{\langle i,j\rangle,s} \left[c_{is}^{\dagger}(1-n_{i,-s})(1-n_{j,-s})c_{js} + \text{h.c.} \right] + J \sum_{\langle i,j\rangle} \vec{S}_i \cdot \vec{S}_j \ . \tag{192}$$
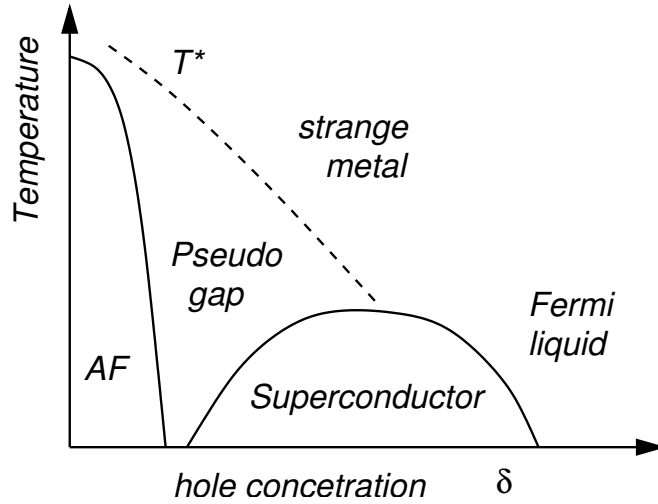
FIGURE 16. Schematic phase diagram of the high-temepature superconductors, temperature versus hole doping concentration.

The first term is formulated as a hopping Hamiltonian for electrons with the matrix element $-t$ ($\sim 0.4eV$) incorporating a strict constraint. The factors $(1-n_{i,-s})(1-n_{j,-s})$ project on a subspace of the usual electron configuration space, ensuring that never more than one electron occupies a site. With this Hamiltonian we describe the interplay between the dynamics of mobile holes and the antiferromagnetic correlations. Despite the simplicity of the Hamiltonian it is absolutely not trivial to extract the low-energy physics of this system.

We may hope that essential features of the weakly hole-doped cuprate are captured by the t-J-model and answer the question of how does the metallic state emerge out of a doped magnetic insulator and eventually gives rise to superconductivity with an unprecedented high transition temperature? The phase diagram, temperature versus hole-concentration, shows that the antiferromagnetic phase is quickly destroyed by doping. The system reaches a state of a strange metal and superconductivity with maximal T_c around a doping concentration of $\delta \approx 0.15$. In the phase diagram Fig.16 there is a intermediate phase between the antiferromagnetic phase and the superconducting dome, which is called pseudo gap phase, due to the reduction of low-energy magnetic excitations below a temperature T^*. In the "strange metal" phase as well as the pseudo gap region the charge carriers do not behave like a standard Fermi liquid. Only for rather large doping the Fermi liquid-like behavior is recovered. However, here the superconductivity disappears eventually. Taking the maximal T_c as a reference point, the so-called optimal doping δ_{opt}, one generally distinguishes two regions, the *underdoped* side with $\delta < \delta_{opt}$ and the *overdoped* side with $\delta > \delta_c$. In the following we address these two regions with different schemes. First we will consider the underdoped regime where correlation effects are very important and where we study to the t-J-Hamiltonian as the basic model. Later we will turn to the overdoped region which we tackle from the viewpoint of a Fermi liquid with strong antiferromagnetic spin fluctuations.

Underdoped Regime and RVB concept

The challenge of description of the underdoped phase lies in capturing the essence of the carrier motion in a background of spins with a strong antiferromagnetic correlation. Anderson proposed shortly after the discovery of high-temperature superconductivity that magnetism would evolve into a resonating valence bond (RVB) state which would be very favorable for Cooper pairing [55]. The RVB phase is characterized by very short-range spin singlet correlation, in contrast to the infinite range correlation of the antiferromagnetic order. This phase embodies the key features to identify the pseudo gap phase and the mechanism of the superconductivity. The t-J-model which we introduced above seems to be most suitable for a theoretical study of this aspect.

One strategy to study ground state properties of the t-J-model is the technique of the Gutzwiller projection which is a variational approach. We consider a suitable "uncorrelated" state $|\psi_0\rangle$ and create a correlated state by projecting out all configurations with doubly occupied sites. This is done with the Gutzwiller projection operator $\hat{P}$:

$$\left|\psi_g\right\rangle = \hat{P}|\psi_0\rangle \quad \text{with} \quad \hat{P} = \prod_i (1 - n_{i\uparrow}n_{i\downarrow}) \tag{193}$$

Among the very best starting states are actually BCS-type of states,

$$|\psi_0\rangle = \prod_{k<k_F} (u_{\vec{k}} + v_{\vec{k}} c^\dagger_{\vec{k}\uparrow} c^\dagger_{-\vec{k}\downarrow})|0\rangle \ . \tag{194}$$

where one finds that variationally most favorable state is the one where Cooper pairs possess $d_{x^2-y^2}$-symmetry (for a very insightful review see [56]).

Gutzwiller's Approximation

Although the structure of $\hat{P}$ is simple, it is generally difficult to calculate with this operator. The expectation value

$$E_g = \frac{\langle\psi_g|\mathcal{H}_{tJ}|\psi_g\rangle}{\langle\psi_g|\psi_g\rangle} = \frac{\langle\psi_0|\hat{P}\mathcal{H}_{tJ}\hat{P}|\psi_0\rangle}{\langle\psi_0|\hat{P}|\psi_0\rangle} \tag{195}$$

and the variational minimization is usually done by means of variational Monte Carlo techniques [56].

An interesting approach which gives an interesting qualitative view of the correlation effects in the t-J-model is called Gutzwiller approximation. The idea of this approximation is to renormalize matrix elements by means of statistical counting of real space configurations. Thus the fully correlated Hamiltonian $\mathcal{H}_{tJ}$ will be replaced by an effective Hamiltonian without constraints.

$$\mathcal{H}_G = -g_t t \sum_{\langle i,j\rangle,s} \left[c^\dagger_{is} c_{js} + \text{h.c.} \right] - \mu \sum_{i,s} n_{i,s} + g_J J \sum_{\langle i,j\rangle} \vec{S}_i \cdot \vec{S}_j \ . \tag{196}$$

Renormalization factors g_t and g_J are determined by comparing the constrained and unconstraint expectation values:

$$\left\langle c_{is}^\dagger c_{js} \right\rangle = g_t \left\langle c_{is}^\dagger c_{js} \right\rangle_0 \quad \text{hopping} \tag{197}$$

$$\left\langle \vec{S}_i \cdot \vec{S}_j \right\rangle = g_J \left\langle \vec{S}_i \cdot \vec{S}_j \right\rangle_0 \quad \text{spin exchange} \tag{198}$$

$$\left\langle c_{i\uparrow}^\dagger c_{j\downarrow}^\dagger \right\rangle = g_\Delta \left\langle c_{i\uparrow}^\dagger c_{j\downarrow}^\dagger \right\rangle_0 \quad \text{pairing} \tag{199}$$

with $\langle \cdots \rangle$ the expectation values in the constrained Hamiltonian and $\langle \cdots \rangle_0$ the expectation values in the unconstrained Hamiltonian. Moreover, a pairing renormalization factor g_Δ is introduced in order to discuss the renormalization of the pairing gap even though it does not explicitly appear in the renormalized Hamiltonian.

First we consider g_t for the particle hopping:

$$\langle \psi | c_{is}^\dagger c_{js} | \psi \rangle = g_t \langle \varphi_0 | c_{is}^\dagger c_{js} | \varphi_0 \rangle \tag{200}$$

where $|\psi\rangle$ is a state where all configurations of double occupancy are absent, while $|\varphi_0\rangle$ is an uncorrelated state with $|\psi\rangle \leftrightarrow \sqrt{g_t}|\varphi_0\rangle$. Only states with one particle on site j and none on site i are relevant in $|\psi\rangle$ so that we approximate g_t through the comparison of configurational probabilities:

$$P(\uparrow, 0) + P(\downarrow, 0) = g_t \left[P_0(\uparrow, 0) + P_0(\downarrow, 0) \right] . \tag{201}$$

Here P and P_0 are the probabilities for constraint and unconstraint configurations, respectively. The left-hand side is the density of electron multiplying the density of holes $n(1-n)$. The right-hand side reads

$$\begin{aligned} P_0(\uparrow, 0) + P_0(\downarrow, 0) &= \left\langle n_{i\uparrow}(1 - n_{j\uparrow}) \right\rangle_0 + \left\langle n_{i\downarrow}(1 - n_{j\downarrow}) \right\rangle_0 \\ &= \langle n_i \rangle_0 - \left\langle n_{i\uparrow} n_{j\uparrow} \right\rangle_0 - \left\langle n_{i\downarrow} n_{j\downarrow} \right\rangle_0 \end{aligned} \tag{202}$$

which yields approximatively $n - n^2/4 - n^2/4$, since electrons are supposed to be uncorrelated. Then, g_t results as

$$g_t \approx \frac{2(1-n)}{2-n} \tag{203}$$

The same reasoning can be done for the exchange renormalization parameter. Now we have

$$\left| s, s' \right\rangle \leftrightarrow \sqrt{g_J} \left| s, s' \right\rangle_0 . \tag{204}$$

Since the process involves two electrons, exactly one on two neighboring sites, the probabilities of configurations give

$$\sum_{s,s'} P(s, s') = g_J \sum_{s,s'} P_0(s, s') . \tag{205}$$

The left-hand side is n^2. For electrons on neighboring sites i and j, the right-hand side is

$$\sum_{s,s'} \left\langle n_{i,s}(1-n_{i,-s})n_{j,s'}(1-n_{j,-s'}) \right\rangle_0 = \left\langle n_i n_j \right\rangle_0 - 2\left\langle n_i n_{j\uparrow} n_{j\downarrow} \right\rangle_0 + 4\left\langle n_{i\uparrow} n_{i\downarrow} n_{j\uparrow} n_{j\downarrow} \right\rangle_0 .$$

(206)

This is approximated as $n^2 - 2n(n/2)^2 + 4(n/2)^4 = (2-n)^2 n^2/4$ so that

$$g_J \approx \frac{4}{(2-n)^2}$$

(207)

Finally we consider the renormalization of the pairing amplitudes, g_Δ. This is an off-diagonal expectation value which couples states with different total number of electrons. Thus the matrix elements take the form

$$\langle \psi(N)| c_{i\uparrow}^\dagger c_{j\downarrow}^\dagger |\psi(N-2)\rangle = g_\Delta \langle \varphi_0(N)| c_{i\uparrow}^\dagger c_{j\downarrow}^\dagger |\varphi_0(N-2)\rangle \Leftrightarrow$$

(208)

$$|\psi(N)\rangle \to \gamma_N |\varphi_0(N)\rangle \quad \text{and} \quad |\psi(N-2)\rangle \to \gamma_{N-2} |\varphi_0(N-2)\rangle ,$$

(209)

with $g_\Delta = \gamma_N \gamma_{N-2}$. The probabilities of the relevant configurations are

$$P(\uparrow,\downarrow) = \frac{n^2}{4} = \gamma_N^2 P_0(\uparrow,\downarrow) = \gamma_N^2 \langle n_{i\uparrow} n_{j\downarrow} \rangle_0 = \gamma_N^2 \frac{n^2}{4}$$

(210)

so that $\gamma_N = 1$. In the same way we evaluate

$$P(0,0) = (1-n)^2 = \gamma_{N-2}^2 P_0(0,0) = \gamma_{N-2}^2 \left\langle (1-n_{i\uparrow})(1-n_{j\downarrow}) \right\rangle = \gamma_{N-2}^2 \left(1-\frac{n}{2}\right)^2 ,$$

(211)

leading to $\gamma_{N-2} = 2(1-n)/(2-n)$ such that

$$g_\Delta = \frac{2(1-n)}{2-n} = g_t ,$$

(212)

Both hopping and pairing are connected with the quasiparticle weight of the electrons at the Fermi surface, which is reduced through the correlation effects. We find that both g_t and g_Δ vanish as we approach half-filling, $n \to 1$. It is obvious that the charge fluctuations under the constraint would be suppressed giving rise to increasing difficulties for hopping due to the lack of free sites. In much the same way the BCS pairing is relying on the availability on configurations with unoccupied sites. On the other hand, we find that g_J takes its maximal (enhanced) value at half filling, since this yields with security configuration where neighboring sites are occupied by just single electrons.

Mean field treatment

The Fermionic operators which we use in $\mathcal{H}_G$ are now not constraint anymore and within our approximation the effect of projections is incorporated by the renormalization factors. Nevertheless, we are still confronted with a many-body problem which we

would like to tackle by means of a mean field ansatz to decouple the Heisenberg part of $\mathcal{H}_G$. It turns out that the following two types of mean fields are giving a description which carries the idea obtained from the above variational treatment:

$$\chi_{ij} = \left\langle c_{is}^\dagger c_{js} \right\rangle_0 \quad \text{and} \quad \Delta_{ij} = \left\langle c_{i\uparrow}^\dagger c_{j\downarrow}^\dagger \right\rangle_0 , \tag{213}$$

where χ_{ij} is a hopping mean field and Δ_{ij} is a BCS-like pairing mean field. Note that we neglect here the staggered magnetic moment as another obvious mean field. These are nearest-neighbor mean fields which are considered to be unform throughout the system with

$$\chi_{i,i+\hat{a}_x} = \chi_x , \; \chi_{i,i+\hat{a}_y} = \chi_y , \; \Delta_{i,i+\hat{a}_x} = \Delta_x , \; \Delta_{i,i+\hat{a}_y} = \Delta_y . \tag{214}$$

The transformation to momentum space leads to the following effective (one-particle) mean field Hamiltonian

$$\mathcal{H}_{MF} = \sum_{\vec{k},s} \xi_{\vec{k}} c_{\vec{k},s}^\dagger c_{\vec{k},s} - \sum_{\vec{k}} \left\{ \Delta_{\vec{k}}^* c_{\vec{k}\downarrow} c_{\vec{k}\uparrow} + \text{h.c.} \right\} + \frac{3Jg_j}{2} \sum_{\vec{k}} \left\{ |\chi_{\vec{k}}|^2 + |\Delta_{\vec{k}}|^2 \right\} \tag{215}$$

with

$$\begin{aligned}
\xi_{\vec{k}} &= -2 \sum_{\alpha=x,y} \left\{ g_t t + g_J \frac{3J}{4} \chi_\alpha \right\} \cos k_\alpha - \mu \\
&= \varepsilon_{\vec{k}} - \mu - g_J \frac{3J}{2} \sum_{\alpha=x,y} \chi_\alpha \cos k_\alpha \tag{216} \\
\Delta_{\vec{k}} &= -g_J \frac{3J}{2} \sum_{\alpha=x,y} \Delta_\alpha \cos k_\alpha \tag{217}
\end{aligned}$$

and $\varepsilon_{\vec{k}} = -2t g_t (\cos k_x + \cos k_y)$. The self-consistence equations lead to a stable solution with

$$\chi_x = \chi_y = \chi \quad \text{and} \quad \Delta_x = -\Delta_y = \Delta \tag{218}$$

for sufficiently low temperatures. The energy spectrum of the Bogolyubov quasiparticles is given by

$$E_{\vec{k}} = \pm \sqrt{\xi_{\vec{k}}^2 + |\Delta_{\vec{k}}|^2} \tag{219}$$

with an energy gap. The mean field $\Delta_{\vec{k}}$ has an onset temperature T^* which gradually decreases from a high value at half filling upon increasing $\delta = 1 - n$ and eventually reaches zero aroung $\delta \sim 0.3$. The onset of the hopping mean field lies higher and has no straightforward physical interpretation.

Despite the formal analogy the mean field $\Delta_{\vec{k}}$ is not the BCS superconducting order parameter which we only obtain with proper renormalization taking the restricted charge fluctuations into account. We find

$$\Delta_{BCS,\vec{k}} = g_\Delta \Delta_{\vec{k}} = \frac{2(1-n)}{2-n} \Delta_{\vec{k}} \tag{220}$$
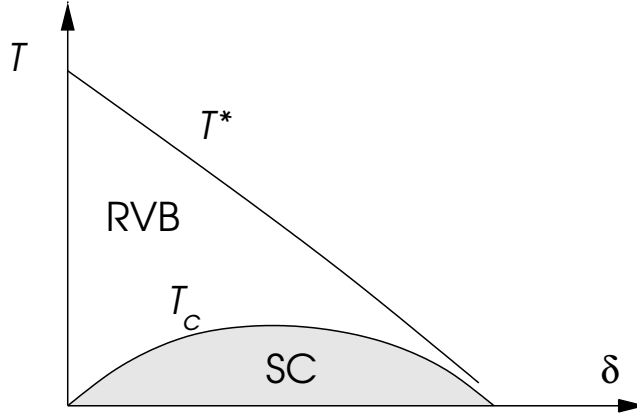
FIGURE 17. Phase diagram obtained from the Gutzwiller approximation with the RVB phase assigned to the pseudogap phase and the dome of superconductivity (SC).

such that the energy scale and correspondingly the superconducting transition temperature lies below T^*. Indeed we find through the renormalization a dome shape as is known from the experiment. Note however that quasiparticle gap measured would correspond to the $\Delta_{\vec{k}}$, the gap of the RVB phase and the reduction for Δ_{BCS} corresponds only to the characteristic temperature scale T_c.

The symmetry of the Cooper pairs is unconventional with a spin singlet even parity state in the D_{4h}-representation B_{1g}:

$$\psi(\vec{k}) = \Delta(\cos k_x - \cos k_y) \tag{221}$$

which corresponds to the $d_{x^2-y^2}$-wave state found in experiment. Beyond the superconducting phase in low-doping region we find a phase with an excitation gap below T^*. Although the onset of this phase is sharp within the present mean field description, it is interpreted as the pseudo gap phase. Experimentally there is no sharp transition at T^*, but a wide crossover. This phase corresponds here to Anderson's RVB phase, a short-ranged spin singlet liquid as well described by the BCS-like state. The superconducting instability is reduced through suppression of charge fluctuations close to half-filling.

Interestingly, this pseudogap phase is predicted to have the same gap structure as the superconducting phase. Indeed experimental results confirm this and can be counted as further supporting evidence for this theory [66]. In this way much of the features of the phase diagram can be reproduced. Antiferromagnetism is spared out, because the mean field theory overestimates the stability o magnetic order.

Alternative approach to the underdoped phase

A similar result is obtained by the so-called slave-boson theory which is an alternative technique to handle non-holonomic constraints such as $\sum_s c_{is}^\dagger c_{is} \leq 1$ [57]. One introduces
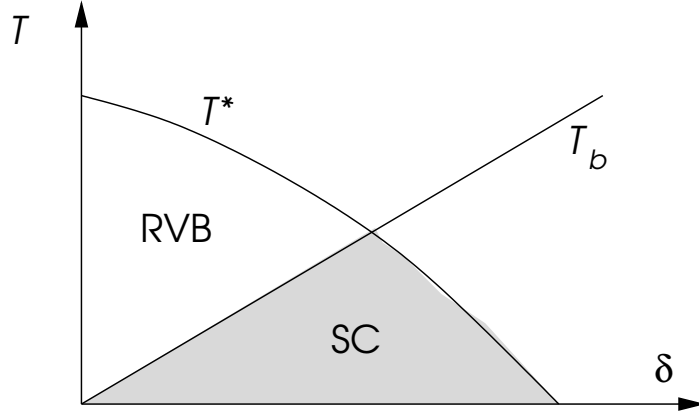
FIGURE 18. Phase diagram obtained from the slave-boson theory: T^* is the onset of the RVB phase corresponding to spinon (df-wave) pairing. T_b is the BEC transition of the holons. Only below both superconductivity (SC) is realized. Note that quasiparticles acquire a coherent part below T_b.

a decomposition of the electron operator:

$$c_{is} = b_i^\dagger f_{is} , \quad c_{is}^\dagger = f_{is}^\dagger b_i \quad \Rightarrow \quad \sum_s f_{is}^\dagger f_{is} + b_i^\dagger b_i = 1 \tag{222}$$

This decomposition splits the electron into a bosonic operator representing the absence of an electron and a fermionic operator for the spin, if an electron is on the site. The former is called *holon* and the latter *spinon*. Within the most simple scheme these two degrees of freedom are behaving independently. This feature corresponds to the concept of spin-charge separation, well-known in the one-dimensional correlated electron systems (Luttinger liquids) [58]. Obviously an electron if extracted from the system would have to combine both degrees of freedom so that this method allows us to give account of the absence of sharp quasiparticles in certain ranges of the phase diagram for the photoemission experiments.

The t-J-model formulated in this composite-fermion language can be again treated by mean field approximation introducing analogous to above

$$\chi_{ij} = \left\langle f_{is}^\dagger f_{js} \right\rangle \quad \text{and} \quad \Delta_{ij} = \left\langle f_{i\uparrow}^\dagger f_{j\downarrow}^\dagger \right\rangle . \tag{223}$$

for the fermionic spinon part and $B = \langle b_i \rangle$ for the bosonic holon part, where B is the mean field of the Bose-Einstein condensation (BEC) of the holons, a coherent state. Note that the real superconducting BCS order parameter is given by

$$\Delta_{ij,BCS} = \left\langle c_{i\uparrow}^\dagger c_{j\downarrow}^\dagger \right\rangle = \langle b_i b_j \rangle \left\langle f_{i\uparrow}^\dagger f_{j\downarrow}^\dagger \right\rangle = b^2 \Delta_{ij} . \tag{224}$$

In this approach the pseudogap phase is a BCS-like phase of the spinons while superconductivity requires the condensation of the holons in addition to the Cooper pairing of the spinons (SC=RVB+BEC) (see Fig.18). Analogous to the Gutzwiller approximation method one finds here an RVB phase below a characteristic temperature T^* and superconductivity appears at lower temperature. The holon condensation temperature grows

linearly with the hole density, while T^* decreases. Where the two temperatures cross we find the maximal T_c (optimal doping). In the overdoped regime we above the superconducting phase no spinon pairing while the holons are condensed. The presence of the condensate allows to find a coherent part in the electron weight, so that one could interpret the normal state here as Fermi liquid-like. The spinon-holon picture is complicated by the fact that two degrees of freedom are coupled by a $U(1)$-gauge field. Hence the spin-charge separation is to some extent a spurious feature of the theory [57].

While the RVB-phase gives an elegant interpretation of the underdoped region, it is difficult to establish this picture firmly. The situation is complicated by the fact that many different states seem to have comparable energy. Disorder can stabilize phase-separated states leading to the formation of charged stripes in a spin background. Other candidates have been the flux state or the d-density wave state which could compete with the RVB phase. Another attempt to explain the pseudogap phase is based on an extended region of superconducting fluctuations. Cooper pairs are created at high temperature but do not form a phase coherent condensate. Each of these proposed phases and concepts relies on a set of experiments for their support. However, no satisfactory description of the emergence of the cuprated physics in the underdoped region out of an antiferromagnetic insulator has been given so far.

Overdoped Regime

In the overdoped regime the normal state properties turn into a more standard metal state. The t-J-model of the weakly-doped system is obsolete here and the description in terms of a Fermi liquid phase with rather strong antiferromagnetic spin fluctuations looks more appropriate. This provides an alternative route to the description of high-temperature superconductivity, sparing out the complications of the underdoped (although there are attempts to extend this kind of analysis into the underdoped region; this is, however, beyond the scope of our lecture) [59]. The starting point is the Hubbard model in two dimensions from which we may derive an effective spin fluctuation based interaction between electrons, which is eventually responsible for the formation of Cooper pairs. Alternatively the spin fluctuations can also be introduced as a phenomenological input.

Effective spin fluctuation model

Restricting to the spin fluctuation induced interaction part we can introduce to following effective Hamiltonian:

$$\mathcal{H}_{sf} = \sum_{\vec{k},s} \xi_{\vec{k}} c^{\dagger}_{\vec{k}s} c_{\vec{k}s} - \frac{1}{2N^2} \sum_{\vec{k},\vec{k}',\vec{q}} \sum_{s_1,s_2,s_3,s_4} v(\vec{q}) \vec{\sigma}_{s_1 s_2} \cdot \vec{\sigma}_{s_3 s_4} c^{\dagger}_{\vec{k}+\vec{q},s_1} c_{\vec{k}s_2} c^{\dagger}_{\vec{k}'-\vec{q},s_3} c_{\vec{k}',s_4} \,,$$

(225)

with the band energy $\xi_{\vec{k}}$ $(= -2t(\cos k_x + \cos k_y) - \mu$ for a simple nearest-neighbor tight-binding model), N as the number of sites of the lattice. The effective interaction has the

form

$$v(\vec{q}) = U + U^2 \chi(\vec{q}) \qquad \text{with} \quad \chi(\vec{q}) = \frac{\chi_0(\vec{q})}{1 - U\chi_0(\vec{q})} \ . \qquad (226)$$

with the approximative RPA form for the static spin susceptibility $\chi(\vec{q})$ where $\chi_0(\vec{q})$ is the spin susceptibility of the free electron system. Since we are concerned with the possibility of Cooper pairing, we ignore all scattering events apart form the pair scattering in the Cooper channel. Hence the interaction part of the Hamiltonian reduces to the following terms in which we separate out the spin-singlet and the spin-triplet part:

$$\mathcal{H}_{pair} = \frac{1}{N^2} \sum_{\vec{k},\vec{k}'} \sum_s \left\{ V^t_{\vec{k},\vec{k}'} (c^\dagger_{\vec{k},s} c^\dagger_{-\vec{k},s} c_{-\vec{k}',s} c_{\vec{k}',s} + c^\dagger_{\vec{k},s} c^\dagger_{-\vec{k},-s} c_{-\vec{k}',-s} c_{\vec{k}',s}) \right.$$

$$\left. + V^s_{\vec{k},\vec{k}'} c^\dagger_{\vec{k},s} c^\dagger_{-\vec{k},-s} c_{-\vec{k}',-s} c_{\vec{k}',s} \right\} , \qquad (227)$$

with the spin-triplet and spin-singlet coupling matrix elements,

$$V^t_{\vec{k},\vec{k}'} = -\frac{1}{4} \left[v(\vec{k} - \vec{k}') - v(\vec{k} + \vec{k}') \right] \quad \text{resp.} \quad V^s_{\vec{k},\vec{k}'} = \frac{3}{4} \left[v(\vec{k} - \vec{k}') + v(\vec{k} + \vec{k}') \right] , \qquad (228)$$

In the sense of the weak-coupling these matrix elements are non-zero only within an energy region of width $2\varepsilon_c$ around the Fermi energy. The interaction contains two parts, a repulsive onsite interaction U preventing to pair in the most simple s-wave form, and a susceptibility dependent part on which we will focus now. The susceptibility can in priniciple be calculated in the RPA scheme using the given band structure. Even more sophisticated approaches developed for itinerant electron systems close to magnetic transitions may be applied such as the self-consistent renormalization scheme [54]. In order to keep matters simple we assume a simple form for the susceptibility which gives the essential features of the interaction. We parameterize $\chi(\vec{q})$ as

$$\chi(\vec{q}) \approx \chi_0[1 - bf(\vec{q})] \qquad \text{with} \qquad f = \cos q_x + \cos q_y , \qquad (229)$$

This $\chi(\vec{q})$ describes antiferromagnetic spin fluctuations, if it is maximal at $\vec{q} = \vec{Q} = (\pi/a, \pi/a)$ (a: lattice constant), i.e. $b > 0$. In contrast, negative b corresponds to ferromagnetic spin fluctuations.

This approximation allows us now to write pairing matrix elements in a particular easy form where we can recognize the pairing symmetries involved. For the spin singlet part we obtain

$$V^s_{\vec{k},\vec{k}'} = \frac{3U}{2} - \frac{3U^2\chi_0}{4} b \left\{ f(\vec{k} - \vec{k}') + f(\vec{k} + \vec{k}') \right\}$$

$$= \frac{3U}{2} - \frac{3U^2\chi_0}{4} b \left\{ (\cos k_x + \cos k_y)(\cos k'_x + \cos k'_y) \right.$$

$$\left. + (\cos k_x - \cos k_y)(\cos k'_x - \cos k'_y) \right\} \qquad (230)$$

and the analog for the spin-triplet part

$$V^t_{\vec{k},\vec{k}'} = \frac{\chi_0 U^2}{4} b \left\{ f(\vec{k} - \vec{k}') - f(\vec{k} + \vec{k}') \right\}$$

$$= \frac{\chi_0 U^2}{2} b \left\{ \sin k_x \sin k'_x + \sin k_y \sin k'_y \right\} .$$

(231)

Owing to this simplification in (229) both matrix elements possess a factorized form from which we immediately read the symmetry of the pair wave function as well as the coupling constant:

$$V_{\vec{k},\vec{k}'} = \sum_n g_n \psi_n(\vec{k}) \psi_N^*(\vec{k}')$$

(232)

with g_n as coupling constant and $\psi_n(\vec{k})$ the corresponding gap function form. Since we are considering here a basically tetragonal system, the symmetry classification of the pairing state for D_{4h} applies, which had given in the previous chapter. We can recognize states belonging to the representations A_{1g}, B_{1g} and E_u. We give here the list of possible states and their names as they are often used in literature:

Γ	gap function	coupling constant	name	type
A_{1g}	1	U	s-wave	repulsive
A_{1g}	$\cos k_x + \cos k_y$	$-\dfrac{3U^2 \chi_0 b}{4}$	extended s-wave	attractive
A_{2g}	$\sin k_x \sin k_y (\cos k_x - \cos k_y)$	$-$	$-$	absent
B_{1g}	$\cos k_x - \cos k_y$	$-\dfrac{3U^2 \chi_0 b}{4}$	$d_{x^2-y^2}$-wave	attractive
B_{2g}	$\sin k_x \sin k_y$	$-$	d_{xy}-wave	absent
E_u	$\{\sin k_x, \sin k_y\}$	$\dfrac{U^2 \chi_0 b}{4}$	p-wave	repulsive

Note that the state called "extended s-wave" is not a real s-wave state although it belongs to the representation A_{1g}. The amplitude of this function vanishes when both electrons are on the same lattice point since

$$\frac{1}{N} \sum_{\vec{k}} (\cos k_x + \cos k_y) = 0 .$$

(233)

For antiferromagnetic spin-fluctuations, only A_{1g} (extended s-wave) and B_{1g} pairing states give rise to an attractive interaction. Both are associated with the spin-singlet channel. (Note that for negative b, i.e. ferromagnetic spin fluctuations, the representation E_u would provide the only channel with attractive interaction.)

We now have to address the instability condition. The linearized gap equation has the form

$$-\lambda \psi(\vec{k}) = -\langle N_0(\hat{k}) V^s_{\vec{k},\vec{k}'} \psi(\vec{k}') \rangle_{\vec{k}',FS}$$

(234)

and look for the highest eigenvalue λ ($N_0(\hat{k})$: angle dependent density of states on the Fermi level). It is easy to see that the instability is not only depending on the coupling

constant which is identical for the extended *s*-wave and the $d_{x^2-y^2}$-wave state, but also the gap function form on the Fermi surface plays a role, in particular the Fermi surface average:

$$I[\psi] = \langle N_0(\hat{k}) | \psi(\vec{k}) |^2 \rangle_{\vec{k},FS} . \tag{235}$$

We find that $I[\psi_{A_{1g}}] < I[\psi_{B_{1g}}]$, i.e. the leading instability results from $d_{x^2-y^2}$ -wave pairing. It is easy to see that the extended *s*-wave state has a small gap function over all the Fermi surface, while the $d_{x^2-y^2}$-wave state has nodes along the (11)-direction, but is largest along the (10)- and (01)-direction where the density of state is largest in the two-dimensional electron system.

The discussion based on the spin fluctuation based mechanism leads to the same pairing state symmetry as the Gutzwiller-approximation for the *t-J*-model. This consistent result is not so surprising in view of the fact that the interaction term in the *t-J*-model is in its structure also a spin fluctuation type of interaction. Moreover the approach (229) leads to the same mathematical structure for both cases. This result is especially satisfactory as the experiments confirm this shape of the pairing interaction.

Testing the Pairing Symmetry

The pairing symmetry has been one of the most important question of the early 1990s also from the experimental point of view. The presence of line nodes constitute one important characteristic feature of the $d_{x^2-y^2}$-wave state. These nodes can be approached by a number of ways. However, the nodes alone do not give the entire picture of the pair wave function. It is also important to establish the phase structure.

Line nodes

The probably first indication for line nodes came from experiments which probe the low-energy (temperature) quasiparticle spectrum. These were the NMR-$1/T_1$ measurements which noted a T^3-powerlaw behavior for $T \to 0$ [61]. Moreover a T-linear behavior has been seen in the low-temperature London penetration depth [62]. Both results are compatible with line nodes. The fact that here T_c is extremely high made it naturally easier to address these powerlaws experimentally than in most other unconventional superconductors.

Evidence of line nodes came also from quasiparticle tunneling spectroscopy, in particular, scanning tunneling microscopy which measures the tunneling conductivity as a function of the applied voltage on *c*-axis facing surfaces [63]. The conductivity gives a picture of the local density of state at given energy $E = -eV$ with V as the voltage. The characteristic V-shape of a quasiparticle spectrum with line nodes was observed.

These experiments indicating line nodes could not decide however on the position of the line nodes. Here the tremendous improvement of the energy resolution of the angle resolved photoemission spectroscopy played a crucial role [64, 65, 66]. This technique allowed to observe for the first time a superconducting gap on the Fermi surface and even
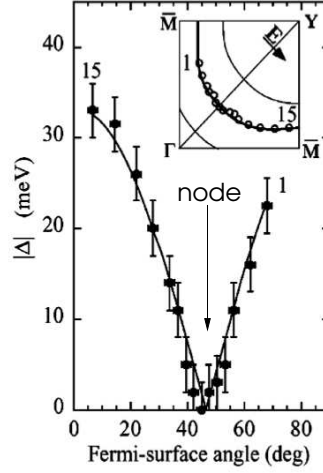
FIGURE 19. The angular dependence of the gap structure obtain by angle resolved photoemission spectroscopy in $Bi_2Sr_2CaCu_2O_{8+\delta}$ [65].

to map out its angular dependence. The results clearly showed nodes along the (11)-direction compatible with the $d_{x^2-y^2}$-wave state (Fig.19 [66]. In this case too the large energy scale of the superconducting gap is essential for the observation of the angular structure of the gap. No similar measurements for other unconventional superconductors have been possibile so far.

Phase sensitive tests - interference and frustration

The above tests provide strong experimental evidence for the $d_{x^2-y^2}$-wave state. However, they do not address the real symmetry aspect of this pairing state. The important point lies in the property that a 90°-rotation around the z-axis leads to a sign change of $\psi(\vec{k}) = \cos k_x - \cos k_y$. The above measurements do not give a direct access to this phase information.

Information on the phase of the order parameter can, however, be obtained from the Josephson effect, the coherent tunneling of Cooper pairs between two superconductors linked by a tunneling contact. The tunneling current depends on the phase of the order parameter on the two sides of the contact interface:

$$I = I_c \sin(\phi_2 - \phi_1) \tag{236}$$

where I_c is the maximal current (Josephson coupling) and $\phi_{1,2}$ are the phases of the order parameter (gap function / pair wave function) on the side 1 and 2, respectively. This standard formula is simple and unproblematic for conventional superconductors. However, in the case of unconventional superconductors geometric aspects of the interface start to play a role. For the $d_{x^2-y^2}$-wave phase the phase of the order parameter is different along the x- and along the y-direction. The phase difference for the two directions is π. Thus, having contacts on two interfaces, x- and y-oriented, then the their current-phase rela-
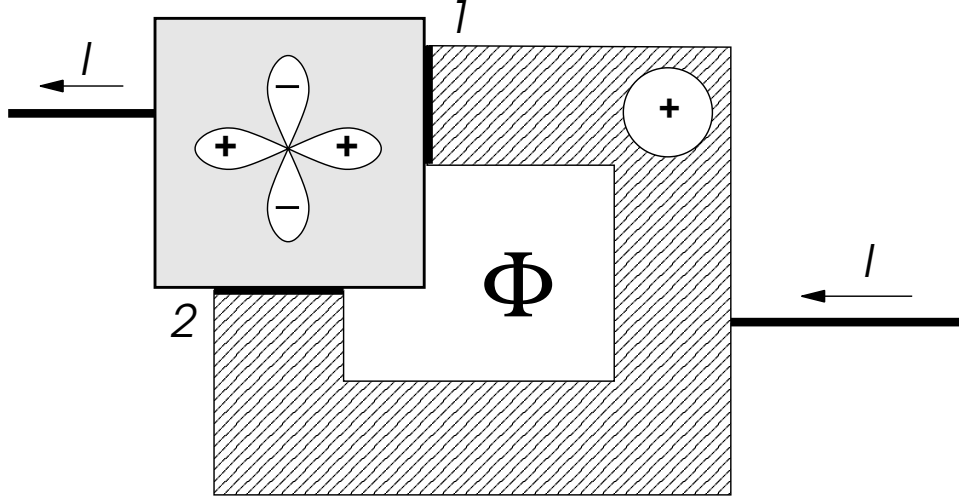
FIGURE 20. Set up for a SQUID phase sensitive probe using a *d*-wave and a conventional *s*-wave superconductor which has Josephson contact along two perpendicular faces [70, 67].

tion would be shifted by π. This property has been used to probe this symmetry feature through an interference experiment.

We consider the configuration as given in Fig.20 where a conventional superconductor is coupled to a $d_{x^2-y^2}$-wave superconductor on two orthogonal faces. This is a typical SQUID (Superconducting QUantum Interference Device) where the flux gives via an Aharanov-Bohm-type effect for the Cooper pairs a periodic interference pattern of the maximal current as a function of the magnetic flux threading the SQUID-loop. The total current through this device consists of the contributions of the two junctions 1 and 2:

$$I = I_1 + I_2 = I_{c1} \sin \varphi_1 + I_{c2} \sin(\varphi_2 + \alpha) \qquad \text{with} \quad \varphi_1 - \varphi_2 = 2\pi \frac{\Phi}{\Phi_0} \qquad (237)$$

with $\Phi_0 = hc/2e$ is the superconducting magnetic flux quantum. The second term involves a phase shift α which is π in the present situation. It is easy to calculate the maximal current assuming $I_{c1} = I_{c2} = I_c$.

$$I_{\max}(\Phi) = I_c \left| \cos \left(\pi \frac{\Phi}{\Phi_0} + \frac{a}{2} \right) \right| . \qquad (238)$$

While the standard SQUID ($\alpha = 0$) shows a maximum for $\Phi = n\Phi_0$, the configuration with the *d*-wave superconductor ($\alpha = \pi$) is shifted by half a flux quantum with a maximum for $\Phi = (n/2 + 1)\Phi_0$ (see Fig.21. This type of experiments have indeed been performed in the specified configuration with $YBa_2Cu_3O_7$ by several groups with a positive result giving an even stronger support for the realization of $d_{x^2-y^2}$-wave symmetry in the cuprate superconductors [71, 72, 73, 67].

Another related experiment addresses the phase frustration effect in a superconducting loop where a π-shift like this is buildt in. We assume that the superconducting loop does
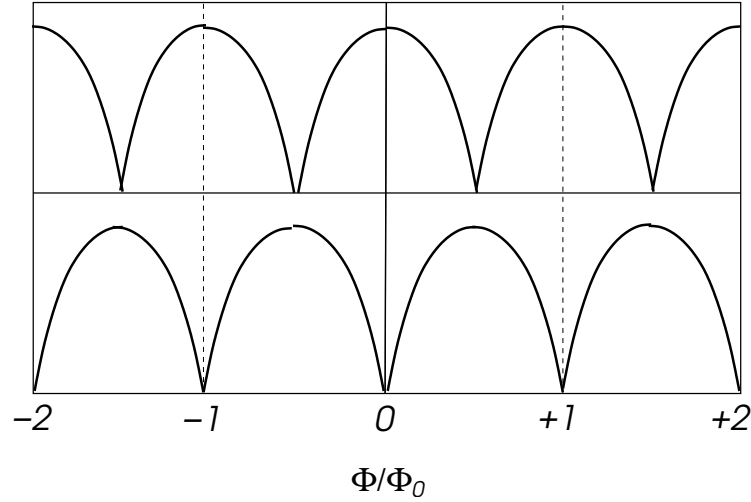
FIGURE 21. Interference pattern of a SQUID: Standard pattern (upper panel); π-shifted pattern (lower panel).

not allow any flux to leak out so that enclosed flux is defined by the following condition

$$0 = \oint d\vec{s} \cdot \left(\vec{\nabla} \phi - \frac{2\pi}{\Phi_0} \vec{A} \right) = 2\pi n + \sum_i \alpha_i - 2\pi \frac{\Phi}{\Phi_0} \tag{239}$$

where the sum runs overall Josephson junction in the loop and α_i denotes the phase shift $(0, \pi)$ (n: integer). Note that these phase shifts are not gauge independent. However, the sum does not change under any gauge transformation in any of the superconducting segments along the loop. One always finds $\sum_i \alpha_i = \pi n'$, either with n' an even or an odd integer, i.e. "even" and "odd" is invariant under gauge transformation. This leads to the following flux quantization:

$$\Phi = \begin{cases} \Phi_0 n & \text{even} \\[2ex] \Phi_0 \left(n + \frac{1}{2} \right) & \text{odd} \end{cases} \tag{240}$$

In case of an even number of π-shifts we have the standard flux quantization in terms of an integer number of flux quanta. In contrast, for an odd number of π-shifts we encounter a "half-integer" flux quantization. A particular consequence of the latter case is that there is no zero-flux situation. We call such a loop frustrated, since there is no situation in which the phase is a constant throughout the loop. The SQUID loop in Fig.20 has an odd number of π-shifts and would carry half-integer flux quanta.

Tsuei and co-workers created small loops of this kind by growing tiny $YBa_2Cu_3O_7$-loop (diameter $\sim 60 \; \mu m$) on top of tricrystalline substrate [74]. In this way arrived at a loop consisting of three differently oriented film segments. The geometry was chosen in a way that the loop would be frustrated. Indeed the measurment of the magnetic flux in the superconducting phase showed that there is a half-integer quantization in this loop,
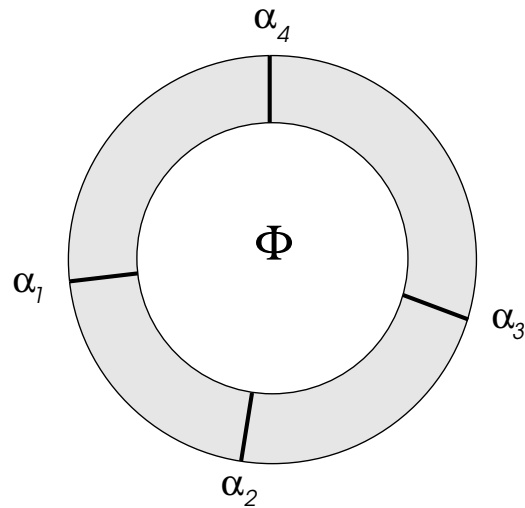
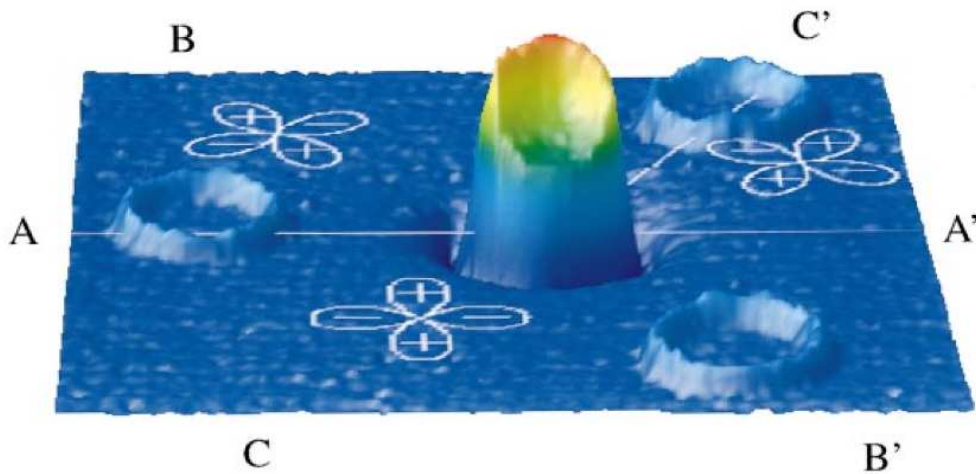**FIGURE 22.** Loop with four segments whose phase shift are α_{1-4}.

FIGURE 23. Magnetic field distribution measured by a scanning SQUID microscope for four $YBa_2Cu_3O_7$ loops on a tricrystal substrate (white lines indicate the grain boundaries). Three loops have no frustration (1,2 and 3) and the center loop 4 is frustrated. There is no magnetic flux in the loops 1, 2 and 3, but half a flux quantum ($\Phi_0/2$ in the loop 4 [74, 13].

while reference loops showed standard flux quantization. These experiments have been repeated for other cuprate superconductors with the same result and are viewed as the most beautiful phase sensitive test for *d*-wave pairing in these materials [13].

Other phase sensitive test based on scattering states

Interestingly potential scattering leads to an additional phenomenon which can be used to obtain information about the phase structure of the pair wave function. Ordinary
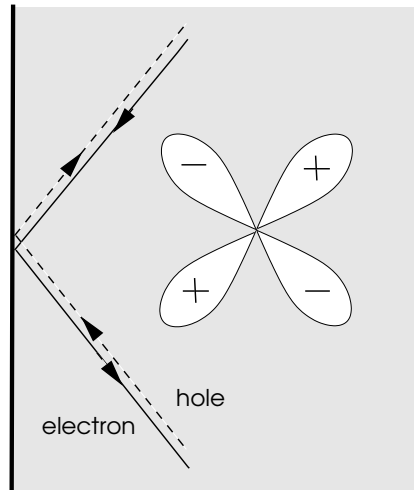
FIGURE 24. Andreev scattering with a specularly scattering surface. The electron and hole path connect two momentum direction where the gap function has opposite sign.

potential scattering from impurities and lattice defects is generally destructive for unconventional pairing. The reason lies in the destructive interference effects, if Cooper pairs are scattered between momenta for which the pair wave function has different phase. Thus one would expect that actually the disorder intrinsic to the doped cuprates would be an obstacle for d-wave pairing. Surprisingly the doping which introduces disorder between the copper-oxide planes has little effect on T_c. Only impurities implanted in the plane acts detrimental to superconductivity, such as the Zn-impurities replacing Cu.

On the level of quasiparticles potential scattering generates localized low-energy states. This is particularly impressive near surfaces with a normal vector (11). Specular surface scattering in the cooper-oxide plane connects Cooper pair states with momenta for which the pair wave functions has opposite sign (Fig.24). If a low-energy (subgap) electron is scattered at the surface back into the condensate it suffers a so-called Andreev reflection resulting in a hole which retraces the trajectory of the electron. In this was the hole returns back to the condensate and releases via Andreev reflection an electron which takes again the path of the original electron. This corresponds to a closed trajectory of a "particle" and hence constitutes a bound state at the surface. It can be shown on general grounds (e.g. by Bohr-Sommerfeld quantization) that such a π-phase shift yields yields to bound quasiparticle states at zero-energy. Since all states of this kind suffering a π-phase shift through scattering have zero energy, this gives rise to a large density of states at $E = 0$. Such states have been successfully observed by inplane quasiparticle tunneling experiments and represent a further strong support for the d-wave symmetry [75, 76, 77]. Also the scattering at an impurities generates similar subgap bound states localized around the scattering center. The typical features for an d-wave pairing state have been observed by STM spectroscopy [78]

The evidence for d-wave pairing is overwhelming. While the spin fluctuation and RVB-based descriptions provide a pairing mechanism which leads to the proper pairing

symmetry, still many questions on the cuprate superconductors remain open, in particular, in the context of the pseudogap phase of the underdoped region of the phase diagram (Fig.16).

SPIN TRIPLET SUPERCONDUCTIVITY IN STRONTIUM RUTHENATES

The discovery of high-temperature superconductivity in quasi-two-dimensional copper-oxide compounds has a initiated the search for other transition metal oxide superconductors of similar structure. In 1994 the team of Maeno and Bednorz reported the discovery of superconductivity in Sr_2RuO_4 which has a layered perovskite structure like La_2CuO_4 [22]. In constrast to the cuprates Sr_2RuO_4 is a low-temperature superconductor with $T_c \approx 1.5K$. In most respects this materials is different from the cuprates. It is in stochiometric composition metallic and displays Fermi liquid behavior at temperature below $\sim 40K$. The conductivity is very different in the basal plane and along the z-axis even a very low temperature, showing that also this material has pronounced two-dimensional behavior. The Fermi liquid parameters indicate strong correlation effects very similar (even on a quantitative level) to the quantum liquid ^{3}He. The analogy with ^{3}He led to the proposal that the superconductivity in Sr_2RuO_4 would be also based on the *odd-parity spin triplet* pairing. Over the years strong evidence has accumulated identifying the superconducting phase as a so-called chiral p-wave state, a time reversal symmetry breaking state: $\vec{d}(\vec{k}) = \hat{z}(k_x \pm i k_y)$ [23, 24].

Electronic structure

The electronic structure is dominated by the $4d$-t_{2g}-orbitals of the Ru-ions which form in each plane a square lattice. There are 4 electrons per ion as Ru^{4+}, which disperse via π-hybridization with the $2p$-orbitals of the O-ions. The result are three essentially two-dimensional bands. The α- and β-band are derived from the two orbital d_{yz} and d_{zx} which each on their own would give a one-dimensional band. Their hybridization via next-nearest-neighbor hopping leads to two two-dimensional Fermi surface a hole- and an electron-like pocket, α and β, respectively. The corresponding Hamiltonian has the form

$$\mathcal{H}_{\alpha\beta} = \sum_{\vec{k},s} \left\{ \varepsilon_{k_y} c^{\dagger}_{\vec{k}1s} c_{\vec{k}1} + \varepsilon_{k_x} c^{\dagger}_{\vec{k}2s} c_{\vec{k}2} + g_{\vec{k}} \left(c^{\dagger}_{\vec{k}1s} c_{\vec{k}2} + c^{\dagger}_{\vec{k}2s} c_{\vec{k}1} \right) \right\} \qquad (241)$$

with $\varepsilon_k = -2t\cos k - \mu$ and $g_{\vec{k}} = 4t' \sin k_x \sin k_y$ (indices $d_{yz} \to c_{\vec{k}1s}$ and $d_{zx} \to c_{\vec{k}2s}$). The third band, γ-band, is decoupled due different parity with respect to the reflection $z \to -z$ as it is derived from d_{xy}. The corresponding Hamiltonian is

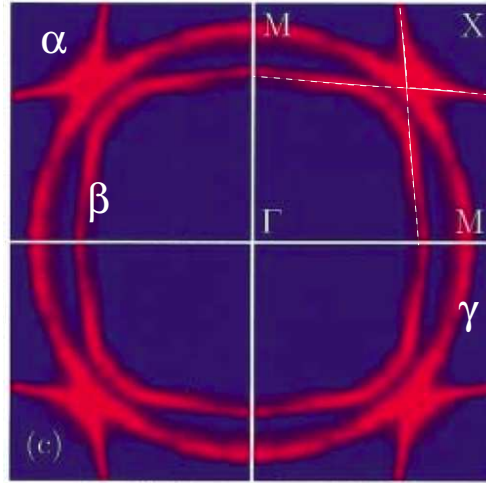$$\mathcal{H}_{\gamma} = \sum_{\vec{k}} \varepsilon'_{\vec{k}} c^{\dagger}_{\vec{k}3s} c_{\vec{k}3} \qquad (242)$$

FIGURE 25. Fermi surfaces of Sr_2RuO_4 measured by ARPES. We distinguish hole-like pockets α and electron-like sheets β and γ. The sheets α and β result from the hybridization of the two crossing one-dimensional bands (dashed white lines) [80].

with $\varepsilon'_{\vec{k}} = -2t(\cos k_x + \cos k_y) - 4t'' \cos k_x \cos k_y - \mu'$ including next-nearest-neighbor hopping ($d_{xy} \to c_{\vec{k}3s}$). The charge distribution is $2:1$ between the (α/β)- and the γ-bands. The resulting Fermi surface agree surprisingly well with the Fermi surfaces observed in detailed de Haas-van Alphen experiments [79] and ARPES [80] measurements (Fig.25).

Possible spin triplet superconducting phases

We now consider the possible superconducting phases in this system from a symmetry point of view. We pose the preconditions that the Cooper pairs consist of electrons in the same RuO_2-plane of the tetragonal crystal lattice and that spin-orbit coupling is now weak. Under these restricting conditions we find the following spin singlet states.

Γ	$\psi(\vec{k})$
A_{1g}	Δ_0
A_{2g}	$\Delta_0 k_x k_y (k_x^2 - k_y^2)$
B_{1g}	$\Delta_0 (k_x^2 - k_y^2)$
B_{2g}	$\Delta_0 k_x k_y$
E_g	–

Note that the two-dimensional E_g-representation does not provide a state. The basis functions have the form $(k_x k_z, k_y k_z)$ and are not inplane pairing states as the presence of the k_z-component shows. The spin triplet gap functions are given by

Γ	$\vec{d}(\vec{k})$	J_z
A_{1u}	$\Delta_0(\hat{x}k_x + \hat{y}k_y)$	0
A_{2u}	$\Delta_0(\hat{x}k_y - \hat{y}k_x)$	0
B_{1u}	$\Delta_0(\hat{x}k_x - \hat{y}k_y)$	± 2
B_{2u}	$\Delta_0(\hat{x}k_y + \hat{y}k_x)$	± 2
E_u	$\Delta_0 \hat{z}(k_x \pm ik_y)$	± 1

For all states we have also given the z-component of the total angular momentum (as defined for a cylindrically symmetric system). We have chosen the time reversal symmetry breaking state for E_u, since it maximizes the weak coupling condensation energy among the possible combinations in this representation.

Interestingly all the spin triplet state listed have a degenerate weak-coupling condensation energy, as this depends only on the quasiparticle gap:

$$\Delta_{\vec{k}} = |\vec{d}(\vec{k})| = \Delta_0 \sqrt{k_x^2 + k_y^2} \tag{243}$$

This degeneracy would be lifted for example by spin-orbit coupling. For the spin singlet case there is no such a problem, since the gap functions possess very distinct anisotropies.

Experimental identification of pairing symmetry

As mentioned earlier there is convincing evidence for spin triplet pairing with the symmetry $\vec{d}(\vec{k}) = \hat{z}(k_x \pm ik_y)$. A first proof for unconventional superconductivity is provided by the sensitivity of the T_c to non-magnetic impurities [81]. The transition temperature is suppressed with increasing impurity concentration. The threshold mean free path of the conduction electrons needs to be longer than roughly 100 nm which corresponds approximately to the zero-temperature coherence length.

A rather direct test for triplet pairing is the measurement of the spin susceptibility which is possible in the superconducting phase via the NMR Knight shift. Early on experiments showed that the spin susceptibility stays constant for magnetic fields in the basal plane indicating a $\vec{d}$-vector parallel to the z-axis [82]. In another experiment, the muon zero-field relaxation rate displays an pronounced continuous increase of the intrinsic magnetic field spread pointing towards a time reversal symmetry breaking

superconducting phase [45]. From our classification we see that under the restriction to inplane pairing there is no spin singlet pairing phase with broken time reversal symmetry. On the other hand, both experiments are consistent with each other in selecting $\vec{d}(\vec{k}) = \hat{z}(k_x \pm ik_y)$.

There is further experimental evidence for this pairing state. Very recently a first phase sensitive test of the SQUID-type has been reported [83]. In contrast to the case discussed for the $d_{x^2-y^2}$-wave spin singlet superconductor, the conditions here is less intuitive. A first problem which has to be settled is the Josephson effect between a spin singlet and a spin triplet superconductor, since the SQUID device contains junctions between the triplet and a conventional superconductor. There are two obstacles to be overcome. The pair wave functions in the two superconductors do not match in the parity of their orbital part and also not in the spin part. The first point is solved through the fact that an interface naturally breaks parity. The second requires magnetically active tunneling, i.e. spin flip processes in tunneling. This appears automatically when the two superconductors are different in spin-orbit coupling, so that the matching of electron spinor wavefunctions removes spin conservation in tunneling. Symmetry considerations lead to the following expression for the coupling:

$$J \propto Im\langle \psi(\vec{k})^* \vec{d}(\vec{k}) \cdot \{\vec{n} \times \vec{k}\}\rangle_{\vec{k},FS} \tag{244}$$

where $\vec{n}$ is the normal vector of the interface on the spin triplet superconductor side. We see that there is only coupling in the basal plane for $\vec{d} \parallel \hat{z}$. The orbital and spin part have no independent selection rules anymore, but only the total angular momentum $\vec{J} \cdot \vec{n}$ perpendicular to the junction. For the gap function $\vec{d}(\vec{k}) = \hat{z}(\eta_x k_x + \eta_y k_y)$ with the normal vector $\vec{n} \parallel x$ we find the the s-wave order parameter couples to the η_y component. In this way $\vec{J} \cdot \vec{n} = 0$ is realized for the Cooper pairs on both sides. The SQUID device follow the basic design proposed by Geshkenbein and co-workers [69] as shown in Fig.26. The s-wave superconductor is attached on two opposite sides so that $\vec{n}$ has opposite sign. In this way there is a phase shift of π in the SQUID loop and, analogously to the d-wave SQUID of the cuprate superconductors, we expect a shift of the interference pattern by half of a flux quantum. This effect has indeed been observed recently by Nelson et al. [83].

The order parameter of $\vec{d}(\vec{k}) = \hat{z}(k_x \pm ik_y)$ has two complex components. This has various consequences. For example the mixed phase is influenced by the nature of the order parameter. The vortex lattice has square coordination for fields along the z-axis, in contrast to the triangular form in the standard case. This was predicted by Agterberg [84] and subsequently experimentally verified by Riseman et al. [85]. Additionally the field distribution in the mixed phase, measured by muon spin relaxation, shows peculiarities which are characteristic for a two-component order parameter [86].

Thermodynamic measurements do not allow to make a clear statement about the order parameter symmetry so far. Many data seem to point towards a phase with line nodes [23]. However, the situations is more complicated due to the presence of several bands which make the data analysis rather complex [87, 88].
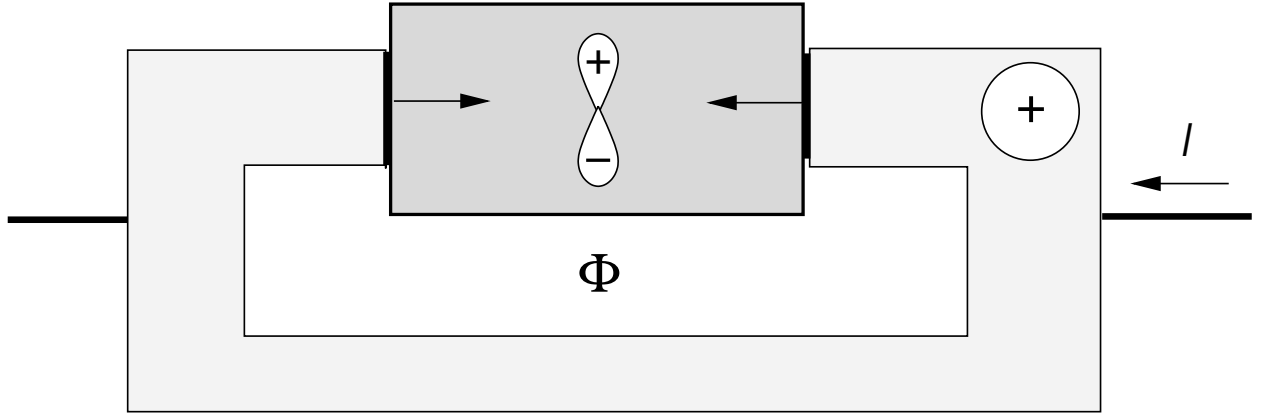
FIGURE 26. SQUID setup with a diametral junction configuration following Geshkenbein et al. [69].

Microscopic origin of the chiral p-wave state

The microscopic origin of the interaction yielding spin triplet pairing is unclear. On the one hand, one may argue that Sr_2RuO_4 would be close to a ferromagnetic phase. The Ruddelson-Popper series of compounds $Sr_{n+1}Ru_nO_{3n+1}$, where n is the number of RuO_2-layers per unit cell, goes towards ferromagnetism with growing n. The infinite-layer compound $SrRuO_3$ is ferromagnetic with $T_C = 165K$. From this viewpoint a mechanism based on ferromagnetic spin fluctuations seems to be an appealing proposal. However, neutron scattering data do not support this idea. Rather strong spin fluctuations at an incommensurate wave vector have been observed [89] which readily can be identified with a nesting vector associated with the α-β bands, a reminiscent of their quasi-one-dimensional nature [90, 105] (see Fig.27). Thus spin fluctuations as a pairing mechanism do not provide a clear-cut picture. Theoretical studies show therefore a wide spread of possible pairing mechanisms [91, 92, 93, 94, 95, 96, 97, 98].

There is another important issue concerning the stability of the chiral p-wave state connected with the degeneracy within the weak-coupling limit. It is spin-orbit coupling which is most relevant for lifting this degeneracy, although it has been shown that certain higher-order feedback effects favor actually the chiral p-wave state [99, 100]. The effect of spin-orbit coupling discussed on the level of the Cooper pairs can be discussed by using a phenomenological approach. Introducing the general order parameter

$$\vec{d}(\vec{k}) = \sum_{\mu=x,y,z} \sum_{i=x,y} A_{\mu i} \hat{\mu} k_i \qquad (245)$$

we find the following second order term in the Ginzburg-Landau free energy in the absence of spin-orbit coupling

$$F_2 = a'(T - T_c)tr(\hat{A}^\dagger \hat{A}) , \qquad (246)$$

i.e. any spin-triplet state has the same T_c. Eventually, the fourth order terms determine the combinations of spin and orbital components in order to maximize the condensation energy. The feedback effects modify the fourth order terms [99, 100]. Spin-orbit
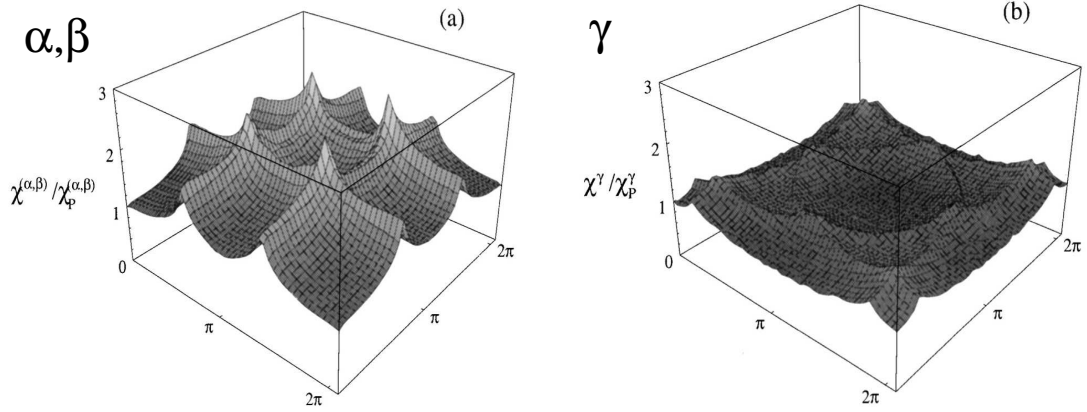
FIGURE 27. Static spin susceptibility $\chi(\vec{q})$ for the two subsystems: (a) the α-β-band with pronounced peak by $\vec{Q}_{ic} \approx (\pi/3, \pi/3, 0)$ due to nesting features; (b) the γ-band with softer features [105].

coupling for a tetragonal material can be cast into following potential for the Cooper pairs

$$\hat{V} = a_1 \vec{L} \cdot \vec{S} + a_2 L_z S_z \quad \text{with} \quad \begin{cases} S_i d_j = -i\varepsilon_{ijl} d_l \\ \\ L_i k_j = i\varepsilon_{ijl} k_l \end{cases} \tag{247}$$

(ε_{ijl}: total antisymmetric tensor). From this we derive the following second order term:

$$\langle \vec{d}(\vec{k})^* \{\hat{V} \vec{d}(\vec{k})\}\rangle_{\vec{k},FS} \quad \Rightarrow \quad F_{so} = -\alpha \sum_{\mu,\nu} \{A^*_{\mu\mu} A_{\nu\nu} - A^*_{\mu\nu} A_{\nu\mu}\} \tag{248}$$

with $\alpha = a_1 + a_2$. These additional terms split the T_c.

$$T_c(a) = T_c(0) - \frac{\alpha}{a'}(|J_z| - 1) . \tag{249}$$

The T_c depends on the total angular momentum J_z and on α. The sign of α determines whether the states with $J_z = \pm 2$ or $J_z = 0$ have the highest T_c. Annoyingly the chiral p-wave state cannot be stabilized in this way [101, 96, 102, 97]

On the microscopic level we can introduce spin-orbit coupling on the Ru-ion acting only within the $4d$-t_{2g}-orbitals:

$$\mathscr{H}_{so} = i\lambda \sum_{m,n,l} \varepsilon_{lmn} \sum_{\vec{k},s,s'} c^\dagger_{\vec{k}ls} c_{\vec{k}ms'} \sigma^n_{ss'} . \tag{250}$$

This added to the tight-binding Hamiltonian (241,242) leads to a modified band structure. Examining this Hamiltonian we find that starting out from the independent orbitals (d_{yz}, d_{zx}, d_{xy}) we can obtain in lowest order perturbation in the spin-orbit coupling and the interorbital hybridization that the degeneracy is lifted by a spin dependent Cooper pair scattering between the orbitals d_{yz} and d_{zx} with the matrix element proportional to

$$\lambda t' \langle k_x k_y \hat{z} \cdot \{\vec{d}_1(\vec{k}) \times \vec{d}_2(\vec{k})\}\rangle_{\vec{k}} \tag{251}$$

where $\vec{d}_1$ and $\vec{d}_2$ are the gap functions associated with the orbital d_{yz} and d_{zx}, respectively. Obviously the $\vec{d}$-vectors have to lie in the x-y-plane in order to reach a finite matrix element. It is easy to verify that the possible states stabilized are characterized by $J_z = 0$ or ± 2 depending on the sign of λ. This is in agreement with the phenomenological analysis above [102].

In order to stabilize the chiral p-wave state an additional indirect spin anisotropy has to enter via the pairing interaction [103, 105, 96, 102]. This means that interactions involving spin densities have to play a certain role in the pairing mechanism in order to pin the orientation of the $\vec{d}$-vector additionally. The spin fluctuation mechanism, for example, involves the anisotropies of the dynamical spin susceptibility resulting from spin-orbit coupling in the multi-band systems (250). The static susceptibility shows very clear properties in this respect:

$$\chi_{zz}(\vec{q}) < \chi_{+-}(\vec{q}) \quad \text{for} \quad \vec{q} \to 0$$

$$\chi_{zz}(\vec{q}) < \chi_{+-}(\vec{q}) \quad \text{for} \quad \vec{q} = \vec{Q}_{ic} \tag{252}$$

where $\vec{Q}_{ic} \approx (\pi/3, \pi/3, 0)$ is the wave vector of the (dominant) incommensurate spin correlation [105, 106]. The small-q contribution is inplane polarized and the incommensurate fluctuations are z-axis polarized [107]. The former favors, of course, inplane equal-spin pairing for the spin triplet channel, since the small-q scattering is favorable for odd-parity pairing[103]. The z-axis polarization on the other hand, is essential for certain spin fluctuation based mechanisms combining the scattering around $\vec{Q}_{ic}$ and special nesting feartures of the Fermi surface to obtained an inplane equal-spin pairing state [92, 94]. While this aspect suggests that spin fluctuations are involved in the pairing mechanism, it is not clear whether they are necessarily the dominant part. In addition the view on the spin dynamics alone neglects contributions from vertex corrections (renormalized coupling matrx elements) which are possibly important for the selection of the pairing state as well [91, 96].

We have two competing trends due to spin-orbit coupling. If the α-β-bands are dominating the superconductivity, then likely the states with $\vec{d} \perp \hat{z}$ will be stabilized. On the other hand, a dominating γ-band would entirely be determined by the contributions of the anisotropic spin fluctuations stabilizing a state with $\vec{d} \parallel \hat{z}$ corresponding to the chiral p-wave phase. Therefore, a γ-band dominating the superconducting instability while the α-β-bands are only passively involved, provides good conditions to favor the chiral p-wave state over the others [104, 96]. This ideas of the dominant γ-band receives strong support from the analysis of various thermodynamic measurements such as the specific heat [88, 108], the London penetration depth [109, 110] etc. These results suggest that the α-β-bands only contribute at rather low temperature noticably to the superconductivity. This aspect makes the search for gap anisotropies, even with nodal features, very challenging [108].

The fact that there are obviously two trends to lift the degeneracy among the different spin triplet states hints that the energy scales involved in the end are rather small despite the rather strong spin orbit coupling ($\lambda \sim 1000K$). There are several renormalizing steps which reduce finally the magnitude of effect on the Cooper pair energy. For example the matrix element (251) is reduced through the fact that contributions to the

$\vec{k}$ average come from the region at the Fermi level where the two bands cross. Also the contribution of the anisotropy of the spin susceptibility can only result in a fraction of T_c. Consequently the anisotropy pinning of the $\vec{d}$-vector is likely weak. Indeed recent Knight shift measurement for fields along the z-axis suggest that for fields of several hundreds of Oe the $\vec{d}$ may have flipped into basal plane [111].

The inhomogeneous 3-Kelvin phase

Finally we would like to briefly review a quite unexpected finding in Sr_2RuO_4. Investigating Ru-Sr_2RuO_4 eutectic samples it was found that an inhomogeneous superconducting phase appears at higher temperature than the bulk superconductivity, roughly around $T^* \sim 3K$. This inhomogeneous phase was then called "3K-phase". Below T^* superconductivity nucleates on islands which eventually grow together to form the uniform bulk phase as the temperature reaches $T_c \approx 1.5K$. The signature of the phase is the gradual drop of the resistance for $T_c < T < T^*$[112]. The Ru-Sr_2RuO_4 eutectic consists of many μm-size Ru-metal inclusions in the otherwise pure Sr_2RuO_4. The experimental evidence points towards the nucleation of superconductivity at the interface between Ru and Sr_2RuO_4 in a way that in a tiny layer the conditions for Cooper pairing is improved [113]. The nucleation of such a filamentary form of superconductivity has been confirmed by measurments of the upper critical field. For filamentary superconductors the temperature dependence of the upper critical field has an exponent $\alpha < 1$ in

$$H_{c2}(T) \propto (T^* - T)^{\alpha} \tag{253}$$

where α has been fitted to the value 0.7. This means a clear deviation from the standard bulk H_{c2} which has a linear dependence [114, 115].

A fascinating aspect of this eutectic system is that the nucleated order parameter has a p-wave component whose lobes lie parallel to the interface. This corresponds to time reversal symmetry conserving phase, so that the bulk transition is not merely a percolation transition as in inhomogeneous conventional superconductors. This transition is time reversal symmetry breaking in order to arrive at the chiral p-wave phase. The study of the structure of the inhomogeneous phase shows that the transition to the bulk phase may be even more complex. The inhomogeneous phase viewed as a network of superconducting islands weakly coupled among each other, which is intrinsically frustrated due to the internal phase structure. Thus, the evolution of the superconducting phase as the temperature is lowered could lead through regimes where spontaneous supercurrents are flowing in the frustrated network, rather similar to the frustrated loops discussed in the context of phase sensitive test for d-wave superconductivity [113]. For such a phase there is so far only indirect evidence by the observation that the critical currents in the 3-K phase are not invariant under the operation $J \rightarrow -J$ [116]. This indicates that in the complex network of superconducting islands the time reversal symmetry has been broken.

It is a lucky coincidence that Sr_2RuO_4 provides us with this highly complex inhomogeneous phase besides much other exciting physics of an unconventional superconduc-

tor. While a great deal of the properties of this superconductor has been understood by now there are still many questions. In particular, the pairing mechanism and its connection to the magnetic properties have not been put into a transparent form. Sr_2RuO_4 will in any case serve in future as an exemplary system for discussing unconventional superconductivity as many of the generic non-trivial aspects are realized here. As a Fermi liquid phase it constitutes also the electronic analog of the most intriguing superfluid, ^{3}He.

CONCLUSION

In this lecture we have covered a few of the essential parts to describe and understand unconventional superconductivity. This field is quickly developing due to impressive progress in the production of high-quality materials during recent years. High quality is mandatory to find unconventional superconductivity, since anisotropic Cooper pairs are easily destroyed by scattering at defects in the samples. Among the unconventional superconductors we do not only find those with the highest T_c but many with fascinating and puzzling properties making them despite most low T_cs a most attractive subject of research. Many of the new superconductors require from us to extend our views and ideas of superconductivity.

Finally I would like to recommend for further reading several reviews and books which go in many parts much deeper than it was possible in this lecture. Among the books to recommend are V.P. Mineev and K.V. Samokhin, *Introduction to Unconventional Superconductivity* (Gordon and Breach, Science Publisher, 1999), K.H. Bennemann and J.B. Ketterson, *The Physics of Superconductors, Vol. I / II* (Springer, 2003). Reviews on recent developments for the heavy Fermion superconductors are by P. Thalmeier and G. Zwicknagl (Handbook on the Physics and Chemistry of Rare Earths, Vol. 34, 135 (2005)), by R.H. Heffner and M.R. Norman (Comments Condens. Matter Phys. 17, 361 (1996)) and specifically on UPt_3, which we had not touched in much detail in the lecture, by R. Joynt and L. Taillefer (Rev. Mod. Phys. 74, 235 (2002)).

ACKNOWLEDGMENTS

REFERENCES

1. P. W. Anderson and P. Morel, Phys. Rev. Lett. **5**, 136-138 (1960); Phys. Rev. **123**, 1911-1934 (1961).
2. R. Balian and N. R. Werthamer, Phys. Rev. **131**, 1553-1564 (1963).
3. A. J. Leggett, Rev. Mod. Phys. **47**, 331-414 (1975).
4. D. D. Osheroff, R. C. Richardson and D. M. Lee, Phys. Rev. Lett. **28**, 885-887 (1972).
5. D. Vollhardt and P. Wölfle, *The superfluid phases of ^3He*, Tayler & Francis, London (1990).
6. F. Steglich, J. Aarts, C.D. Bredl, W. Lieke, D. Meschede, W. Franz and H. Schäfer, Phys. Rev. Lett. **43**, 1892 (1979).
7. H.R. Ott, H. Rudigier, Z. Fisk and J.L. Smith, Phys. Rev. Lett. **50**, 1595 (1983).
8. G.R. Stewart, Z. Fisk, J.O. Willis and J.L. Smith, Phys. Rev. Lett. **52**, 679 (1984).
9. D. Jerome, A. Mazaud, M. Ribault and K. Bechgaard, J. Phys. Lett. (Paris) **41**, L95 (1980).
10. S.S.P. Parkin, E.M. Engler, R.R. Schumaker, R. Lagier, V.V. Lee, J.C. Scott and R.L. Greene, Phys. Rev. Lett. **50**, 270 (1983).
11. J.G. Bednorz and K.A. Müller, Z. Phys. B **64**, 189 (1986).
12. D.J. Scalapino, Phys. Rep. **250**, 329 (1995).
13. C.C. Tsuei and J.R. Kirtley, Rev. Mod. Phys. **72**, 969 (2000).
14. B. Batlogg and C. Varma, Physics World, Feb. 2000, p. 33. (http://physicsweb.org/article/world/13/2/8)
15. F.M. Grosche, S.R. Julien, N.D. Mathurand G.G. Lonzarich, Physica B **223-224**, 50 (1996).
16. N.D. Mathur, G.M. Grosche, S.R. Julian, I.R. Walker, D.M. Freye, R.K.W. Haselwimmer, G.G. Lonzarich, Nature (London) **394**, 39 (1998).
17. J.D. Thompson, R. Movshovich, Z. Fisk, F. Bouquet, N.J. Cueeo, R.A. Fisher, P.C. Hammel, H. Heeger, M.F. Hundley, M. Jaime, P.G. Pagliuso, C. Petrovic, N.E. Philips, J.L. Sarrao, J. Magn. Magn. Mater. **226-230**, 5 (2001).
18. C. Petrovic, R. Movshovich, M. Jaime, P.G. Hundley, J.L. Sarrao, Z. Fisk, J.D. Thompson, Europhys. Lett. **53**, 354 (2001).
19. S.S. Saxena, P. Agarwal, K. Ahllan, F.M. Grosche, R.K.W. Haselwimmer, M.J. Steiner, E. Pugh, I.R. Walker, S.R. Julian, P. Monthoux, G.G. Lonzarich, A. Huxley, I. Shelkin, D. Braithwaite, and J. Flouquet, Nature (London) **406** , 587 (2000).
20. D. Aoki, A. Huxley, E. Ressouche, D. Braithwaite, J. Flouquet, J.-P. Brison, and E. Lhotel, Nature **413**, 613 (2001).
21. C. Pfleiderer, J. Magn. Magn. Mater, **226-230**, 23 (2001).
22. Y. Maeno, H. Hashimoto, K. Yoshida, S. Nishizaki, T. Fujita, J.G. Bednorz and F. Lichtenberg, Nature (London) **372**, 532 (1994).
23. A.P. Mackenzie and Y. Maeno, Rev. Mod. Phys. **75**, 657 (2003).
24. Y. Maeno, T.M. Rice and M. Sigrist, Physics Today **54**, 42 (2001).
25. E.D. Bauer, N.A. Frederick, P.-C. Ho, V.S. Zapf, and M.B. Maple, Phys. Rev. B **65**, 100506 (R) (2002).
26. K. Takada, H. Sakurai, E. Takayama-Muromachi, F. Isumi, R.A. Dilanian and T. Sasaki, Nature (London) **422**, 53 (2003).
27. M. Hanawa, Y. Muraoka, T. Tayama, T. Sakakibara, J. Yamaura and Z. Hiroi, Phys. Rev. Lett. **87**, 187001 (2001).
28. S. Yonezawa, Y. Muraoka, Y. Matsushita and Z. Hiroi, J. Phys. Cond. Matter **16** , L9 (2004).
29. E. Bauer, G. Hilscher, H. Michor, C. Paul, E.W. Scheidt, A. Gribanov, Y. Seropegin, H. Noel, M. Sigrist and P. Rogl, Phys. Rev. Lett. **92**, 027003 (2004).
30. P. W. Anderson and P. Morel, Phys. Rev. **125**, 1263-1271 (1962).
31. W. L. MacMillan, Phys. Rev. **167**, 331 (1968).
32. W. Kohn and J.M. Luttinger, Phys. Rev. Lett. **15**, 524-526 (1965).
33. N.F. Berk and J.R. Schrieffer, Phys. Rev. Lett. **17**, 433-435 (1966).
34. D. Fay and J. Appel, Phys. Rev. B **22**, 3173-3182 (1980).
35. P. Monthoux and G.G. Lonzarich, Phys. Rev. B **59**, 14598 (1999); Phys. Rev. B**63**, 054529 (2001).
36. T. Akazawa, H. Hidaka, T. Fujiwara, T.C. Kobayashi, E. Yamamoto, Y. Haga, R. Settai and Y. Onuki, J. Phys.: Condens. Matter **16**, L29 (2004); T. Akazawa, H. Hidaka, T.C. Kobayashi,T. Fujiwara E. Yamamoto, Y. Haga, R. Settai and Y. Onuki, J. Phys. Soc. Jpn. **73**, 3129 (2004).

37. P.W. Anderson and W.F. Brinkman, included in P.W. Anderson *Basic Notions of Condensed Matter Physics*, Frontiers in Physics Nr. 55, Addison-Wesley (1984).
38. P.W. Anderson, J. Phys. Chem. Solids **11**, 26 (1959).
39. P.W. Anderson, Phys. Rev. B**30**, 4000 (1984).
40. P.W. Anderson and W.F. Brinkman, Phys. Rev. Lett. **30**, 1108 (1973).
41. A.A. Abrikosov, *Fundamentals of the Theory of Metals*, North-Holland, Chapter: 21.4 (1988).
42. L.P. Gorkov, Sov. Sci. Rev. A Phys. **9**, 1 (1987).
43. M. Sigrist and K. Ueda, Rev. Mod. Phys. **63**, 239 (1991).
44. G.E. Volovik and L.P. Gorkov, JETP **61**, 843 (1985).
45. G.M. Luke, Y. Fudamoto, K.M. Kojima, M.I. Larkin, J. Merrin, B. Nachumi, Y.J. Uemura, Y. Maeno, Z.Q. Mao, Y. Mori, H. Nakamura and M. Sigrist, Nature (London) **394**, 558 (1998).
46. R.H. Heffner, J.O. Willis, J.L. Smith, P. Birrer, C. Baines, F.N. Gygax, B. Hitti, E. Lippelt, H.R. Ott, A. Schenk and D.E. MacLaughlin, Phys. Rev. B **40**, 806 (1989).
47. H.R. Ott, H. Rudigier, E. Felder, Z. Fisk and J.L. Smith, Phys. Rev. B **33**, 126 (1986).
48. H.R. Ott, J. Low Temp. Phys. **95**, 95 (1994).
49. G.M. Luke, A. Keren, L.P. Le, W.D. Wu, Y.J. Uemura, D.A Bonn, L. Taillefer and J.D. Garrett, Phys. Rev. Lett. **71**, 1466 (1993).
50. R.A. Fisher, S. Kim, B.F. Woodfield, N.E. Phillips, L. Taillefer, K. Hasselbach, J. Flouquet, A.L. Giorgi and J.L. Smith, Phys. Rev. Lett. **62**, 1411 (1989).
51. K. Hasselbach, L. Taillefer and J. Flouquet, Phys. Rev. Lett. **63**, 93 (1989).
52. Y. Aoki, A. Tsuchiya, T. Kanayama, S.R. Saha, H. Sugawara, H. Sato, W. Higemoto, A. Koda, K. Ohishi, K.Nishiyama and R. Kadono, Phys. Rev. Lett. **91**, 067003 (2003).
53. F.C. Zhang and T.M. Rice, Phys. Rev. B **37**, 3759 (1988).
54. T. Moriya, *Spin fluctuations in itinerant electron magnetism*, Springer Series in Solid-State Sciences 56 (1985).
55. P.W. Anderson, Science **237**, 1196 (1987).
56. P.W. Anderson, P.A. Lee, M. Randeria, T.M. Rice, N. Trivedi and F.C. Zhang, J. Phys. Condens. Matter **16**, R755 (2004).
57. P.A. Lee, N. Nagaosa and X.G. Wen, cond-mat/0410445.
58. N. Nagaosa, *Quantum Field Theory in Strongly Correlated Electronic Systems*, Springer (1998).
59. T. Moriya and K. Ueda, Adv. Phys. 49, 555 (2000).
60. T. Tanamoto, H Kohno and H. Fukuyama, J. Phys. Soc. Jpn. 63, 2739 (1994).
61. J.A. Martindale, S.E. Barrett, K.E. O'Harea, C.P. Slichter, W.C. Lee and D.M. Ginsberg, Phys. Rev. B **47**, 9155 (1993).
62. W.N. Hardy, D.A. Bonn, D.C. Morgan, R. Liang and K. Zhang, Phys. Rev. Lett. **70**, 3999 (1993).
63. B. Barbiellini, O. Fischer, M. Peter, C. Renner and M. Weger, Physica C **220**, 55.
64. Z.X. Shen, D.S. Dessau, B.O. Wells, D.M. King, W.E. Spicer, A.J. Arko, D. Marshall, L.W. Lombardo, A. Kapitulnik, P. Dickinson, S. Doniach, J. DiCarlo, A.G. Loeser and C.H. Park, Phys. Rev. Lett. **70**, 1553 (1993).
65. H. Ding, M.R. Norman, J.C. Campuzano, M. Randeria, A.F. Bellman, T. Yokoya, T. Takahashi, T. Mochiku and K. Kadowaki, Phys. Rev. Lett. **54**, 9678 (1996).
66. A. Damascelli, Z. Hussain and Z.X. Shen. Rev. Mod. Phys. **75**, 473 (2003).
67. D.J. Van Harlingen, Rev. Mod. Phys. **67**, 515 (1995).
68. V.B. Geshkenbein and A.I. Larkin, JETP Lett. **43**, 395 (1986).
69. V.B. Geshkenbein, A.I. Larkin and A. Barone, Phys. Rev. B **36**, 235 (1987).
70. M. Sigrist and T.M. Rice, J. Phys. Soc. Jpn. **61**, 4283 (1992).
71. D.A. Wollman, D.J. Van Harlingen, W.C. lee, D.M. Ginsberg and A.J. Leggett, Phys. Rev. Lett. **71**, 2134 (1993).
72. D. Brawner and H.R. Ott, Phys. Rev. B **50**, 6530 (1994).
73. A. Mathai, Y. Gim, R.C. Black, A. Amar and F.C. Wellstood, Phys. Rev. Lett. **74**, 4523 (1995).
74. C.C. Tsuei, J.R. Kirtley, C.C. Chi, L.S. Yu-Jahnes, A. Gupta, T. Shaw, J.Z. Sun and M.B. Ketchen, Phys. Rev. Lett. **73**, 593 (1994).
75. C.-R. Hu, Phys. Rev. Lett. **72**, 1526 (1994).
76. S. Kashiwaya and Y. Tanaka, Rep. Prog. Phys. **63**, 1641 (2000).
77. G. Deutscher, Rev. Mod. Phys. **77**, 109 (2005).
78. A.V. Balatsky, I. Vekhter and J.-X. Zhu, cond-mat/0411318 (2004).

79. C. Bergemann, S.R. Julian, A.P. Mackenzie, S. Nishizaki and Y. Maeno, Phys. Rev. Lett. **84**, 2662 (2000).
80. A. Damascelli, D.H. Lu, K.M. Shen, N.P. Armitage, F. Ronning, D.L. Feng, C. Kim, Z.X. Shen, T. Kimura, Y. Tokura, Z.Q. Mao and Y. Maeno, Phys. Rev. Lett. **85**, 5194 (2000).
81. A.P. Mackenzie, R.K.W. Haselwimmer, A.W. Tyler, G.G. Lonzarich, Y. Mori, S. Nishizaki and Y. Maeno, Phys. Rev. Lett. **80**, 161 (1998).
82. K. Ishida, H. Mukuda, Y. Kitaoka, K. Asayama, Z.Q. mao, Y. Mori and Y. Maeno, Nature (London) **396**, 658 (1998).
83. K.D. Nelson, Z.Q. Mao, Y. Maeno and Y. Liu, Science **306**, 1151 (2004).
84. D.F. Agterberg, Phys. Rev. Lett. **80**, 5184 (1998).
85. T.M. Riseman, P.G. Kealey, E.M. Forgan, A.P. Mackenzie, L.M. Galvin, A.W. Tyler, S.L. Lee, C. Ager, D. McK. Paul, C.M. Aegerter, R. Cubitt, Z.Q. Mao, T. Akima and Y. Maeno, Nature (London) **396**, 242; Nature (London) **404**, 629 (2000).
86. P.G. Kealey, T.M. Riseman, E.M. Forgan, A.P. Mackenzie, L.M. Galvin, S.L. Lee, D.McK. Paul, R. Cubitt, D.F. Agterberg, R. Heeb, Z.Q. Mao and Y. Mao, Phys. Rev. Lett. **84**, 6094 (2000).
87. D.F. Agterberg, T.M. Rice and M. Sigrist, Phys. Rev. Lett. **78**, 3374 (1997).
88. M.E. Zhitomirsky and T.M. Rice, Phys. Rev. Lett. **87**, 057001 (2001).
89. Y. Sidis, M. Braden, P. Bourges, B. Hennion, W. Reichardt, Y. Maeno and Y. Mori, Phys. Rev. Lett. **83**, 3320 (1999).
90. I.I. Mazin and D.J. Singh, Phys. Rev. Lett. **82**, 4324 (1999).
91. T. Nomura and K. Yamada, J. Phys. Soc. Jpn. **69**, 2678 (2000); J. Phys. Soc. Jpn. **71**, 404 (2002);J. Phys. Soc. Jpn. **71**, 1993 (2002).
92. T. Kuwabara and M. Ogata, Phys. Rev. Lett. **85**, 4586 (2000).
93. M. Sato and K. Kohmoto, J. Phys. Soc. Jpn. **69**, 3505 (2000).
94. K. Kuroki, M. Ogata, R. Arita and H. Aoki, Phys. Rev. B **63**, 060506 (2001).
95. I. Eremin, D. Manske, C. Joas and K.H. Bennemann, Europhys. Lett. **58**, 871 (2002).
96. Y. Yanase and M. Ogata, J. Phys. Soc. Jpn. **72**, 673 (2003).
97. I. Eremin, D. Manske, S.G. Ovchinnikov and J.F. Annett, Annalen der Physik **13**, 149 (2004).
98. R. Arita, S. Onari, K. Kuroki and H. Aoki, Phys. Rev. Lett. bf 92, 247006 (2004).
99. J. Goryo and M. Sigrist, J. Phys.: Condens. Matter **12**, L599 (2000).
100. J. Goryo and M. Sigrist, Europhys. Lett. **57**, 578 (2002).
101. M. Sigrist and M.E. Zhitomirsky, J. Phys. Soc. Jpn. **65**, 3452 (1996).
102. J.F. Annett, G. Litak, B.L. Gyorffy and K.L. Wysokinski, cond-mat/0411169.
103. M. Sigrist, D.F. Agterberg, A. Furusaki, C. Honerkamp, K.K. Ng, T.M. Rice and M.E. Zhitomirsky, Physica C **317-318**, 134 (1999).
104. K.K. Ng and M. Sigrist, Europhys. Lett. **49**, 473 (2000).
105. K.K. Ng and M. Sigrist, J. Phys. Soc. Jpn. **69**, 3764 (2000).
106. I. Eremin, D. Manske and K.H. Bennemann, Phys. Rev. B **65**, 220502 (2002).
107. M. Braden, P. Steffens, Y. Sidis, J. Kulda, P. Bourges, S. Hayden, N. Kikugawa and Y. Maeno, Phys. Rev. Lett. **92**, 097402 (2004).
108. K. Deguchi, Z.Q. Mao, H. Yaguchi and Y. Maeno, Phys. Rev. Lett. **92**, 047002 (2004); K. Deguchi, Z.Q. Mao and Y. Maeno, J. Phys. Soc. Jpn. **73**, 1313 (2004).
109. I. Bonalde, B.D. Yanoff, D.J. Van Harlingen, M.B. Salamon and Y. Maeno, Phys. Rev. Lett. **85**, 4775 (2000).
110. H. Kusunose and M. Sigrist, Europhys. Lett. **60**, 281 (2002).
111. H. Murakawa, K. Ishida, K. Kitagawa, Z.Q. Mao and Y. Maeno, Phys. Rev. Lett. **93**, 167004 (2004).
112. Y. Maeno, T. Ando, Y. Mori, E. Ohmichi, S. Ikeda, S. Nishizaki and S. Nakatsuji, Phys. Rev. Lett. **81**, 3765 (1998).
113. M. Sigrist and H. Monien, J. Phys. Soc. Jpn. **70**, 2409 (2001).
114. H. Yaguchi, M. Wada, T. Akima, Y. Maeno and T. Ishiguro, Phys. Rev. B **67**, 214519 (2003).
115. M. Matsumoto, C. Belardinelli and M. Sigrist, J. Phys. Soc. Jpn. **72**, 1623 (2003).
116. J. Hooper, Z.Q. Mao, K.D. Nelson, Y. Liu, M. Wada and Y. Maeno, Phys. Rev. B **70**, 014510 (2004).